NTNU
Norwegian University of
Science and Technology

Case Hardening of Hardox 450 Steel for Increased Ballistic Strength

Tor Arne Buberg

Materials Science and Engineering
Submission date: June 2011
Supervisor: Jan Ketil Solberg, IMTE

Norwegian University of Science and Technology
Department of Materials Science and Engineering

Preface

The work of this master's thesis has been conducted at the Department of Materials Science and Engineering and at the Structural Impact Laboratory (SIMLab) at the Norwegian University of Science and Technology (NTNU) during the spring of 2011. The thesis is a part of a larger research project from the Centre for Research-based Innovation (CRI).

The master's thesis was carried out independently and in accordance with the examination regulations of NTNU.

Trondheim 27.06.2011

Tor Arne Buberg

Abstract

Steel alloys are the material that is most used in protective constructions today. The reason is the overall good properties of steels, with its high strength and hardness, high ductility, high formability and relatively low cost compared to other materials. Even though armour steels are affordable, work is done to limit expenses from production or come up with new and less expensive alloys.

Case hardening is a technique for production of steel with a very hard and durable surface while still maintaining a tough and ductile core. Case hardened products have hard, durable and fatigue resistant surfaces and tough and durable cores. Case hardening is typically applied to machine parts that are exposed to heavy wear and high loads such as gears, bearings, screws and nuts, shafts, etc

In 2010, Lou et al. managed to significantly increase the penetration resistance of a low-cost steel (NVE36) by case hardening. Encouraged by this, Hans Magne Thorseth wrote his master's thesis "*Optimalisering av stål i beskyttelseskonstruksjoner*" in 2010. His attempt to improve the ballistic strength of Hardox 450 steel by case hardening did not have the desired results. The ballistic limit velocity was reduced from approximately 800 m/s for the original Hardox 450 to approximately 770 m/s for the case hardened steel. The probable reasons for the reduction of the ballistic limit velocity was a too low carbon content increase from the carburizing and thus a too low hardness increase, in addition to deterioration of the metal core properties from the heat treatment. The objective of this master's thesis was to improve the case hardening process used by Hans Magne Thorseth in his master's thesis.

The improvement work was divided into two parts, a preliminary project work and this master thesis. The project was carried out in the autumn of 2010, and the aim was to find the optimum case hardening process to produce steel with improved ballistic properties. This involved testing of different carburizing potentials to increase the surface carbon content of the metal and to find carburizing heat treatments that would retain the core properties of the carburized steel. Based on the results from the preliminary project it seemed possible to produce case hardened steel with surface hardness over 1000 HV, but a slight reduction of core hardness was difficult to avoid.

The present master's thesis was written during the spring of 2011. The key results from the preliminary project work were used to determine a range of case hardening courses. A total of 11 case hardening courses were tested, of which six courses employed carbon

potential of 0.9% and five courses employed a carbon potential of 1.1%. Different hardening courses were tested, including direct hardening, a modified single hardening process and traditional and modified versions of double and triple hardening. Before the case hardening the plates were sandblasted to remove a corrosion-resistant primer that was applied to the plates. The primer was believed to limit the diffusion of carbon into the steel. In the preliminary project the primer was ground away and grinding was the preferred solution in this work as well, however, due to capacity issues sandblasting was employed.

The ballistic limit velocity of the case hardened and the original Hardox 450 target plates were calculated from results obtained by ballistic experiments. The ballistic limit velocities of the case hardened samples, with approximately 787 m/s as the highest, were lower than that of the original Hardox 450, being approximately 800 m/s.

Surface hardness measurements of the steel revealed a poor effect from the carburization, the hardest surface was measured at 735 HV. This could be explained by a probable surface decarburization of the original Hardox 450, which was discovered by microstructure examinations and hardness measurements. In contrary to in the preliminary project where this layer was ground away, the sandblasting did not remove the decarburized layer. Due to this, the case hardening did not have the desired effect on the steel surface, resulting in a too low surface hardness.

The core hardness proved difficult to retain, the highest core hardness value obtained was below 460 HV, compared to the original Hardox 450 with core hardness of 475 HV. This could be another reason for the lower ballistic limit velocity of the carburized steel plates. However, the original Hardox 450 did not have the highest cross-sectional hardness integral value, so the ballistic properties probably also depend to some degree on ductility. A main reason for the superior ballistic limit velocity of the original Hardox 450 was therefore believed to be related to cracking of the rear side of the case hardened target plates during projectile penetration. The cracking seemed to be a result of the harder, and thus more brittle, outer surface layer.

Table of Contents

1 Introduction 1

2 Theory 3

2.1 Protective materials 3

2.2 Impact dynamics 5

2.3 Case hardening 11

2.4 Previous work 20

3 Experimental 25

3.1 Base metal 25

3.2 Preliminary project work post-examinations 25

3.3 Case hardening 26

3.4 Ballistic experiments 30

3.5 Sample preparation, microscopy and hardness measurement 33

4 Results 35

4.1 Preliminary project work post-examinations 35

4.2 Ballistic experiments 39

4.3 Case hardening 47

5 Discussion 57

6 Conclusion 63

7 Acknowledgements 65

8 References 66

Appendix

1 Introduction

The need for protective materials is present all over the world for different purposes. Constructions exposed to collisions, explosions, bullet or fragment impacts, etc. require sturdy materials to keep personnel and equipment safe and secure. Oil installations, armoured vehicles and nuclear facilities are examples of such constructions. Small-arms and light weapons represent a major threat to human security in particular civilian situations and in military conflict zones. According to Small Arms Survey [1], firearms are used in 40 % of all homicides worldwide and an estimated 60 to 90 % of all direct conflict victims are killed with a firearm.

Even though there are a number of materials with properties that make them suitable for protection purposes, such as ceramics, polymers and aluminium among other metals, steel alloys are still the dominating material [2]. The reasons for this are the good overall properties of steels; high strength and hardness, high ductility, high formability and relatively low cost compared to other materials. High-quality armour steels are still expensive and work is done to limit the expenses attached to these steels or manufacture new and less expensive steel alloys with properties suitable for protection purposes.

Experiments performed by Lou et al. (2009) showed significantly increased penetration resistance of a low-cost steel (NVE36) after a case hardening process [10]. Based on this, Hans Magne Thorseth wrote his master's thesis "*Optimalisering av stål i beskyttelseskonstruksjoner*" in the spring of 2010 [11], where a hard, wear-resistant steel quality, Hardox 450, was case hardened to increase the hardness of the surface and thus increase the ballistic strength. However, the results of the experiments were not as desired, possibly due to a number of reasons. The carbon content of the steel surface was 0.6 % after the carburizing, which was significantly lower than the content aim of 0.9 %. This resulted in a lower surface hardness than expected. In addition, the hardness of the core material (not carburized) was lowered due to the heat treatment of the case hardening process.

The objective of this master's thesis is to improve the case hardening process used by Thorseth, and thus improve the ballistic strength of the Hardox 450 steel. The work was divided in two, a preliminary project work and the master's thesis. The project was carried out in the autumn semester of 2010, and the aim was to find the optimal case hardening process to produce steel with improved ballistic properties [19]. This involved testing of different carburizing potentials to increase the surface carbon content of the metal and to find

carburizing heat treatments that would retain the core properties of the carburized steel. The master's thesis is written in the spring semester of 2011. The key results from the preliminary project work will be used to determine a range of case hardening courses. Target plate samples will go through the case hardening courses before being exposed to ballistic experiments, i.e. the plates will be shot at. The main parameter used to determine ballistic strength is the ballistic limit velocity, which is calculated from the experiments. Afterwards the target plates will be examined to find their metallurgical properties.

As the master's thesis is a direct continuation of the preliminary project work, some parts of the project report is used in the master's thesis report. This includes most of this introduction and parts of the theory chapter.

2 Theory

This chapter consists of a short introduction to different materials used as protective applications, an introduction to impact dynamics and the theory behind the case hardening process. Some key conclusions from previous work are also mentioned.

2.1 Protective materials

Protective materials come in most material categories. Among metals the most used are steels. The main reasons for this are the good overall properties of steel, with high strength and hardness while retaining relatively high ductility and formability. The high strength enables the use of thin sheet dimensions and thereby reduces weight. Steel has excellent load carrying capability, i.e. it is not necessary with additional support for the construction itself. Steels are also less expensive than most other protective materials.

Another often used metal is aluminium. Extruded panels are used against collisions, impacts and explosions on oil platforms, bridge decks and train and ship components, in addition to military applications. In offshore environments massive steel or concrete constructions are not desirable due to their high weight, and therefore aluminium protection systems with its lower weight can be a good alternative. Reasons for this are the high specific strength, low density, high specific energy absorption capacity and high thermal conductivity of aluminium. High thermal conductivity gives a higher resistance against adiabatic shear bands (ASB), than for example steel. However, when comparing aluminium to steel there are some disadvantages, as steel has higher strength, Young's modulus, ductility and thermal melting point [3].

Ceramic materials are used as protective materials due to their very high hardness and compressive strength. Ceramics also have low density, which gives low specific weight compared to steel and composites. Ceramic materials are used in different armour configurations, with one being ceramic panels that are added to ballistic vests to increase protection against high-power armour-piercing weapons, mainly in the small-arms and heavy machine gun category. Commonly used ceramic materials include alumina (Al_2O_3), boron carbide (B_4C), silicon nitride (S_3N_4), silicon carbide (SiC) and titanium diboride (TiB_2). The

ballistic properties, price, availability, production technology and workability decide where the different ones are utilized. Alumina is the most economical and thus most commonly used ceramic material [4]. While ceramics are very hard, they are also very brittle and may easily crack as a consequence of the tension waves developed when subjected to impacts. Ceramic panels in ballistic vests also lower the comfort, mobility and flexibility of the user.

Polymers are used as protective material in civilian, police and military life. A lot of sports use protective gear made of polymer materials, e.g. helmets in bicycling, baseball and American football. Police and military forces also utilize armour suits made of rigid polymers in anti-riot situations. Light-weight and soft ballistic vests are commonly made of unidirectional or woven high tensile strength polymer fibers. The most common fibers of this use are ballistic nylon, para-amids (Kevlar® and Twaron ®), Ultra High Molecular Weight Polyethylenes (UHMWPE) (Dyneema® and Spectra®) and Polyphenylene-2,6-benzobisoxazole (PBO) (Zylon®) [5]. These materials can also be encapsulated in a resin matrix to produce a rigid composite often used in ballistic helmets. However, the light-weight vests cannot withstand high-power weapons, therefore ceramic or metal plates are added to the armour for additional protection, as mentioned before.

Most armour systems are actually composites, i.e. they consist of multiple different protective materials or material types, such as metals, polymers and ceramics. The aim is a composite system with a hard outer layer of a metal or ceramic that is supposed to deform the projectile and reduce kinetic energy. Behind the hard layer is a softer layer that is supposed to absorb the rest of the energy along with possible fragments. Soft metals such as aluminium, or fibrous polymers are often used for this purpose. Larger structural armor panels can also be composites to reduce weight while maintaining penetration resistance [6]. Bullet- or blast-proof windows are composites. A typical bullet-proof window can be made of a hard glass outer layer with a inner layer of a tough and ductile polymer, with an adhesive in between. For further protection additional layers of glass and polymer can be added [7].

2.2 Impact dynamics

2.2.1 Projectile impact dynamics – an introduction

To be able to understand impact dynamics it is necessary to define certain words, phrases and parameters.

Impact is defined as the collision between two or more solids, where the interaction between the bodies can be elastic, plastic or fluid, or any combination of these [15]. Ballistics is defined as the accelerating of objects by use of an engine, and deals with the motion, forces and impact of projectiles [15]. Ballistics is usually divided into three sub-categories. The first, interior ballistics, is the study of the motion and forces acting on an object while still in the launcher. The second, exterior ballistics, is the study of the motion and forces acting on an object during free flight, while the third, terminal ballistics, describes the interaction between the object and the target during impact [15]. Of the three, the terminal ballistics is of greatest interest in this study. Penetration is defined as the entry of the projectile into any region of a target. During impact the projectile may penetrate the target in several ways, and some definitions include perforation, where the projectile passes through the target with a final residual velocity, embedment, where the target is stopped during contact with the target, and ricochet or rebound, where the projectile is deflected from the target without being stopped [17].

The ballistic limit velocity of a material is the average of two velocities, where the first is the highest velocity only giving partial penetration (no perforation), and the second is the lowest velocity giving complete perforation [15]. In addition to the ballistic limit velocity, the ballistic limit curve (or residual velocity curve) is an important measure in structural impact. The curve gives the residual velocity of the projectile as a function of initial projectile velocity [15]. An illustration of the ballistic limit velocity and curve is shown in Figure 1. Also illustrated in the figure, is the ballistic limit line (or residual velocity line) i.e. the ballistic limit curve for a target of zero thickness. The calculation of the ballistic limit velocity is given in chapter 2.3.2.

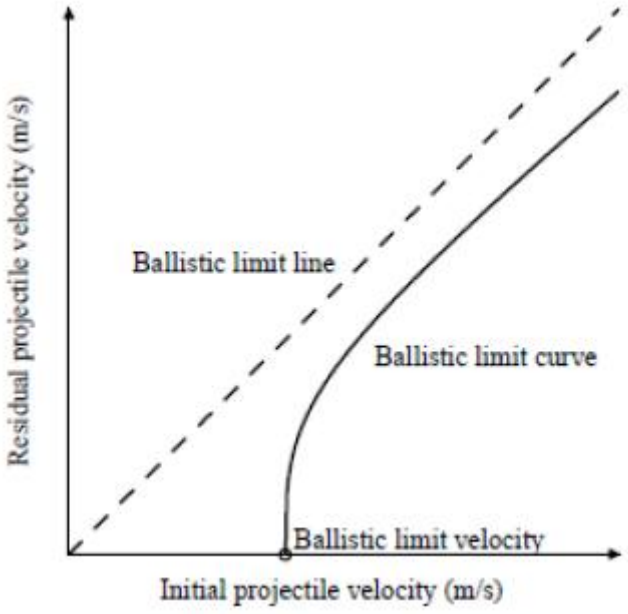

Figure 1. Ballistic limit curve with ballistic limit line [15].

The term projectile is used for any item that can be launched, but usually refers to objects for general ballistic performance that serves specific ballistic functions (bullets, bombs artillery shells, etc.), in contrast to e.g. missiles, which are usually self-propelled and can be guided during flight, or fragments, which are pieces separated from a body by breaking [16]. Projectile hardness is an important parameter during impact. Projectiles can be defined as soft, semi-hard or hard depending on the material used, the degree of nose deformation and the coupling between target deformation and impact loading [15]. Hard projectiles are used in this study as most military-applied projectiles, designed to perforate a target, are in this category. Hard projectiles can be recognized by a low and often negligible plastic deformation of the projectile during penetration, while the target can suffer from significant plastic deformations and local breakage [15]. The shape of the projectile is another important parameter. Figure 2 shows an illustration of flat, conical, truncated cone, hemispherical, and ogival ended projectile noses. The projectile nose affects the characteristics of the fracture during penetration.

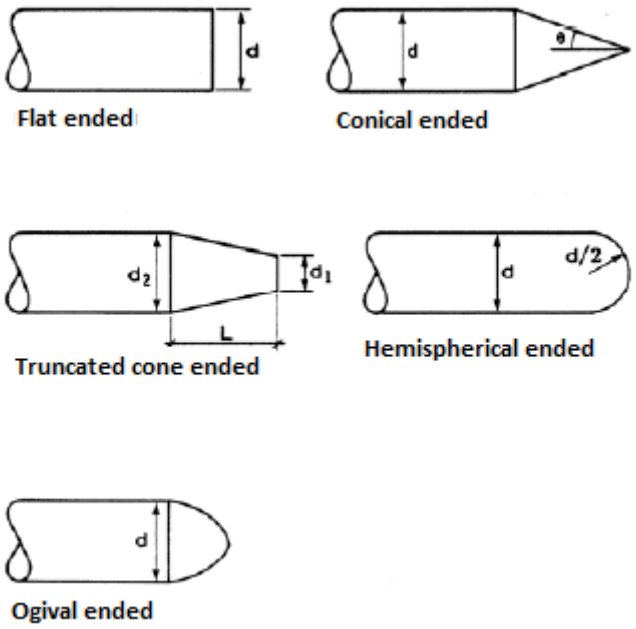

Figure 2. Illustration of different projectile nose shapes. Displayed here is flat ended, conical ended, truncated cone ended, hemispherical ended and ogival ended [11] [15].

The target is defined as any moving or stationary object struck by the projectile and identified by structural and functional unity [15]. Targets can be classified by thickness. A target is defined as: Thin, if stress and deformation gradients throughout its thickness may be neglected, intermediate, if the rear surface exerts considerable influence on the deformation process during all (or nearly all) of the penetration motion, thick, if the rear surface experience the penetration process only after substantial projectile travel into the target, or infinite, if the rear surface experience no effects from the penetration process [17]. The fracture mechanisms change with varying target thickness. Tests show a slight increase of local work with increasing target thickness at first. At a critical thickness the rate of local plastic work will increase. Global plastic work is of largest concern where the target thickness is significantly less than the projectile diameter. The plastic work of the projectile can be neglected at low velocities and thin targets. The elastic work of all target thicknesses is insignificant [11] [15].

A number of parameters will influence the impact dynamics. Projectile diameter, nose shape and hardness, and target thickness and hardness are important factors. The angle of incidence or projectile trajectory is important as well [15]. However, the projectile velocity is the dominant factor and may override most other considerations [15] [17]. The initial velocities in this study will all be inside the "Ordnance velocity regime" (500-1300 m/s), where most of

the kinetic energy is converted into plastic work both in the projectile and the target, without any significant material erosion. The material strength is an important parameter, but material density is getting gradually more important with increasing velocity. The activated part of the target is very small, typically 2-3 projectile diameters from the impact zone, and hardly any global deformation of the target is seen [15].

Target response on impact is commonly divided into non-failure and failure modes. Non-failure modes include elastic deformation with no damage, plastic deformation that only gives local bulging and global dishing, and cratering for very thick targets [15]. The many different failure modes are of interest in this study. The actual mechanisms depend on variables such as material properties, impact velocity, projectile nose shape and trajectory, target support and relative dimensions of projectile and target. Although one of these may dominate the failure process, several mechanisms usually interact [15]. Some of the most common failure modes for thin and intermediate thickness targets are shown in Figure 3.

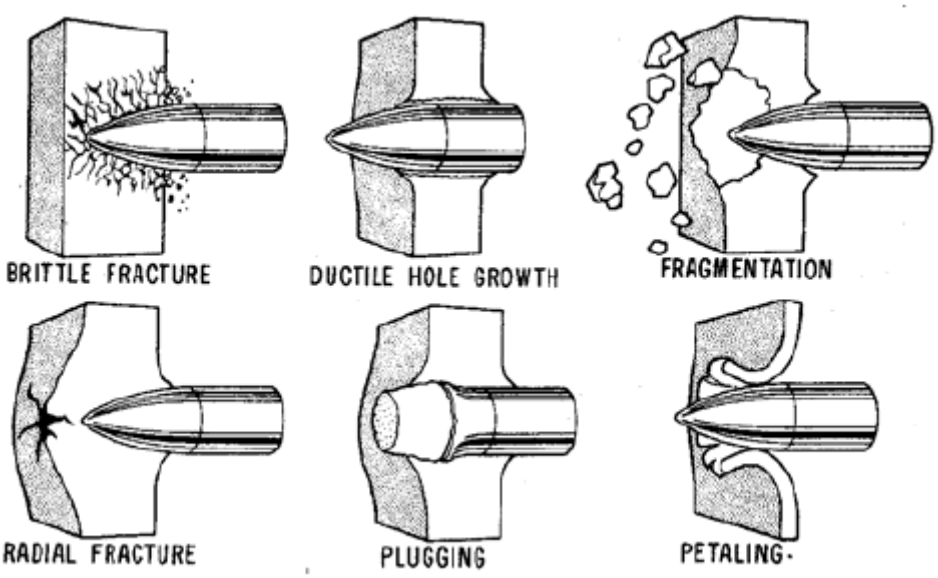

Figure 3. Illustration of common failure modes for thin and intermediate thickness targets [18].

Brittle fracture may occur when the fracture is a result of local inhomogeneities and anisotropy. Brittle fracture is common for brittle materials with low tension and high compression capacities, and can result from explosions [11 15]. Ductile hole growth usually happens in ductile materials where projectiles with conical or ogival nose shape have been employed. Perforation is the result of hole expansion due to the high radial pressure from the projectile. The result is an increase in thickness in the zone near the hole [11 15]. Fragmentation

is typical for brittle materials and high velocities. The material in front of the projectile fractures and the results are fragmentation of the target plate [11 15]. Radial fracture is typical for brittle materials as well. This fracture mode is recognized by the wave of tension resulting from radial motion of particles, and fracture will occur when the target plate tension capacity is lower than the applied tension [11 15]. Plugging is usually the result of flat ended projectiles, where the projectile presses out a plug from the target plate with approximately the same diameter as the projectile. A shear zone arises around the zone of penetration, and the fracture is initiated here. Depending on the mechanisms the plug can be cylindrical, conical or invert conical. The tendency of plugging increases with increasing target plate strength [11 15]. Petaling occur on thin target plates when either low velocity conical or ogival nose shaped projectiles, or high velocity (near the ballistic limit velocity) flat projectiles are employed [11 15].

2.2.2 Numerical calculation of the ballistic limit velocity

The ballistic limit velocity, V_{BL}, is defined as the average of the lowest projectile velocity that gives perforation, and the highest velocity that do not give perforation.
The initial projectile velocity, V_I, and the residual projectile velocity (if any), V_R, are measured during experiments. The experimental data points can be fitted to a model proposed by Lambert in order to calculate residual projectile velocity (V_R) as a function of the measured initial projectile velocity (V_I) and the experimental obtained ballistic limit velocity (V_{BL}), as seen in Equation 1 [15]:

$$V_R = a(V_I^p - V_{BL}^p)^{\frac{1}{p}} \quad (1)$$

The parameters a, p and V_{BL} can be defined as empirical material constants. Recht and Ipson proposed a model where a is defined as in Equation Y, where m_P is the projectile mass and m_{PL} is the total mass of the projectile hole fragments. The constants a and p are often set to be 1 and 2, respectively, which is valid if the plastic deformation of the projectile and the mass of fragments during perforation is negligible [15].

$$a = \frac{m_P}{m_P + m_{PL}} \tag{2}$$

2.2.3 Adiabatic shear bands

Shear bands are the result of high strain rates, and may emerge during machining, forging, ballistic penetration and fragmentation. When the creation of shear bands is related to rapid local heating they are called adiabatic shear bands (ASB) [11]. During plastic deformation large parts of the work introduced is transformed to heat. If the strain rate is sufficiently high, the heat will not be able to diffuse away from the deformation zone, with softening of the zone as a result. The plastic deformation will lose stability if the loss in strength from softening is larger than the increase in strength from strain hardening, and if this is the case, ASB will be the result [11]. ASB is most easily formed in materials with low density, such as titanium and aluminium, but can also be found in steel [11]. ASB is identified as martensite in steel. This implies that the temperature has climbed above the A_3 temperature of the steel, and caused complete austenitizing. The temperature can reach 1000 °C locally. Afterwards, the austenite is quenched from the cooler surroundings and transformed to martensite. Shear bands in steel typically appear as thin white bands after etching in nital. ASB often have a thickness between 10 and 100 μm while the length may reach several millimeters [11]. ASB are very brittle compared to the matrix and will be a potential passage for brittle fractures, and thus they act as weak zones in the material [11]. This is in particular for constructions that are exposed to cyclic impact loads, such as protective constructions. Brittle fractures are most common in phase transformed ASB. Fracture occur after the formation and cooling of the ASB, and may propagate longitudinally or perpendicular to the shear band, depending on the local strain conditions [11]. The critical strain for ASB formation is varying with hardness, and decrease with increasing initial hardness of the material [11].

2.3 Case hardening

Case hardening is a technique for producing steel with a very hard and durable surface while still maintaining a tough and ductile core. Steel with a base content of 0.10-0.25 weight-percent carbon is normally used. The metal surface is carburized, i.e. the carbon concentration in the metal surface is increased through a diffusion controlled process, and with succeeding heat treatment and quenching the surface will be significantly harder than the metal core. A carbon concentration of approximately 0.9 % is typical for the surface, and this concentration decrease rapidly towards the metal core, where the carbon concentration is at the base content. After hardening the result is a hard, durable and fatigue resistant surface and a tough and durable core. Case hardening is typically applied to machine parts that are exposed to heavy wear and high loads such as gears, bearings, screws and nuts, shafts, etc [8 9].

2.3.1 Carburizing

Carburizing is performed in a carbon-enriched environment at temperatures from 790 to 1190 °C, although most common from 850 °C to 950 °C. At these temperatures the steel is in the austenitic phase and is able to absorb a lot of carbon, which diffuse into the material. The material is generally held for 2-10 hours. To avoid grain growth aluminium-killed steel is often used. There are several available carbon-enriched environments used for carburizing, such as gas carburizing and vacuum carburizing (gas atmosphere), molten salt (liquid carburization), pack carburizing and paste carburizing (solid atmosphere) [8 9]. The carbon concentration of the atmosphere is called the carbon potential.

The atmosphere is regulated so that the metal surface obtains a concentration of usually 0.85-0.95% carbon. Higher carbon concentration will most likely result in retained (residual) austenite due to a lowered M_f-temperature. This retained austenite is very soft and thus unwanted. At the high temperatures of 850-950 °C carbon will rapidly diffuse into the steel, and Figure 4. shows different carbon profiles for different carburizing holding times.

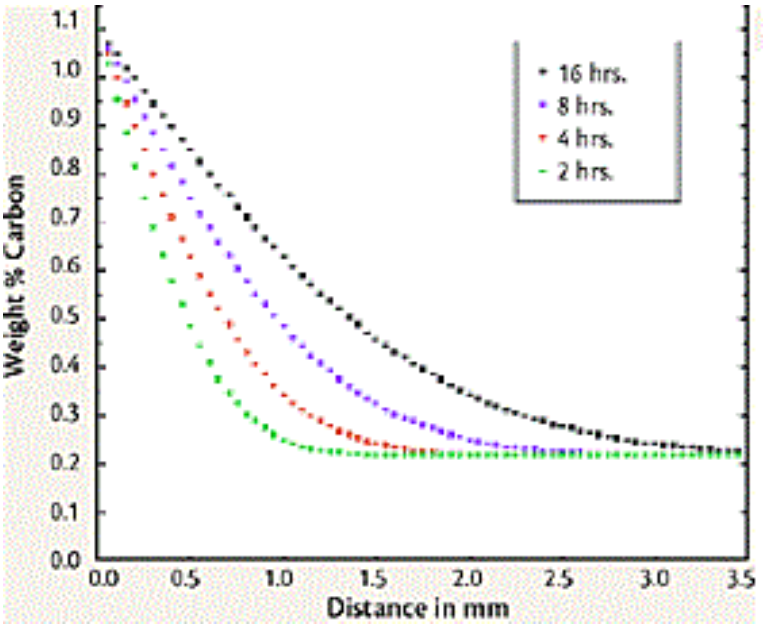

Figure 4. Carbon profiles of different carburization holding times at a carburizing potential of approximately 1.1 %.

2.3.2 Gas carburizing

Gas carburizing is the most dominant method used today, and was the carburizing method utilized in this project. In general, gas atmosphere is more effective than solid or liquid environment for carburizing, with deeper and higher carbon content cases obtained more rapidly. Thus, gas carburizing is more economical and more adaptable for mass production than the other carburizing processes [8].

The most common source of carbon for gas carburizing is natural gas, either as methane or propane. Propane is too rich to use directly, so that small volumes (5 to 20 %) are mixed with a carrier gas, usually an endothermic gas. The main components of the gas in the atmosphere are CO, N_2, H_2, CO_2, H_2O and CH_4. The nitrogen is inert and acts as a diluent. The mass ratio CO/CO_2 and H_2/H_2O is important for the carbon potential, and is determined by the reversible reaction [8 11]:

$$CO + H_2O \leftrightarrow CO_2 + H_2 \qquad (3)$$

The reactions involved in the carburizing are not known in detail, but the following reversible reactions for adsorption and desorption of carbon in steel is known [8 11]:

$$2CO \leftrightarrow C_{\gamma\text{-}Fe} + CO_2 \quad (4)$$

$$CO + H_2 \leftrightarrow C_{\gamma\text{-}Fe} + H_2O \quad (5)$$

$C_{\gamma\text{-}Fe}$ is adsorbed carbon in austenite. As seen, the decomposition of CO is the reactions that give the carburizing. Methane and propane is the main sources for carbon through the reactions [8 11]:

$$CH_4 + CO_2 \leftrightarrow 2CO + 2H_2 \quad (6)$$

$$CH_4 + H_2O \leftrightarrow CO + 3H_2 \quad (7)$$

The reactions (6) and (7) will generate CO and H_2. The sum of the reactions (4), (5), (6) and (7) is [8 11]:

$$CH_4 \leftrightarrow C_{\gamma\text{-}Fe} + 2H_2 \quad (8)$$

The components of the atmosphere are not in equilibrium with each other, and the atmosphere is not in equilibrium with the steel surface that is carburized. Based on the composition of the gas, the carburizing rate can be calculated if the carburizing potential, temperature and time are constant. When the equilibrium composition of the gas is known, the carbon potential can be determined by the equilibrium expression of reaction (4) [8 11]:

$$K_2 = \frac{a_C P_{CO_2}}{P_{CO}^2} \quad (9)$$

P_{CO} and P_{CO2} are the partial pressures of CO and CO_2, respectively, a_C is the carbon activity and K_2 is the equilibrium constant of reaction (4). K_2 can be calculated from Gibbs free energy for the formation of CO and CO_2 at the relevant temperature [8 11]:

$$\Delta G^0_{CO_2} - 2\Delta G^0_{CO} = -RT \ln K_2 \quad (10)$$

$\Delta G^0_{CO_2}$ and ΔG^0_{CO} are the Gibbs free energy of CO and CO_2, respectively, R is the gas constant and T is the temperature in Kelvin. Equation (11) is relating the carbon activity (a_C) to the carbon content in austenite (w) [8 11]:

$$\log a_C = \frac{2300}{T} - 0.920 + \frac{17950w}{T(100-w)} + \log\left(\frac{4.65w}{100-5.65w}\right) \tag{11}$$

Here, w is given as % carbon in austenite, equal to the carbon potential. The equation cannot be solved directly, one has to try and fail to get a satisfying solution.

2.3.3 Carburizing depth

Carburizing depth is defined as the depth, x, under the surface where the carbon content has the mean value of the carbon content of the surface and the core, which remains uncarburized. The carburizing depth is dependent on different parameters that will be explained below.

The carbon concentration gradient that emerges during carburizing is dependent on carbon potential, temperature, time and chemical composition of the steel. The carbon potential can be altered by regulation of the CO/CO_2 ratio of the carburizing atmosphere. At the same time, the carbon content in the steel is limited by the solubility of carbon in austenite, which can be seen as the A_{cm} curve in the Fe-C phase diagram, a section of this phase diagram can be seen in Figure 5a). In carburizing the carbon content rarely exceeds 1.3 wt% carbon. The carbon potential is usually regulated to be around 0.85-0.95 wt%, and the temperature is around 850 °C to 950 °C. In cases where large carburizing depths is required the temperature is generally higher. For thin or narrow carburized layers the temperature is kept low, because the depth is more easily controlled with lower diffusion rates. The rate of carburization increases rapidly with increasing temperature, an increase from 815 °C to 925 °C will double the rate. The rate of carburization is proportional to the square root of time, i.e. the depth increases most in the start of the carburization. Figure 5b) shows how the carburization depth changes as a function of time for different carbon potentials (C_P) and temperatures [11].

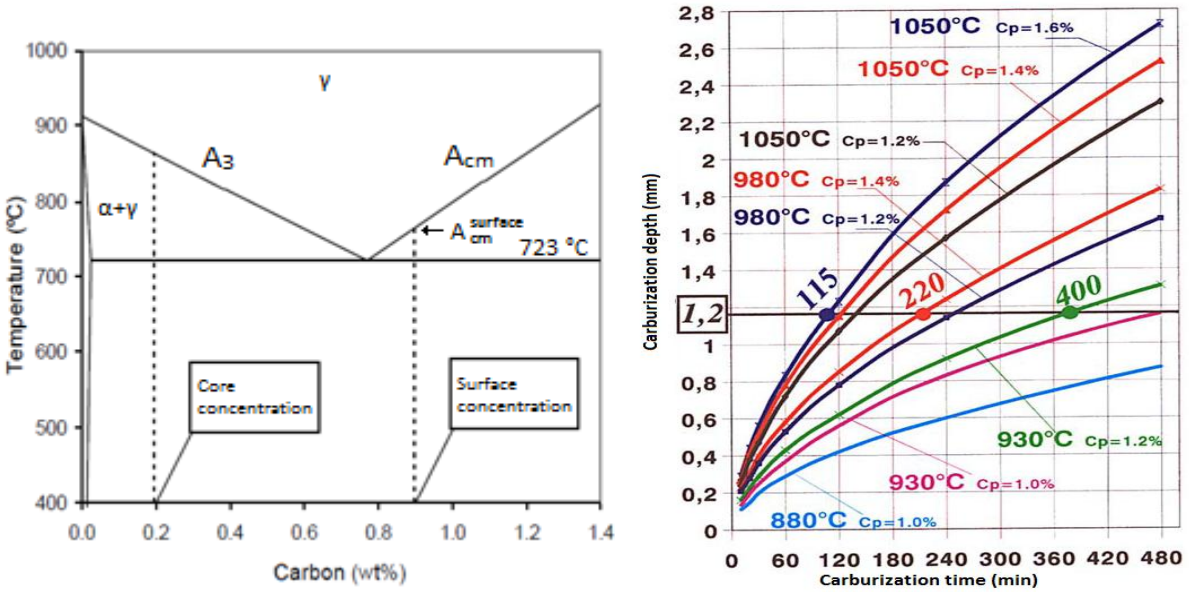

Figure 5. Left: a) Section of the Fe-rich Fe-C phase diagram [11]. Right: b) Carburization depth as function of time for different temperatures and carbon potentials [11].

Fick's second law can be applied to describe the carbon concentration from the surface and in towards the core of the material. The solution is shown in the equation (12). The error function is shown in equation (13).

$$C(x,t) = C_0 + (C_S - C_0)\left\{1 - erf\left(\frac{x}{2\sqrt{Dt}}\right)\right\} \tag{12}$$

$$erf\left(\frac{x}{2\sqrt{Dt}}\right) = \frac{2}{\sqrt{\pi}} \int_0^{\frac{x}{2\sqrt{Dt}}} e^{-y^2} dy \tag{13}$$

$C(x,t)$ is the carbon content as a function of the distance from the surface, x, and a given time, t. C_S is defined as the carbon content at the surface, C_S will in practice be equal to the carbon potential C_P. C_0 is the original carbon content of the steel before carburization. D is the diffusion constant of carbon in austenite, and is defined by:

$$D = D_0 \exp\left(-\frac{Q}{RT}\right) \tag{14}$$

Here D_0 is the diffusivity coefficient and Q is the activation energy of carbon in austenite. With input values for the constants D_0 and Q that is valid for temperatures between 900 °C and 1050 °C, gives D as [11]:

$$D = 0.15 \exp\left(-\frac{135000}{RT}\right) \quad \left[\frac{cm^2}{s}\right] \tag{15}$$

By using equation (12) together with pre-calculated values of the error function, the carburization depth for all temperatures, X, can be calculated:

$$X \approx 0.95\sqrt{Dt} \tag{16}$$

2.3.4 Heat treatment

While the carburization gives a hardening effect due to increased carbon content, the heat treatment of the case hardening process also provides hardening effects, e.g. through quenching. Case hardening is used when the aim is a hard, wear resistant surface layer and a tough, brittle fracture resistant core. Correct heat treatment is essential to achieve desired hardness of the surface, but also to conserve the core properties.

As the carbon content through the carburized layer will vary, the microstructure will vary as well. Changes in microstructure are depending on the local content of carbon and heat treatment after the carburization. From the surface and in towards the core there is a gradual change from a high-carbon to a low-carbon microstructure. For some steels this is simply a change from high-carbon to low-carbon martensite. In other cases there can be a change from perlite with proeuteutectoid cementite to a ferrite structure [8 11].

With increased carbon contents at and near the surface there is an increased possibility of carbide precipitation and the formation of retained austenite after quenching. Composition, austenitic temperature and cooling rate are factors that will determine the maximum carbon content in the surface that is able to keep the amount of precipitates and retained austenite at a satisfactory level [8 11]. Retained austenite in the carburized layer is undesirable, due to the reduction of hardness it causes. A retained austenite amount up to 30 % is generally accepted.

Increasing carbon content of steel will lower the M_s and M_f temperatures, and thus increase the amount of retained austenite (Figure 6). Ordinary carbon steel can take carbon contents of up to 1.1 wt% without deteriorating the mechanical properties significantly.

Alloying elements in steel will cause the optimum carbon content to decrease. Sufficient hardenability is necessary to obtain desired properties of the carburized layer. Maximum hardenability is reached near the eutectoid composition (approximately 0.8 wt% carbon). Carbon contents higher than this composition may reduce the hardness, if the alloying elements added to increase hardenability leads to formation of carbides. However, these carbides may also have a positive effect on the hardness if they are small, spherical and evenly distributed in the metal, and therefore produce a precipitation hardening effect in the metal [8].

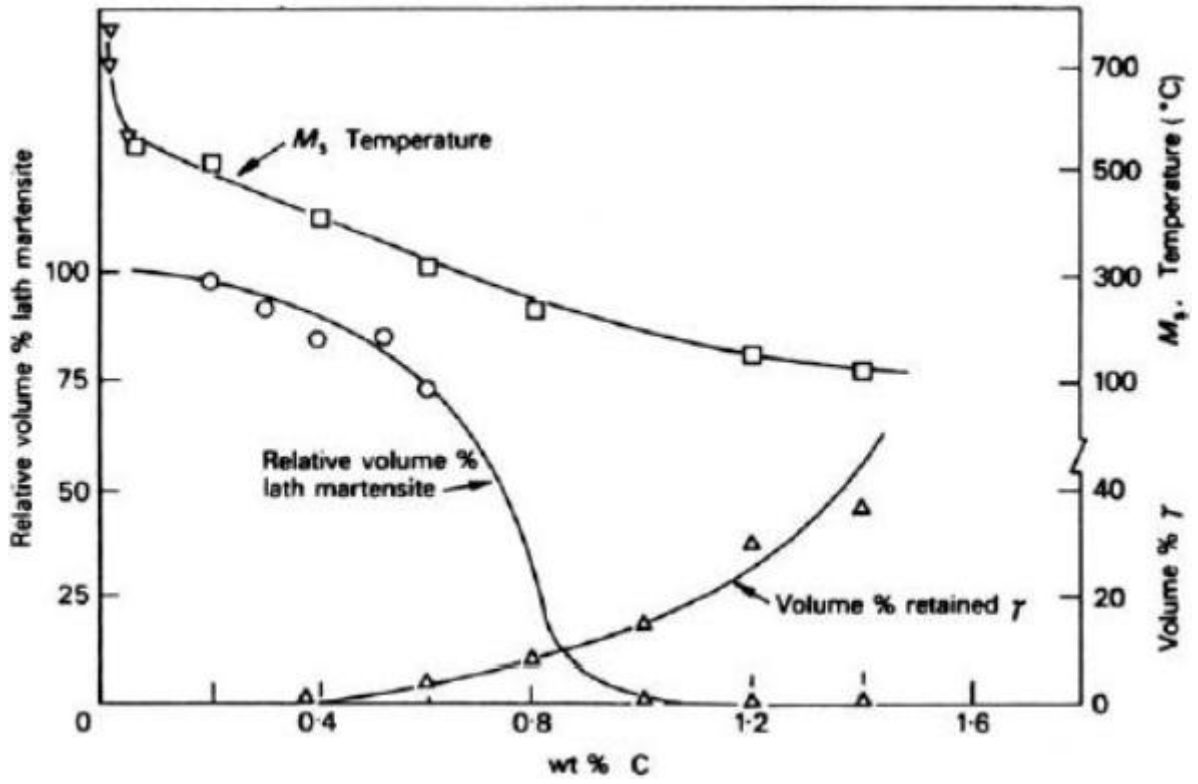

Figure 6. Effect of carbon on martensite structure, M_s temperature and retained austenite [11].

There are a number of different heat treatments applied in case hardening. The most common method is called direct hardening. After being carburized, the components are quenched, to obtain a martensitic or bainitic microstructure in the surface layer. This is the simplest way to harden and is widely used due to the efficiency and thus, low cost of the method. As shown in Figure 7a), the material is carburized at a temperature just above A_3

before quenching. The holding time above A_3 is normally between 2 and 10 hours. To limit the amount of retained austenite, the holding temperature can be lowered to between the A_3 and A_{cm} temperatures for some time before quenching (Figure 7b). This will lower the carbon content of the surface in accordance with the A_{cm} curve in the phase diagram. The excess carbon will diffuse into the metal [9].

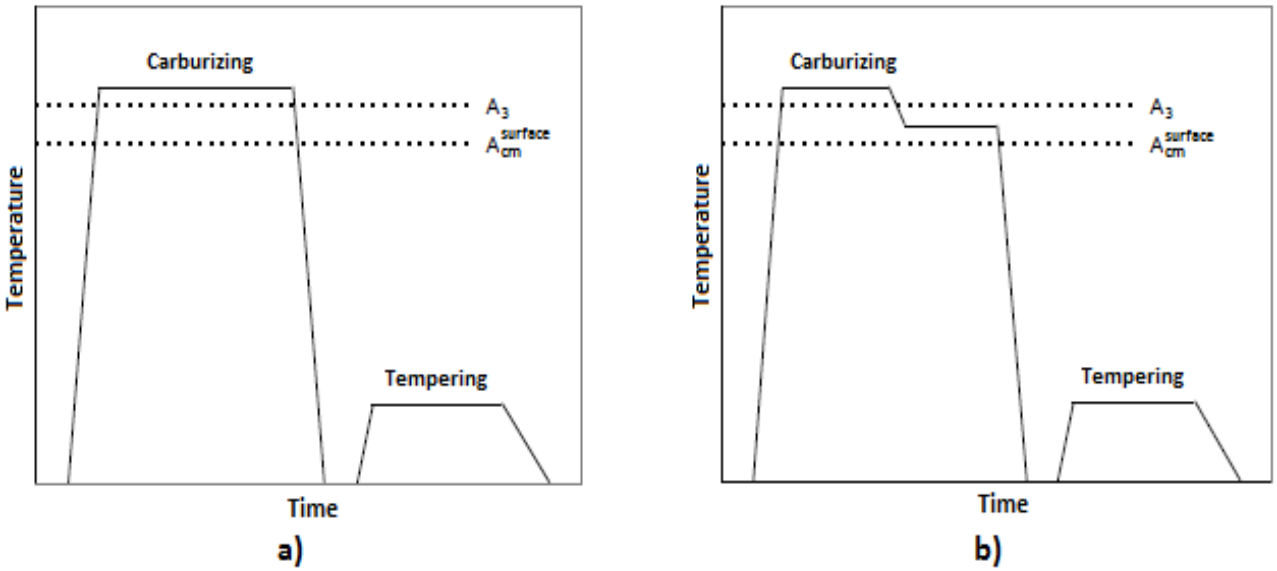

Figure 7. Two different variants of direct hardening [9].

Single hardening is another method used in case hardening. The metal is not quenched from above the A_3 temperature, but cooled slowly in air. The low cooling rate will give a microstructure consisting of perlite near the surface and ferrite/perlite in the core. After the cooling, the metal is reheated to a temperature under A_3, but over the surface A_{cm} temperature for some time, and then quenched, as seen in Figure 8. The quenching will allow the formation of martensite in the surface. In addition, the metal surface achieves a grain refinement during austenite-martensite transformation. This extra hardening step can be necessary to control shape and distribution of carbides in the carburized layer. Grain boundary cementite will dissolve as well [9].

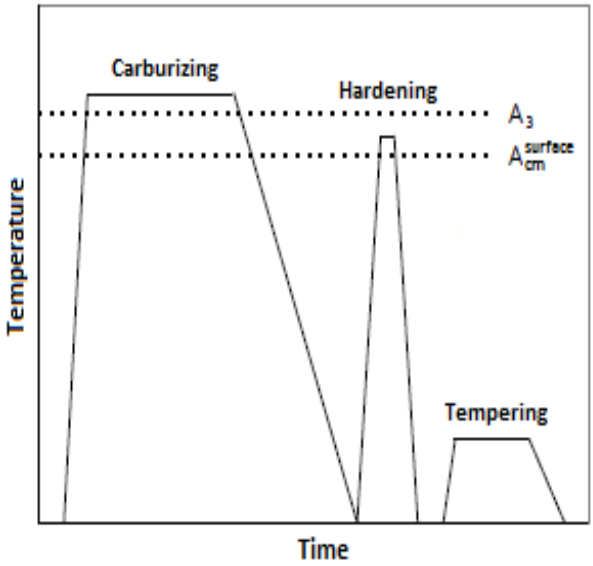

Figure 8. Sketch of the heat treatment of the single hardening method [9].

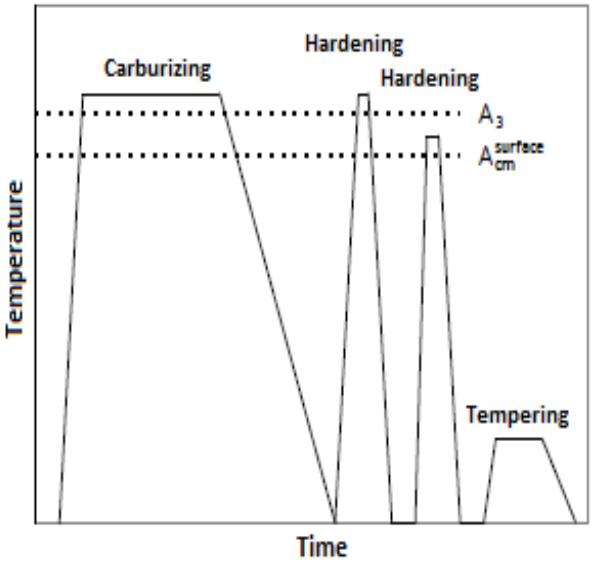

Figure 9. Sketch of the heat treatment of the double hardening method [9].

Double hardening can provide a strong core as well as a hard surface. The heat treatment is shown in Figure 9. The steel is cooled at a low rate, as with single hardening. The difference is the first hardening step, where the metal is heated to over the A_3 temperature. After the holding time, the steel is quenched. This will give grain refining and hardening effects through the whole metal. The last hardening step is similar to the last step in single hardening. When quenching, the surface will harden. The newly grain refined core will undergo a strong tempering during the last step. Double hardening often requires alloying elements to obtain hardening of the core [9].

After carburization and further heat treatment the metal is tempered. The temper temperatures are normally between 150 °C and 250 °C, and are the same for direct, single and double hardening methods. Carburizing typically gives a carbon content of 0.9 wt% at the surface and the content is reduced inwards until the original core content is obtained. In areas with carbon contents of over approximately 0.20 wt%, ε-carbides will precipitate. In areas with lower carbon content the carbon will merge in zones. Increasing tempering temperatures generally give decreasing hardness, but tempering in the low temperature areas will not have a significant effect on the hardness. Tempering temperatures below 150 °C have been observed to give an increase in hardness, due to precipitation hardening of the martensite by ε-carbides. Retained austenite can be transformed to bainite at temper temperatures over 200 °C [9 11].

2.4 Previous work

2.4.1. Application of the case hardening process to increase penetration resistance in steel plates

Lou et al. [10] examined the ballistic limit of a ferrite/perlite steel (NVE36), which was case hardened using pack carburizing. A new heat-treatment process using a self-protective diffusion paste was introduced. Advantages of this process is the self-protectiveness of the paste, easy handling, quick production time, suitability for partial treatment of the steel surface and the treatment can be carried out in a wide variety of furnaces. The NVE36 steel was carburized at 950 °C for 6 hours and thereafter tempered at 245 °C for 2 hours. This resulted in an increase of the ballistic limit of the NVE36 steel (yield stress of 355 MPa). The ballistic limit increased to a value slightly higher than for a Hardox 400 wear resistance steel (yield stress of approximately 1200 MPa). The ammunition used in the experiments to calculate the ballistic limit was 7.62 mm APM2 (armour-piercing).

Based on the results of Lou et al., Hans Magne Thorseth wrote his master's thesis "Optimalisering av stål i beskyttelseskonstruksjoner" in the spring of 2010 [11]. The thesis aimed at increasing the ballistic limit of Hardox 450 wear resistant steel by case hardening. After several experiments to optimize the heating process, the steel was carburized at 910 °C for 6 hours, quenched in oil and tempered at 245 °C for 2 hours. The ballistic limit of the original Hardox 450 quality and the case hardened quality was calculated on the basis of shooting experiments with 7.62 mm APM2 ammunition. The ballistic limit of the original steel was approximately 800 m/s, while the case hardened steel showed a slight reduction with a ballistic limit of approximately 770 m/s. The reason for the reduction of the ballistic limit was concluded to be related to the carburized layer of the metal. The carbon concentration of the surface was approximately 0.6%, significantly lower than the desired carbon concentration of 0.9%. Consequently, the hardness of the metal surface was lower than expected, and the average hardness over the cross-section of the plate was reduced because of the simultaneous hardness reduction of the core from the heat-treatment.

There are also at least two patents on this topic. One patent from 1925, "Process of manufacture of armour plate", belongs to Johnson and Daniels [12]. Another patent from 1989, "Case-hardened plate armour steel and method of making", is written by Karst et al. [13].

2.4.2 Preliminary project work

In an attempt to improve the results obtained by Thorseth, a project work was carried out in the autumn of 2010 by the present author, where the objectives was to modify or improve the case hardening process used by Thorseth, i.e. obtain a higher content of carbon in the surface layer and, desirably, retain or improve the core properties. The modification involved testing different carburizing potentials and testing of different heat treatments, among other slight adjustments [19]. The heat treatment experiments, carried out at NTNU in Trondheim, were performed to see how the sample core would act when exposed to different heat treatments. Six different heat treatments, including modified versions of single and double hardening and a triple hardening process, were tested, before the sample cores were subjected to hardness measurements and examined in light microscopy [19]. The carburizing, carried out by Raufoss Industrial Tools AS in Raufoss, was performed to see how the metal surface would absorb carbon from different carbon potentials and surface conditions [19]. The hardness values of the case hardened steel surface were measured, as increasing carbon content will give increasing hardness values. The main results from the experiments are presented in Figure 10 and Figure 11 [19].

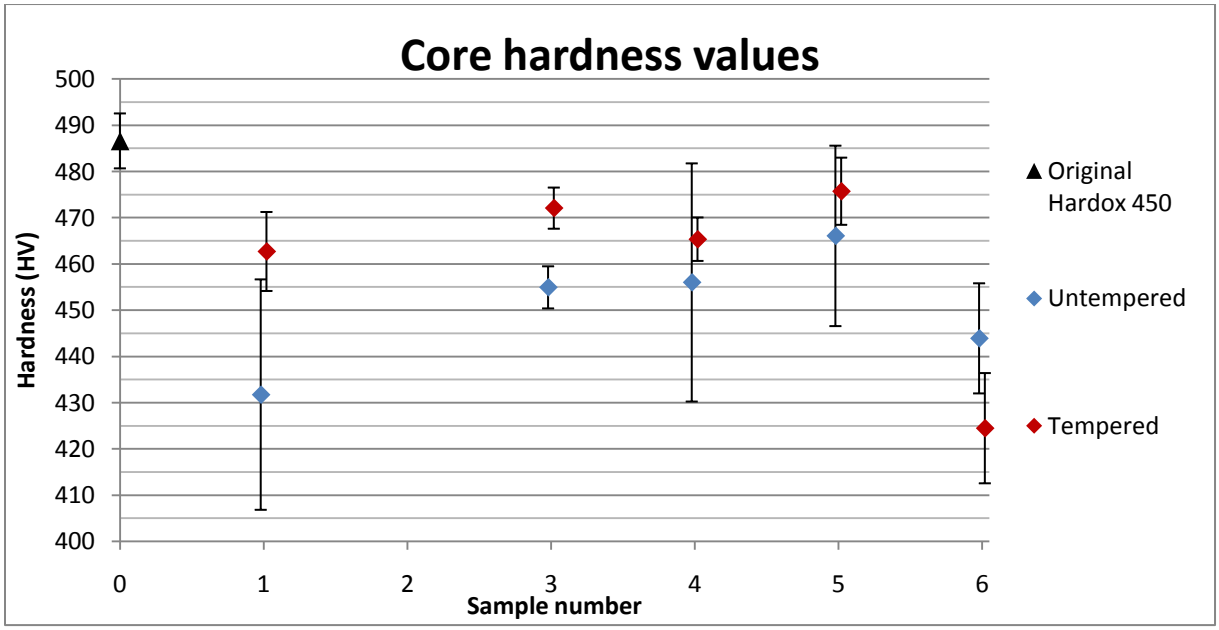

Figure 10. Core hardness values of the heat treated samples and the original Hardox 450 (sample number 0) with standard deviations. Each value is an average of 6 measurements. Sample 2 had a hardness value under 400 HV [19].

The results from Figure 10 shows that the core hardness was difficult to retain even through heat treatments specifically designed for that purpose. Heat treatment number 5, a modified double hardening case hardening process, produced the least softened steel with hardness of approximately 476 HV, compared to the untreated reference sample with hardness of approximately 486 HV. The tempering seemed to give an increase in hardness in most cases. This was not expected, as the hardness is usually decreased after tempering.

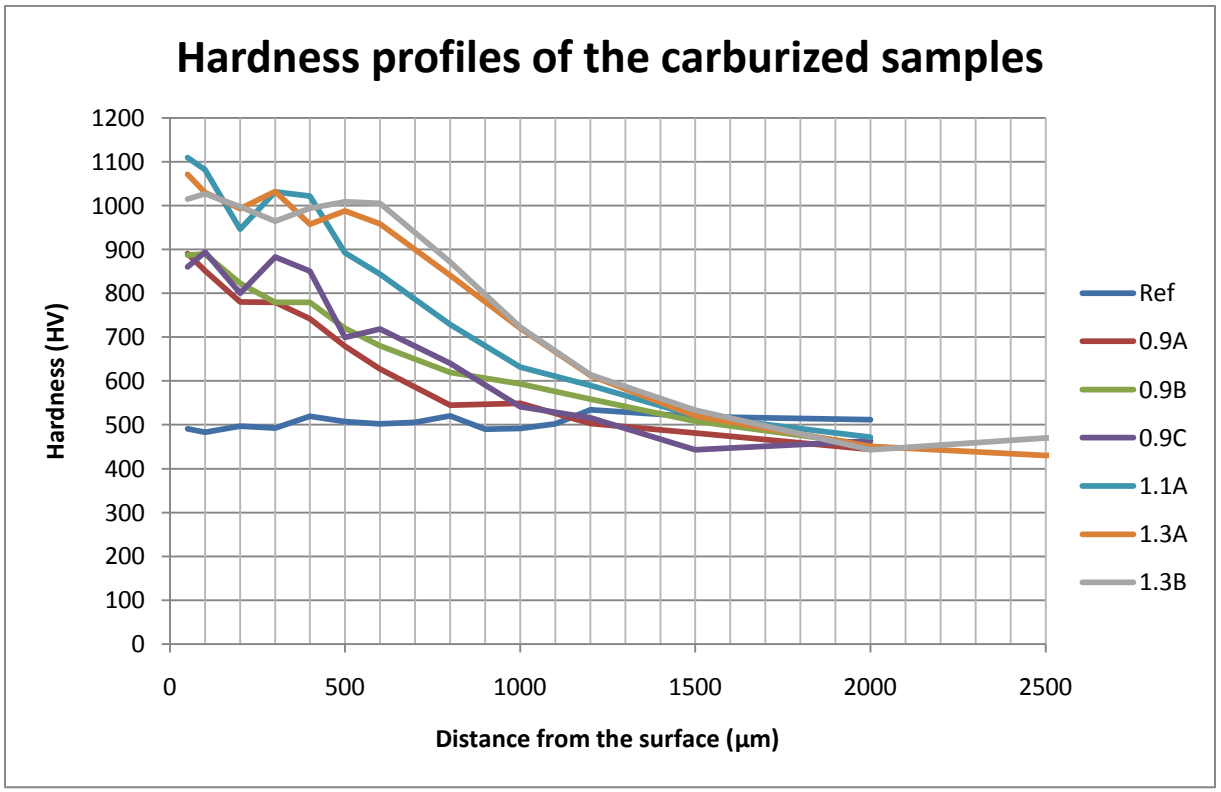

Figure 11. Hardness profiles of the carburized samples. The samples 0.9A, 0.9B and 0.9C were carburized at a carbon potential of 0.9%, sample 1.1A at a carbon potential of 1.1%, and samples 1.3A and 1.3B at a carbon potential of 1.3%. The hardness was measured from the sample surface and in towards the sample core. Each value is an average of three measurements [19].

The carburization gave an obvious hardness increase in all samples. As expected, sample 1.1A had higher hardness than samples 0.9A, 0.9B and 0.9C. Samples 1.3A and 1.3B, however, suffered from a drop in the hardness increase rate close to the surface, probably due to the high carbon content that caused high amounts of the soft retained austenite.

From microscopic examinations it seemed that sample 6 (triple hardening) had the finest microstructure, ahead of sample 4 (traditional double hardening), although this was not confirmed by grain size measurements [19].

An increase in carbon content in the carburized surface layer was merely indicated with the hardness measurements. Experiments performed with Electron Probe Micro Analyzer (EPMA) to verify an increase in carbon concentration, gave very limited increase in carbon content in the supposed carburized area. This was more likely to be because of problems during testing, than the lack of carbon increase, however, this should be investigated further [19].

Some of the heat treatments looked interesting for further investigation and experiments. The modified double hardening method produced the hardest core metal (sample 5) [19]. The triple hardening method produced, seemingly, the finest microstructure and might therefore give the most tough and ductile metal, as indicated by the relatively low hardness (sample 6) [19]. However, the traditional double hardening method produced, seemingly, the second finest microstructure and the second hardest steel and could be a good alternative (sample 4) [19].

The carburization experiments showed that it was possible to get metal with hardness values up to 1100 HV at the surface. This was positive; as the intention was to crush the projectile upon impact with the hard surface metal, while the core metal took up the rest energy and possible fragments [19].

3 Experimental

3.1 Base metal

The metal used in the experiments was Hardox 450. The metal was produced and delivered by Swedish Steel AB (SSAB). Hardox is described by SSAB as "an all-round wear resistant plate", and had a hardness of 425-475 HBW (Hardness Brinell, tungsten carbide indenter) [14]. The steel was delivered with a corrosion resistant primer. The alloy composition of the steel, measured by SSAB, is given in Table 1. The composition was determined with use of optical emission spectrometer. The steel was rolled, in quenched condition and was delivered as a 12 mm thick plate [11].

Table 1. Hardox 450 alloy composition.

Element	**C**	**Si**	**Mn**	**P**	**S**	**Cr**	**Ni**	**Mo**	**B**
Amount (wt%)	0.19	0.52	1.40	0.007	0.001	0.26	0.04	0.011	0.002

The A_1 and A_3 temperatures of the steel was determined to be 730 °C and 860 °C, respectively, by a dilatometer test [19]. The A_{cm} temperature for different carbon contents was found in the Fe-C phase diagram.

The original Hardox 450 was also characterized by use of light microscopy and hardness tests. Sample preparation, microscopy and hardness tests are described in detail later.

3.2 Preliminary project work post-examinations

3.2.1 Verification of carbon content with use of Electron Probe Micro Analyzer

To verify an increase in carbon content from the carburization, examinations were performed by wavelength dispersive spectroscopy (WDS) in a JEOL JXA-8500F Electron Probe Micro Analyzer (EPMA). Cut-out samples of the carburized plates were cast in Clarocit, ground and polished by standard metallurgical methods (described later in this

chapter). After polishing, the samples were removed from the cast. This was done by freezing the cast-in samples in liquid nitrogen, and then crushing the clarocit casts to extract the bare metal samples. The reason for this was to obtain the best possible connection between the sample and the sample table for an optimum electron leading path. Two reference samples, with 0.19% carbon content and 0.95% carbon content, respectively, were used as standard specimens for the carbon measurement. The employed accelerating voltage was 10 kV, the probe current was 3×10^{-8} A, the probe diameter was 1 μm, and the interval between each measurement was 1 μ. The measurement started approximately 10 μm outside the sample surface and travelled 2.5 mm towards the sample center. The analyzing crystal was a LDE6H (Cr/C) synthetic crystal. These settings gave carbon profiles from the carburized surface into the steel sample cross-section.

3.2.2 Microstructure

The techniques and equipment used to explore the microstructure is described in chapter 3.5.1.

3.3 Case hardening

From the preliminary project some hardening processes looked better than others. However, as plate metal was no limitation, it was decided to try all the hardening courses in complete case hardening processes. The case hardening procedures were tested with 0.9% and 1.1% carbon potential. Due to severe crack formation observed in microscopic examinations of miniature dummy specimens, the 1.3% carbon potential was not tested. Illustrations of the 0.9% carbon potential case hardening courses are displayed in Figure 12. Sample 1 went through a direct case hardening process with deep quenching (-72 °C) after the carburizing at 940 °C for 6 hours. Samples 2 – 6 were cooled in air after the carburizing. Sample 2 went through a modified single hardening process with one hardening step at 880 °C for 30 minutes, before deep quenching at -72 °C. The idea was that hardening above A_3 (860 °C for

a core carbon content of 0.2%) would give the whole sample (surface and core) a hardening and grain refining effect. Sample 3 went through a traditional double hardening process with hardening steps at 880 °C and 810 °C (above A_{cm}-temperature at 0.9 % carbon content), respectively, for 30 minutes each. The first hardening step was not followed by deep quenching, but quenching in oil at 70 – 80 °C before cooling in water to room temperature. Sample 4 went through the same treatment as sample 3, except it was modified, i.e. the second hardening step was at 880 °C instead of 810 °C. This modification was done to give the whole cross-section of the sample hardening and grain refinement (see sample 2). Sample 5 went through a triple hardening treatment. Two hardening steps at 880 °C for 30 minutes and quenching in oil was followed by a third hardening step at 810 °C for 30 minutes and deep quenching at -72 °C. Sample 6 went through the same treatment as sample 5, except that it was not deep quenched after the last hardening step, instead it was quenched in oil. When quenched in oil at 70-80 °C the plates where held in the oil for approximately 25 minutes before being washed in water. The deep quenching included quenching in oil at 70-80 °C for approximately 25 minutes, washing, and then put in a -72 °C freezer, where it was held for minimum 5 hours. The total time from furnace to freezer was approximately 30 minutes. All samples were tempered at 245 °C for 2 hours.

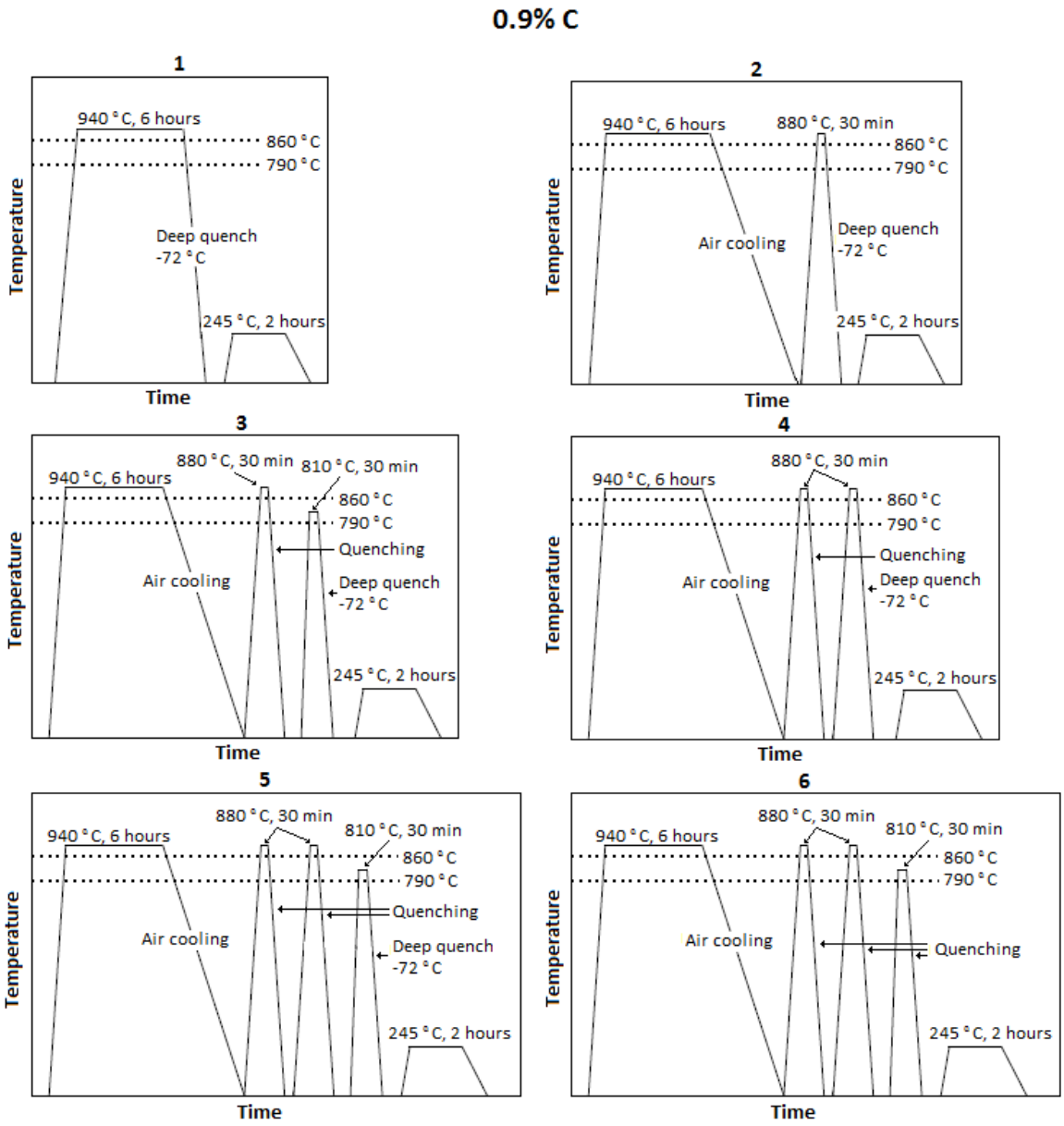

Figure 12. Illustration of 0.9% carbon potential case hardening courses.

Illustrations of the 1.1% carbon potential case hardening courses are displayed in Figure 13. Sample 7 went through a direct case hardening process with deep quenching at -72 °C after the carburizing at 940 °C for 6 hours. The samples 8 – 11 were cooled in air after the carburizing. With increasing carbon content the A_{cm}-temperature will increase (Figure 5a), and at 1.1% C the A_{cm} is approximately the same as the core A_3-temperature. Because of this, hardening between A_3 and A_{cm} is difficult to accomplish and as a result all hardening steps reaches temperatures above the A_3. Sample 8 was single hardened and deep quenched, sample 9 was double hardened and sample 10 and 11 was triple hardened. All hardening steps were at 880 °C for 30 minutes. Samples 9 and 10 were quenched in oil (70 – 80 °C) after the

intermediate hardening steps and then deep quenched after the final hardening step. Sample 11 was quenched in oil after all hardening steps, i.e. no deep quenching. All samples were tempered at 245 °C for 2 hours.

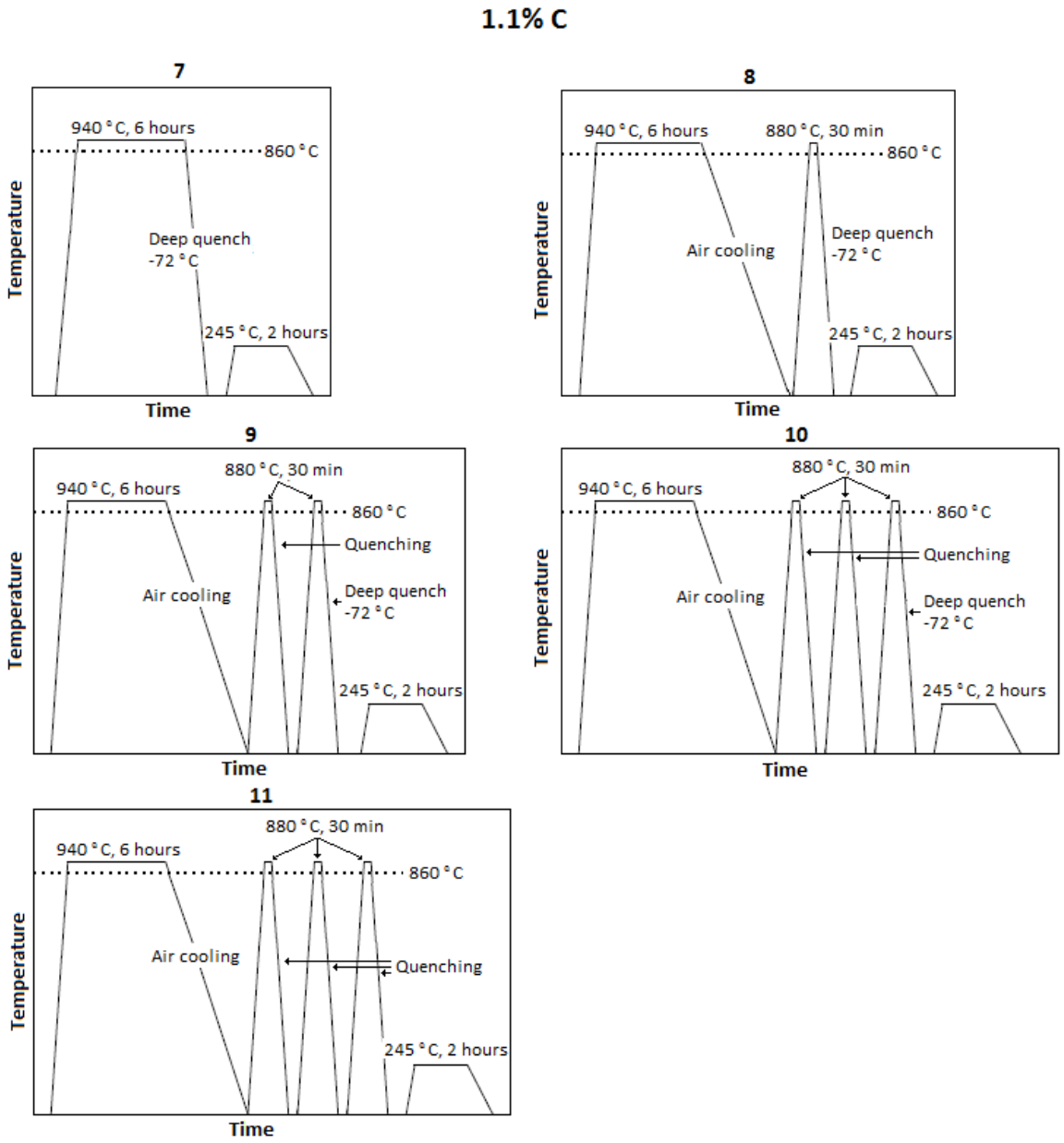

Figure 13. Illustration of 1.1% carbon potential case hardening courses.

The case hardening was carried out by Bandak Raufoss (former Raufoss Industrial Tools AS).The plates were 300×300×12 mm^3 in size. Due to capacity issues, the plates were sandblasted prior to the case hardening to remove the corrosion resistant primer, instead of ground as in the preliminary project. The primer was believed to limit the diffusion of carbon

into the steel. The furnace employed was an Ipsen T5, a gas-tight multi-purpose two chamber furnace with an integrated oil quench tank (Figure 14). The carbon-enriched atmosphere was a mixture of propane and air. Before every heat treatment, either carburizing for 6 hours or hardening for 30 minutes, the plates where heated to the target temperature in inert atmosphere for 30 minutes in the first chamber. After heating, the plates were transferred to the next chamber with the selected carbon potential atmosphere and held for the specified amount of time, before quenching in the integrated oil bath. After quenching in oil, the plates were washed and dried. The plates that should be deep quenched were then placed in a freezer with temperature of -72 °C.

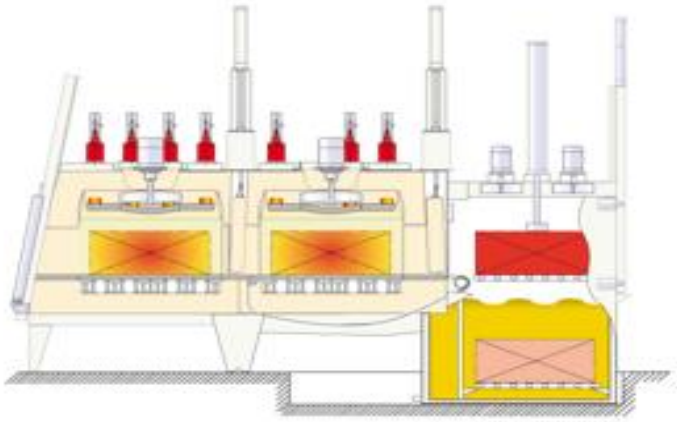

Figure 14. Illustration of Ipsen TQ-2-Type furnace [20]. Note the two separate chambers and integrated oil quench chamber. The products are loaded on the left hand side, then heat treated in the two separate chambers, quenched in the integrated oil tank and finally unloaded on the right hand side.

3.4 Ballistic experiments

The ballistic experiments were executed at the Department of Structural Engineering at NTNU. The experiments were carried out to estimate the ballistic limit velocity of the different case hardened plates. A 7.62mm×63mm bolt-action Mauser rifle was used. The stock was removed so that only the barrel, bolt-action mechanism and trigger mechanism was remaining (Figure 15). The barrel was 1 m long and smooth-bored. It was rigidly mounted to ensure the same hit point for every shot. In front of the muzzle there was a plate with a hole for the projectile. This hole was covered with tape before every shot to limit muzzle flame.

On the opposite side of the plate there was a photocell system that measured the initial velocity of the projectile.

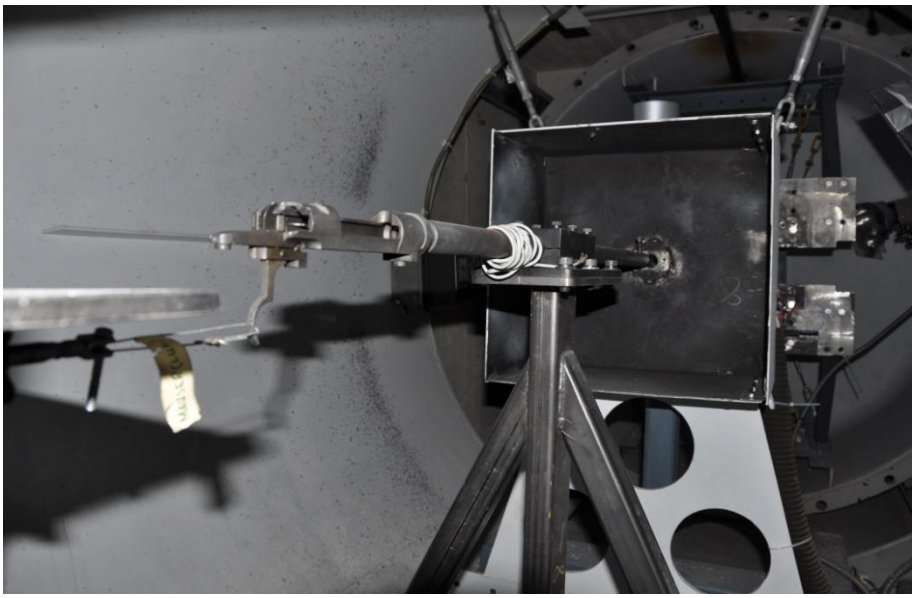

Figure 15. The mounted Mauser barrel and trigger. The bolt is not inserted in this picture.

The target plate was rigidly mounted approximately 1 m from the muzzle. Each plate was shot at five times, four corner shots that were 100mm from each other and from the plate edges, and one shot in the middle of the corner shots (Figure 16).

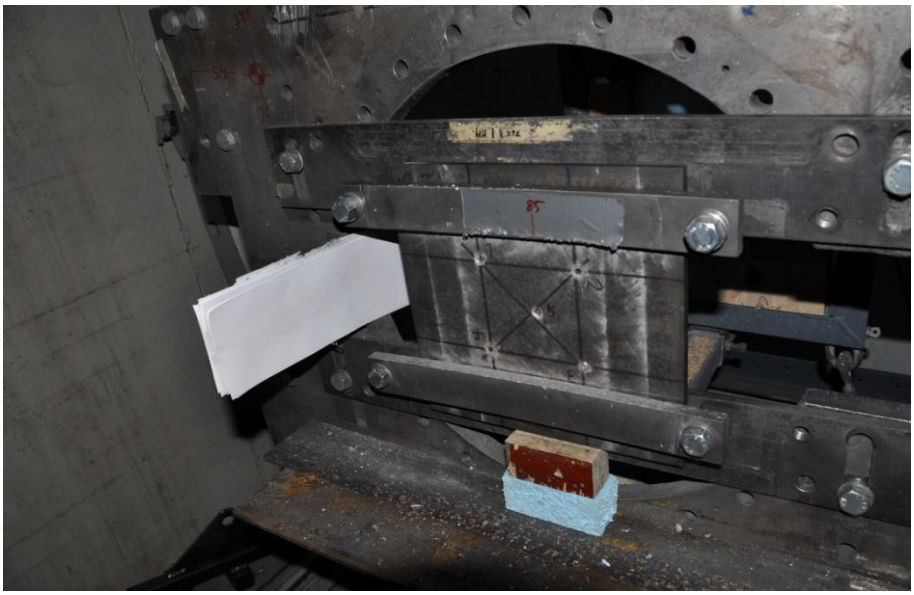

Figure 16. A mounted target plate. This plate has been shot at five times, 4 corner shots and one middle shot.

The whole set-up was inside a 16 m^3 chamber that was closed during all shots. The chamber can be seen in Figure 17. The trigger was operated from outside the chamber. The chamber had windows, and a Photron SA1.1 High Speed Camera was mounted outside the chamber and recorded all projectile impacts. The initial and residual velocity of the projectile was calculated from the high-speed recordings. The initial velocity from the photocell and high-speed recordings was compared to ensure correct measurements and calculations.

Figure 17. The chamber surrounding the Mauser rifle and the target plate [11].

The ammunition in the experiments was 7.62mm×63mm armor piercing rounds. The projectile consists of a hard steel core, a lead cap (for stabilization during flight) and brass jacket and sabot as displayed in Figure 18. The core material was 1007 tool steel with a hardness of 800 HV. The velocity of the projectile was determined from the amount of gunpowder in the cartridge. Less gunpowder gives lower velocity. However, the velocity will vary slightly with constant amount of gunpowder, as the ignition process is difficult to control. Geometries, mass and alloying elements of the projectile parts is given in Table 2.

Table 2. Summary of geometries, mass and alloying elements of the different projectile components [11].

Jacket (CuZn10)			Sabot (CuZn10)			Core (1007 tool steel)			Cap (PbSb10)		
l (mm)	d_{max} (mm)	m(g)	l (mm)	d_{max} (mm)	m(g)	l (mm)	d_{max} (mm)	m(g)	l (mm)	d_{max} (mm)	m(g)
34.9	7.9	4.4	4.0	6.2	0.4	27.6	6.1	5.0	9.3	5.1	0.7

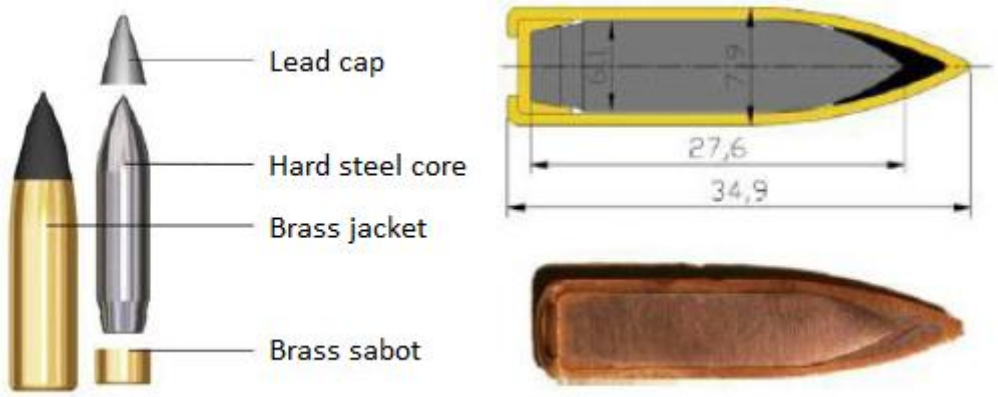

Figure 18. Illustration of a 7.62mm×63mm AP projectile [11]. The scale is millimeters.

3.5 Sample preparation, microscopy and hardness measurement

All sample preparation, microscopy and hardness measurement was performed at the Department of Materials Science and Engineering at NTNU.

3.5.1 Sample preparations and microscopy examinations

Before examination, the sample plates were cut to reveal the interesting surfaces, using a Struers Discotom-5 saw, and cast in Clarocit. The cast samples were ground and polished down to 1 µm by standard metallographic methods. For examinations of microstructure in light microscopy, the samples were etched in a solution with 2 % nital for 5-15 seconds. To reveal austenite grain boundaries, the samples were etched in a solution consisting of 28 ml 10% oxalic acid, 4 ml hydrogen peroxide and 80 ml water for 45 seconds. Grain size was measured according to ASTM standard E112-96 [11]. The length of 50 grains was measured, and this was then divided by 50 to find the average diameter of one grain. All results are

averages of 8 length measurements in the core of each sample. The light microscope used was a Leica MEF4M. The camera used for taking images was a Progress C10.

3.5.2 Hardness measurements

Hardness measurements of the case hardened sample cores were performed with a Matsuzawa Seiki DVK-1S. The loading force was 5 kgf, and the loading time was 15 seconds. The hardness value of each of the samples is an average of 5 measurements in the center of the cross-section. The hardness values are in Hardness Vickers (HV).

The surface hardness of the case hardened samples was measured by a Leica VMHT MOT microhardness tester. The loading force was 0.3 kgf, and the loading time was 15 seconds. Hardness profiles of the samples were measured. All profiles were averages of three parallel profile measurements on each sample. The profiles started at the carburized surface and ended approximately 2.5 mm into the metal. The hardness values are in Hardness Vickers (HV).

4 Results

4.1 Preliminary project work post-examinations

4.1.1 Electron Probe Micro Analyzer (EPMA)

Results from the EPMA examinations of three test samples that were carburized during the project work at carbon potentials of 0.9%, 1.1% and 1.3%, respectively, are displayed in Figure 19. Three parallel line analyses were measured on each sample, whereas only one parallel from each sample is included in the figure. All parallels show an evident increase in carbon content, from approximately 0.2% C in the core to approximately 0.9%, 1.1% and 1.3% carbon content at the sample surface. EPMA examinations of all the other samples revealed the expected increase in carbon content, and thus verified the carburizing effect. The rest of the EPMA results are displayed in Appendix A.

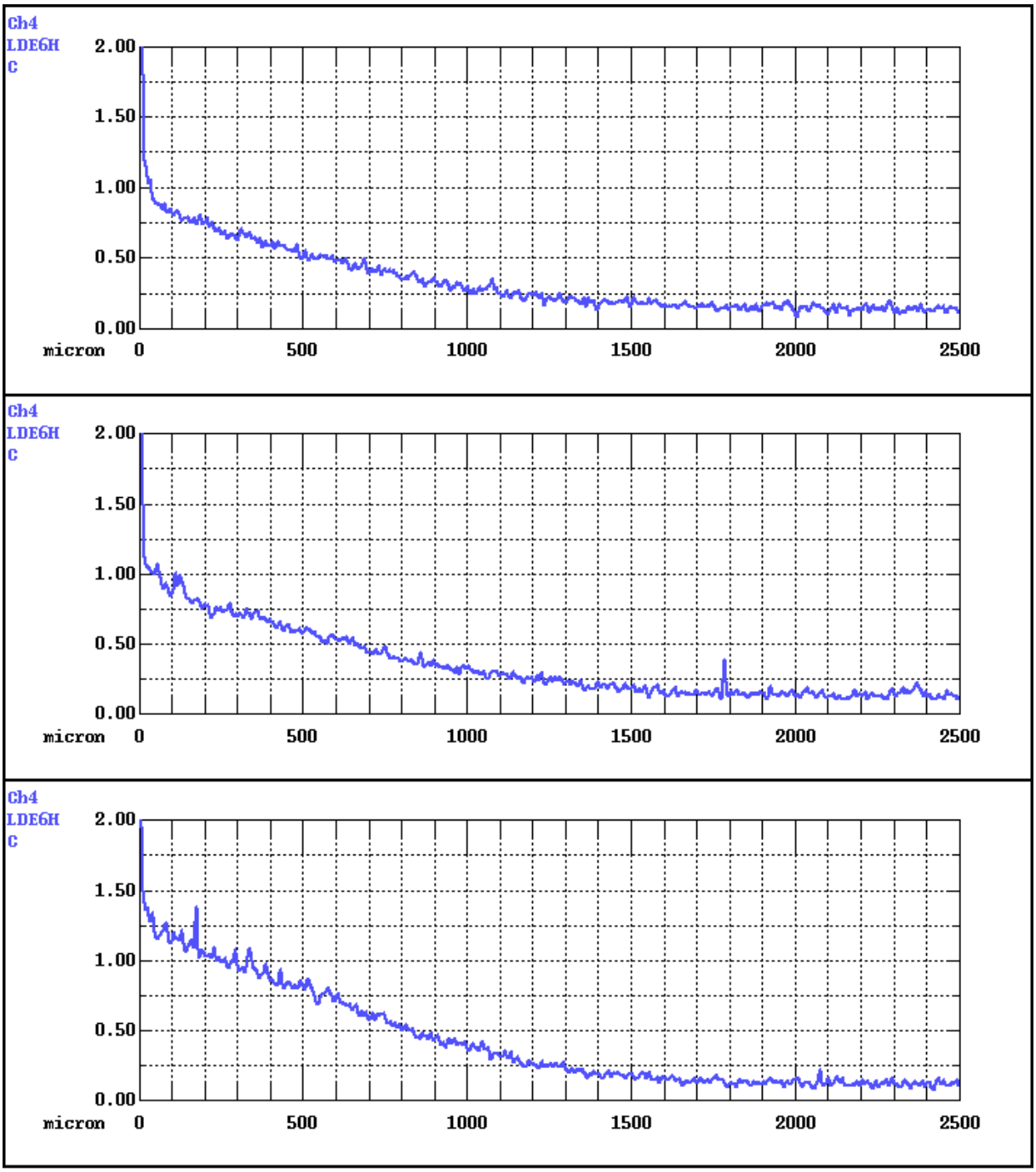

Figure 19. The results from the EPMA examinations of three samples that were carburized at carbon potentials of 0.9% (top), 1.1% (middle) and 1.3% (bottom), respectively. The x-axis shows the distance from the sample surface in µm. The y-axis shows the carbon content in atomic%. The sudden increase of carbon near the surface indicate carbon content measurements from the cast material, while carbon content peaks further inside the sample indicate contaminations or impurities.

4.1.2 Microstructure

The core microstructure of the case hardened samples 0.9A, 0.9B, 0.9C (0.9% carbon potential), 1.1 (1.1% carbon potential) 1.3A and 1.3 B (1.3% carbon potential) were low-carbon martensitic. The core microstructure of the original Hardox 450 reference sample was low-carbon martensitic as well noticeably smaller grains than the case hardened samples. The microstructure of sample 0.9B and the reference sample is displayed in Figure 20. The austenite grain size of all samples were measured, this is displayed in Figure 21. The grain size of all the carburized samples were ranging from 20 µm to 22 µm, while the reference sample had a grain size of 10 µm.

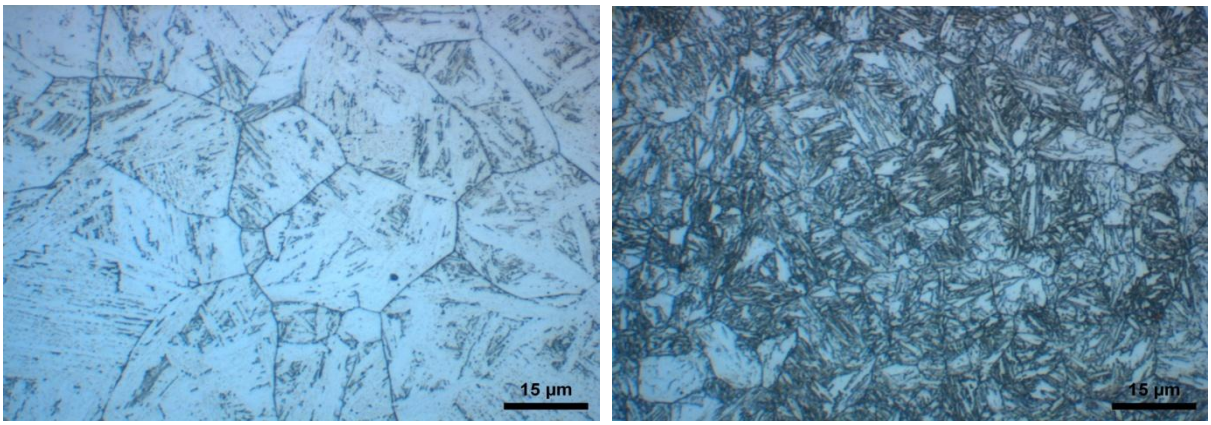

a) **b)**

Figure 20. High magnification images of sample 0.9B (a) and the reference sample (b).

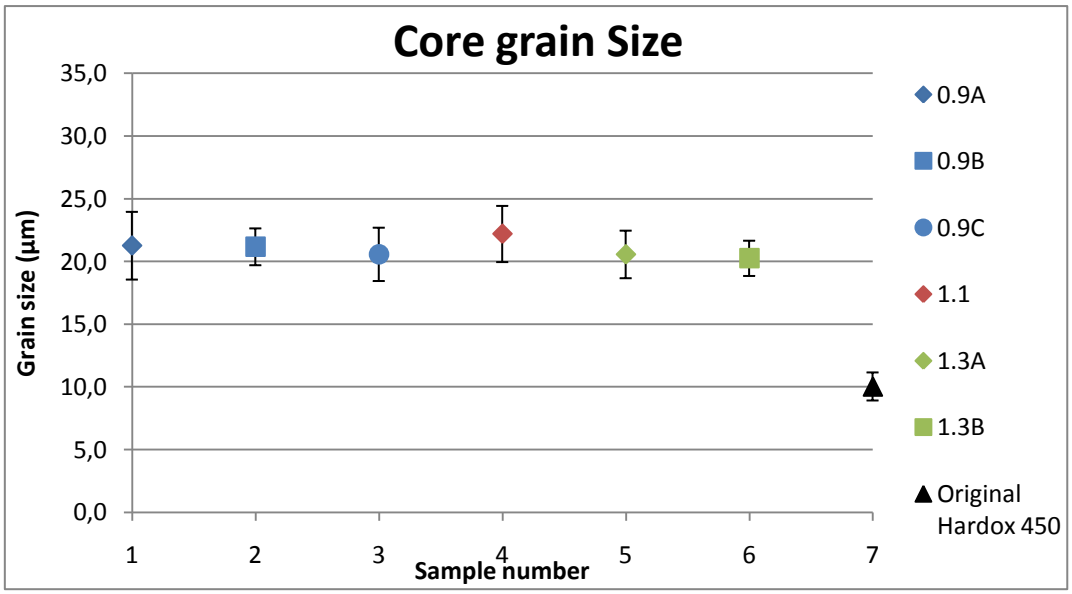

Figure 21. Core grain sizes of the case hardened samples and the reference sample.

The light microscope examinations revealed cracks in most carburized test samples from the project work. The samples with 1.3% carbon potential had the most and longest cracks, while the 0.9% carbon potential specimen had fewest and shortest cracks. All cracks were located on the lower side of the samples, i.e. the surface which faced the metal basket during carburizing and quenching. The cracks were thin (< 10 µm) and had lengths up to approximately 900 µm. Figure 22 shows a low magnification of the surface layer of a sample that was carburized with carbon potential of 1.3%. The crack to the far right is over 800 µm long.

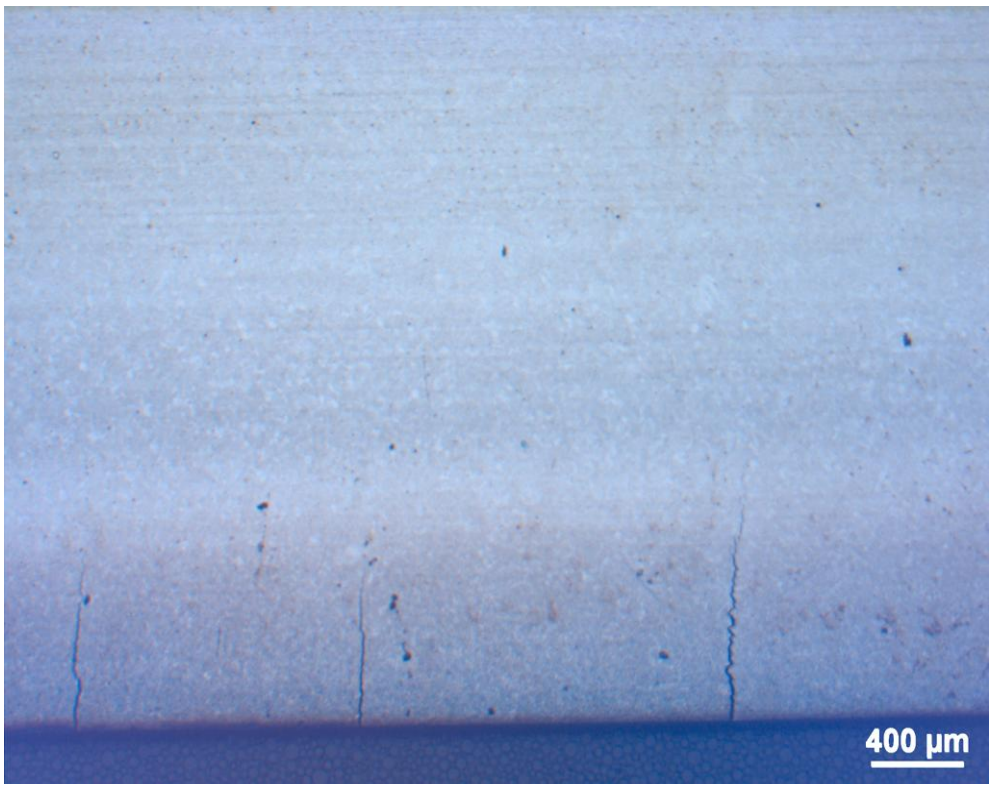

Figure 22. Low magnification image of a sample that was carburized at carbon potential of 1.3%. The dark blue layer at the bottom of the picture is the Clarocit cast material. Three cracks can be seen from the surface of the sample and stretching in towards the sample core.

The examinations also revealed that the microstructure changed from the core and out to the surface. This is expected, as the carburizing and quenching will give different effects at different distances from the surface. This can be seen in Figure 20 as well, note the change in color from the surface of the sample (bottom of image) and towards the core (top of image).

4.2 Ballistic experiments

4.2.1 Ballistic limit velocities

The results from the ballistic experiments performed on the 30×30×12 mm^2 plates during the work of this thesis are displayed as ballistic limit curves. The ballistic limit curves of the samples 1-6, carburized at a carbon potential of 0.9%, are displayed in Figure 23. The ballistic limit velocity was calculated to be 779, 770, 726, 713, 728 and 710 m/s, respectively.

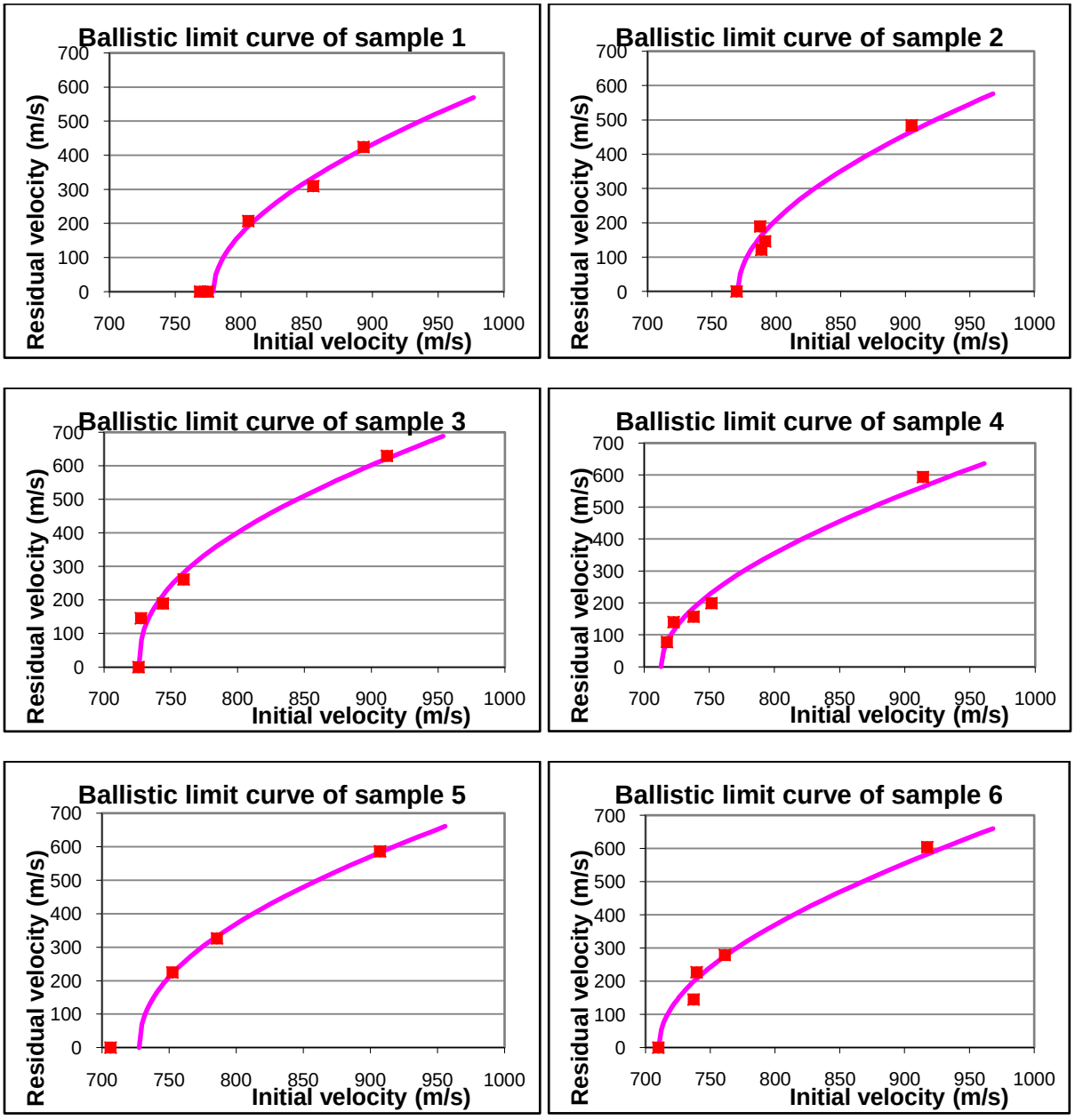

Figure 23. The ballistic limit curve of samples 1-6.

The ballistic limit velocity of sample 1 and sample 2 are near equal around 775 m/s, but the samples 3-6 has significantly lower ballistic limit velocities, with as much as 50-65 m/s reduction from samples 1 and 2.

The ballistic limit curves of the samples 7-12, carburized at carbon potential of 1.1%, are displayed in Figure 24. The ballistic limit velocity was calculated to 787, 767, 759, 783, 775 and 797 m/s, respectively.

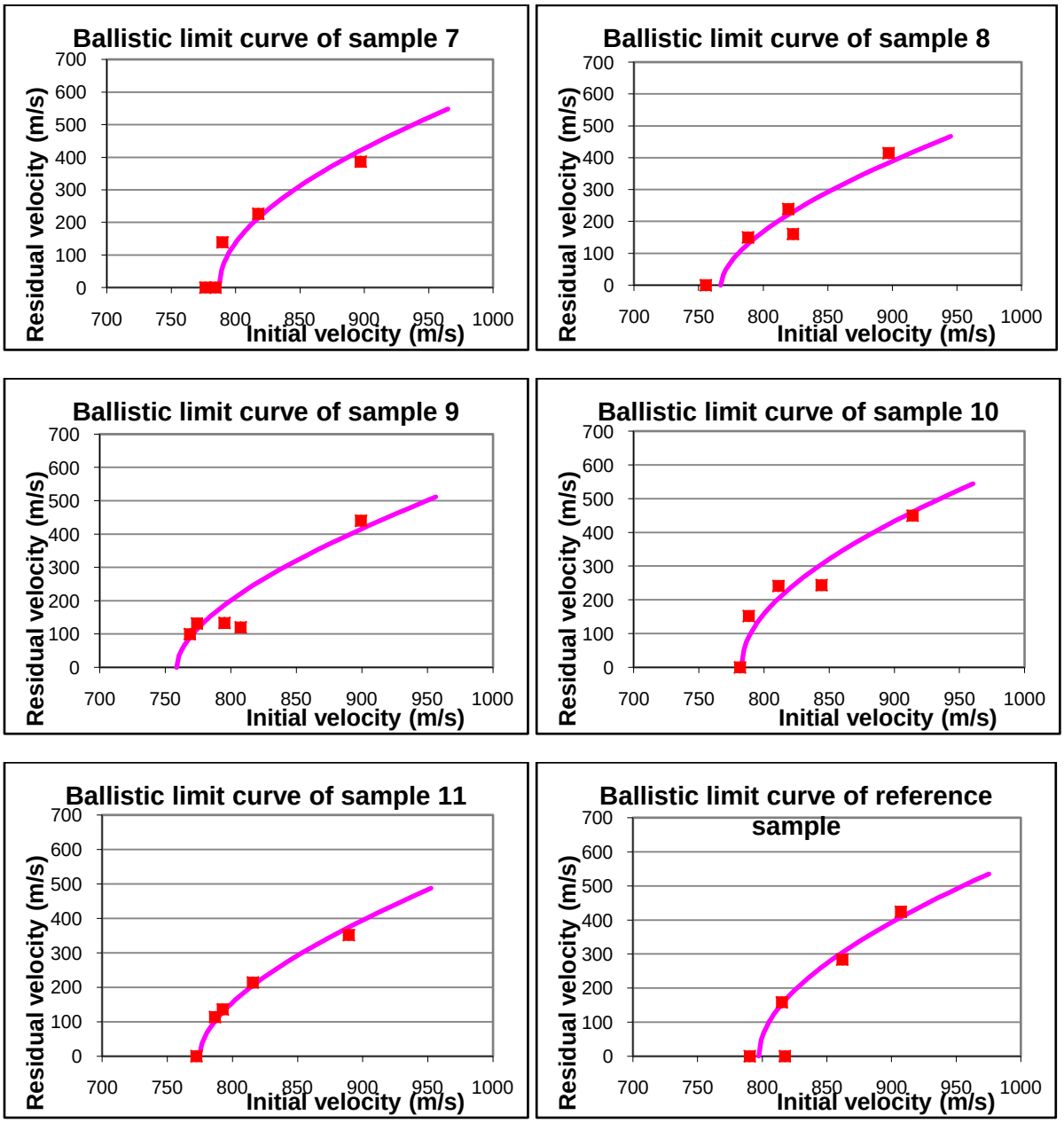

Figure 24. The ballistic limit curve of the samples 7-11 and the original Hardox 450 reference sample.

The ballistic limit velocity of the samples 7-11 are ranging from 759-787 m/s, somewhat lower than the ballistic limit velocity of the original Hardox 450 reference sample at 797 m/s.

The ballistic limit velocities of all samples are summarized in Figure 25.

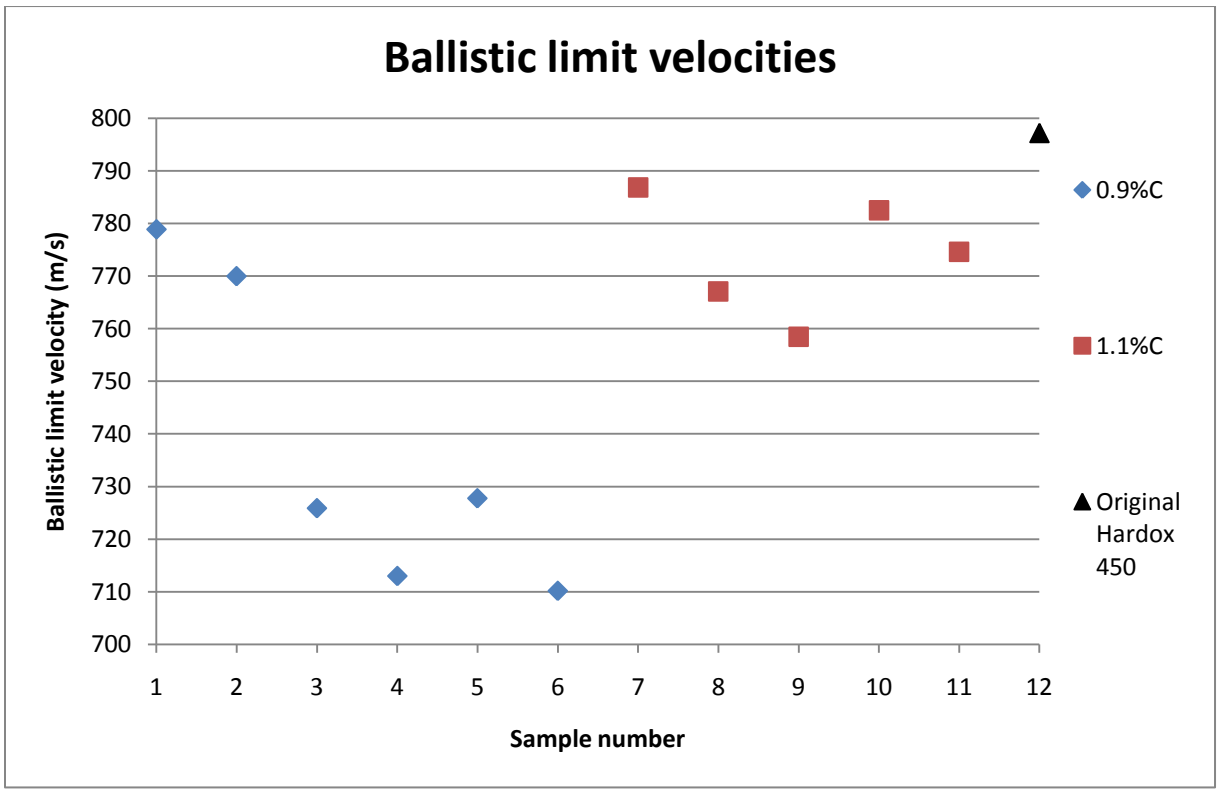

Figure 25. Ballistic limit velocities of all samples. The samples 1-6 are all case hardened with a carbon potential at 0.9 % C, while samples 7-11 are all case hardened with a carbon potential of 1.1 % C. Sample 12, the original Hardox 450 reference sample, is not case hardened at all.

The results show that the case hardening process has not improved the ballistic limit velocity, in fact, the ballistic limit velocity has been reduced. The smallest reduction is 10 m/s (sample 7), and the largest is 87 m/s (sample 6).

4.2.2 Metallographic examination of the penetration zone

Cut-out cross-sections of the penetration zone of the samples 1, 6, 10 and the Hardox 450 reference sample are shown in Figure 26.

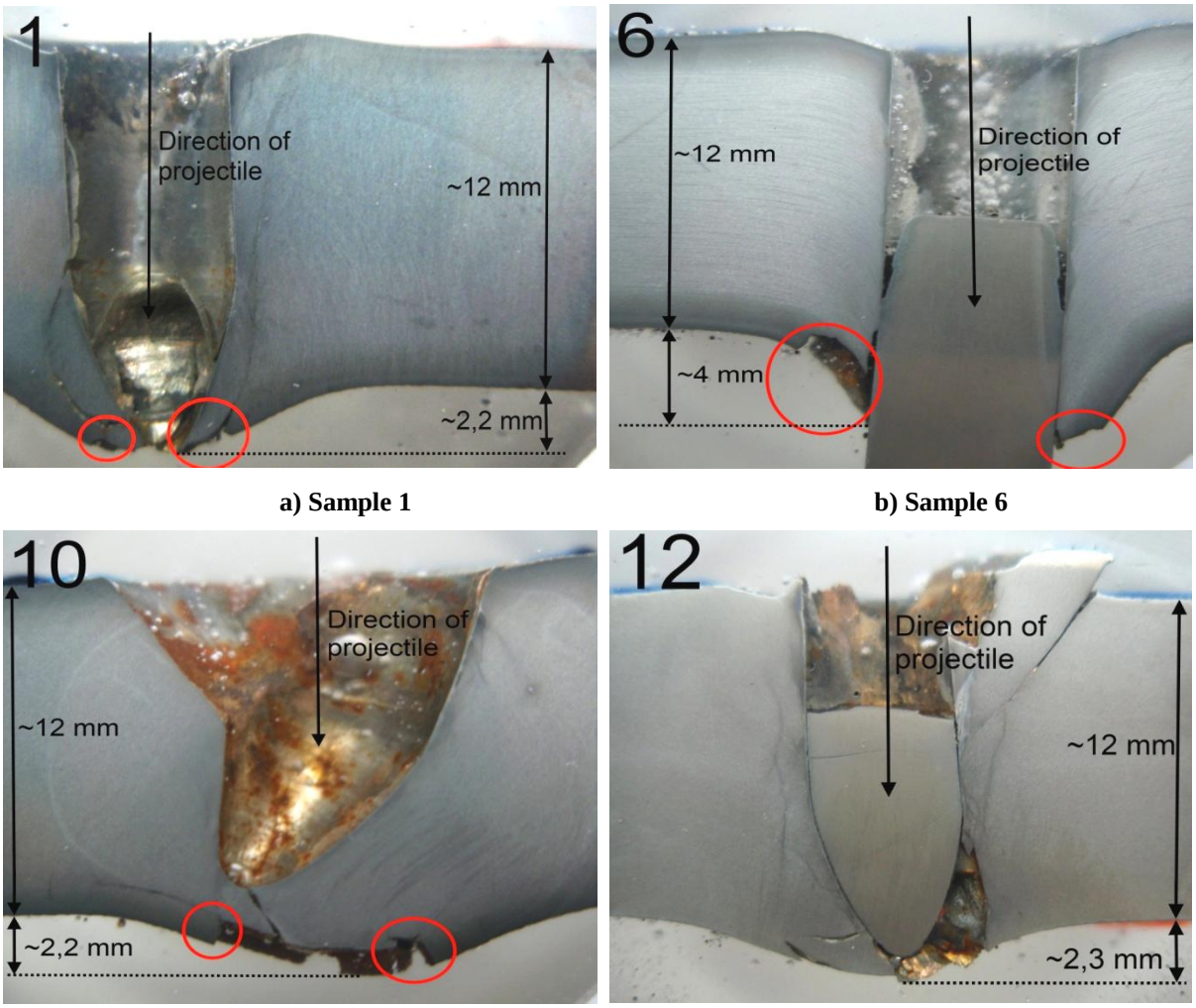

a) Sample 1 **b) Sample 6**

c) Sample 10 **d) Sample 12**

Figure 26. Cross-section images of the penetration zone of sample 1, 6, 10 and the original Hardox 450 (sample 12). Notice that the images are not in scale.

All of the above images show samples where the projectile was embedded in the steel, i.e. the initial projectile velocity was close to the ballistic limit velocity (the projectile itself is not present in Figure 26 a and c). In samples 1, 6 and 10 the carburized layer can be seen as the dark layer at the surfaces. The reference sample 12 does not have this layer. The carburized layer seemed to be very brittle because it had cracked due to the stress caused by the projectile. The cracks seemed to propagate in the transition area between carburized and

uncarburized metal. This can be seen in Figure 27 that contains high magnification images captured within the red circles in Figure 26b) and c).

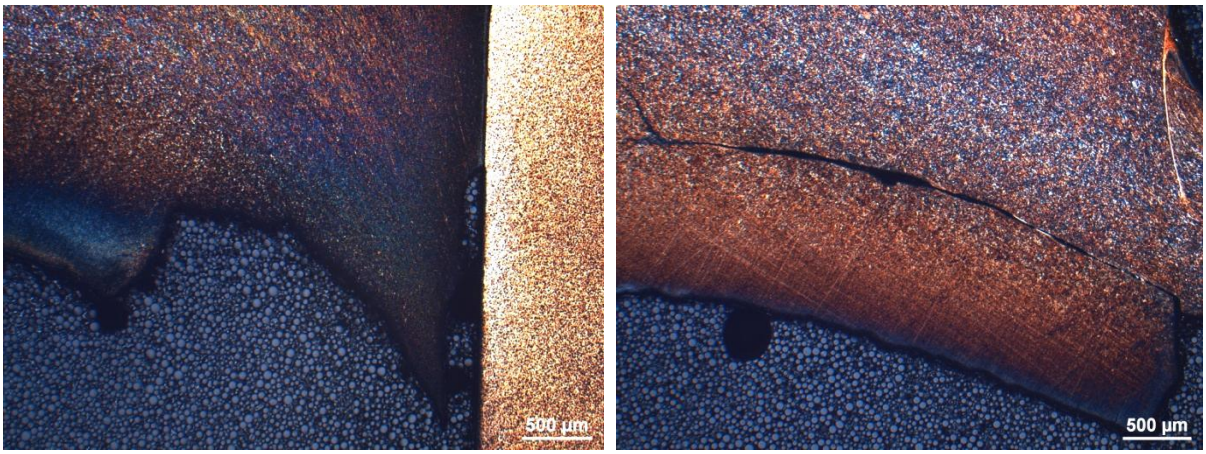

a) **b)**

Figure 27a. Magnification of the area in the red ring on the left hand side of Figure 26b (sample 6). Most of the carburized layer has been removed, probably due to cracks in the transition area between carburized and uncarburized metal.

Figure 27b. Magnification of the area in the red ring on the left hand side of Figure 26c (sample 10). The crack seems to grow in the area between carburized and uncarburized metal. The bright stripe on the right hand side of the image is an adiabatic shear band (ASB).

Sample 6 seemed to be more ductile than the other samples, due to high deformation in the penetration zone. Sample 6 also had less adiabatic shear bands (ASB) than the other samples, another indication of sample 6 being softer and more ductile, as the possibility of ASB increases with increasing hardness. Low magnification images of ASBs in the different samples can be seen in Figure 28.

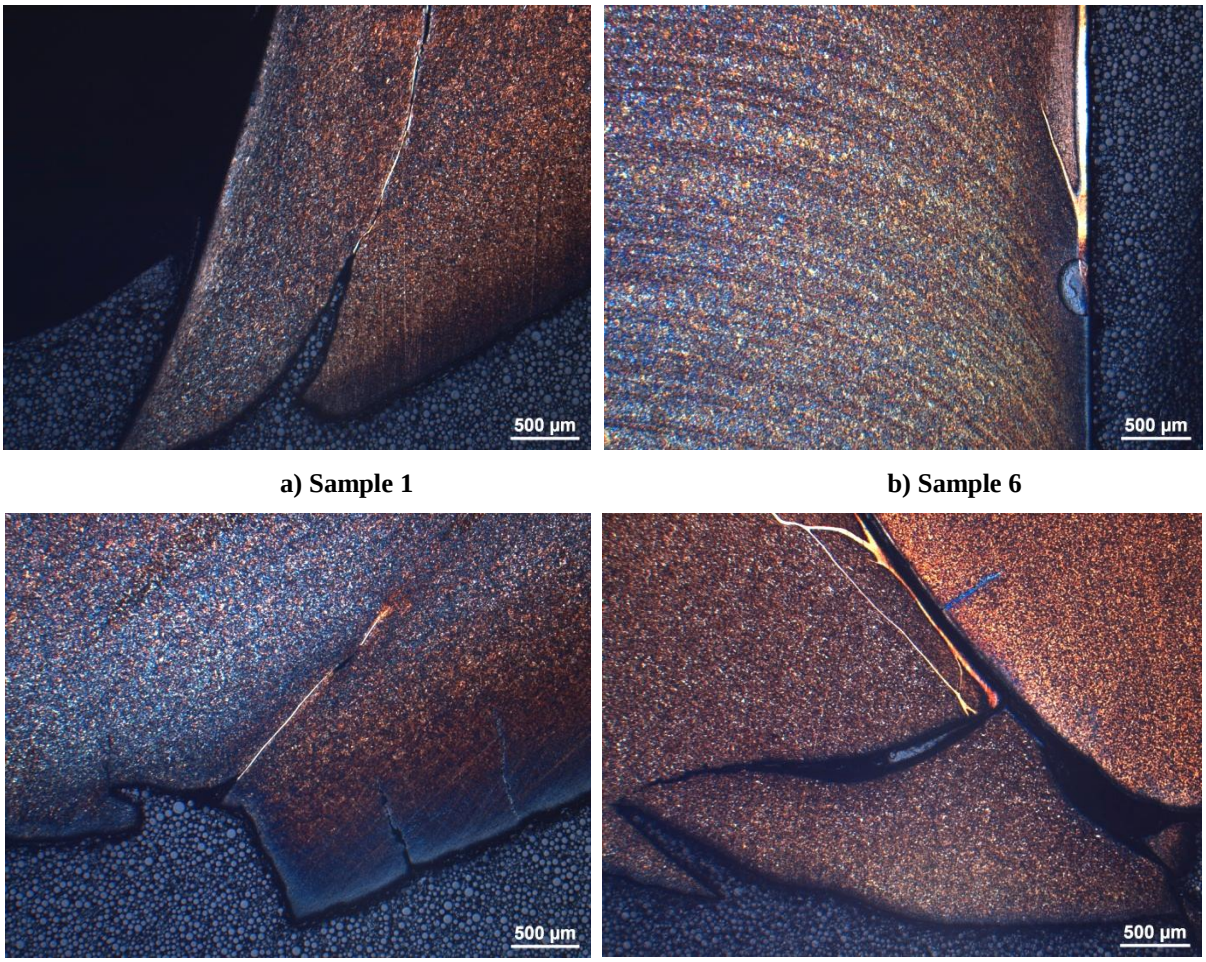

a) Sample 1 **b) Sample 6**

c) Sample 10 **d) Sample 12**

Figure 28. Low magnification of ASB in the samples 1, 6, 10 and the reference sample 12.

The ASBs in sample 6 were formed at the interphase between target and projectile (Figure 28b). The ASBs in the other samples were formed at the target-projectile interphase as well, but seemed to reach further into the target. In the samples 1 and 10, ASBs were formed in the transition area between carburized and uncarburized metal, where they acted as crack initiators (Figure 28 a and c). The cracks from the lower surface and upwards in Figure 28c, sample 10, could be cracks formed prior to the ballistic test, as was observed in the preliminary project work (Figure 22), however this is probably not the case as similar cracks were not observed in the other samples. High magnification images of the ASB in Figure 28c are displayed in Figure 29.

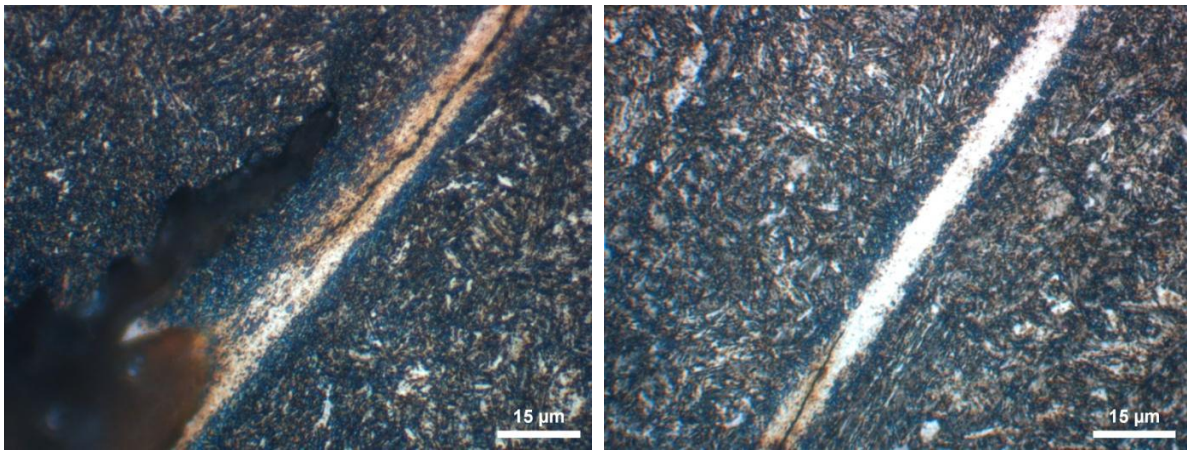

Figure 29. High magnification of crack in ASB in sample 10.

Images of all projectile entry- and exit- holes were captured. Some of them are displayed in Figure 30. The samples 3-6, exemplified by sample 3 in Figure 30a, showed signs of radial fracture, with the carburized layer separated from the uncarburized core, and possibly some ductile hole growth. The samples 1, 2 and 7-11, exemplified by sample 7 in Figure 30b, showed signs of radial fracture with fragmentation to some extent. The carburized layer was separated from the uncarburized core here as well. The entry hole also had some cracks around it. The original Hardox 450 reference sample showed signs of fragmentation with no or little evidence of radial fracture or separation of the metal near the surface. Images of all entry- and exit-holes in all samples can be found in Appendix B.

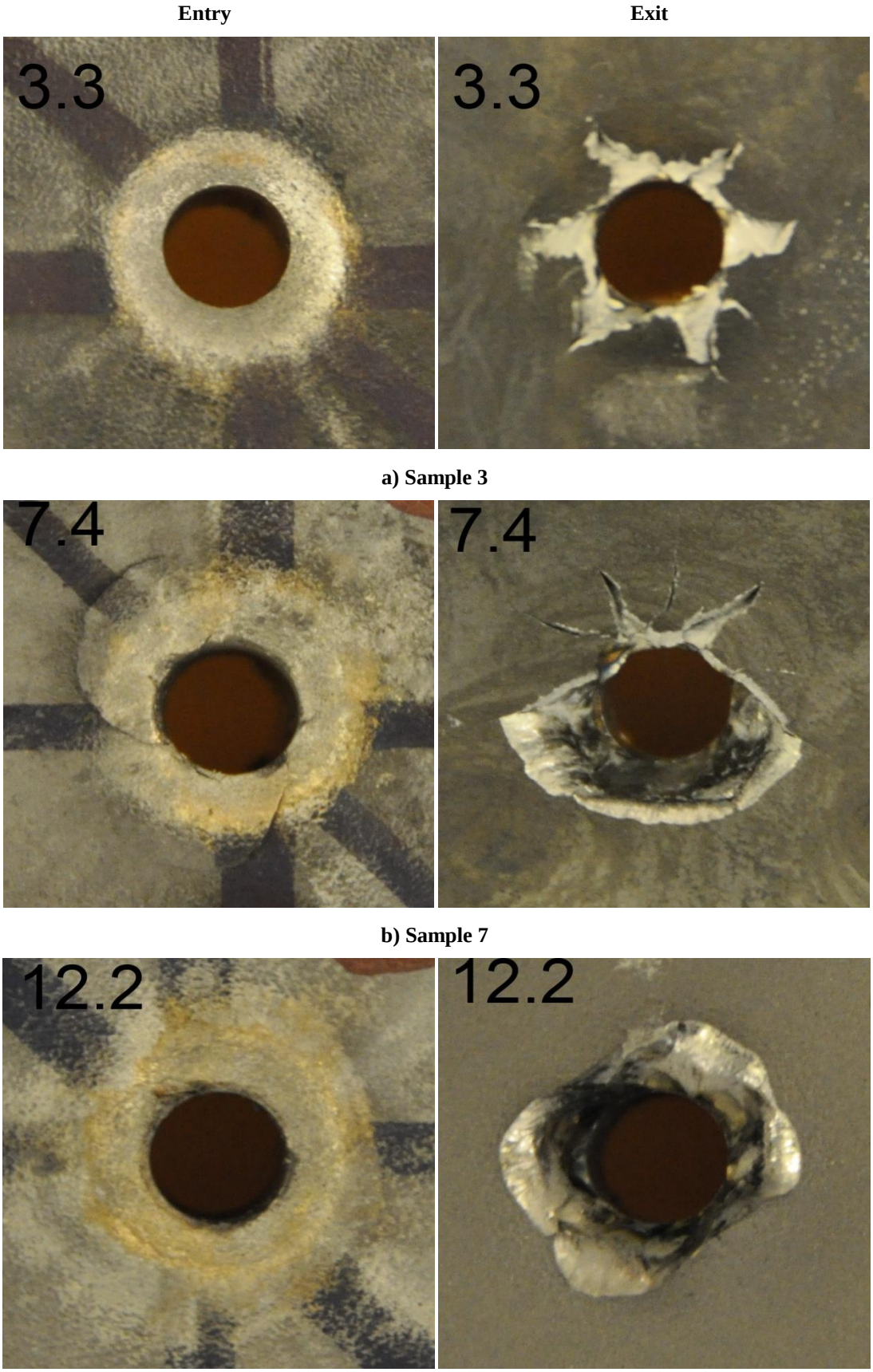

a) Sample 3

b) Sample 7

c) Sample 12

Figure 30. Entry- and exit-holes of samples 3 (a), 7 (b) and the reference sample 12 (c).

4.3 Case hardening

4.3.1 Core hardness

The core hardness values of the case hardened samples and the original Hardox 450 are given in Figure 31.

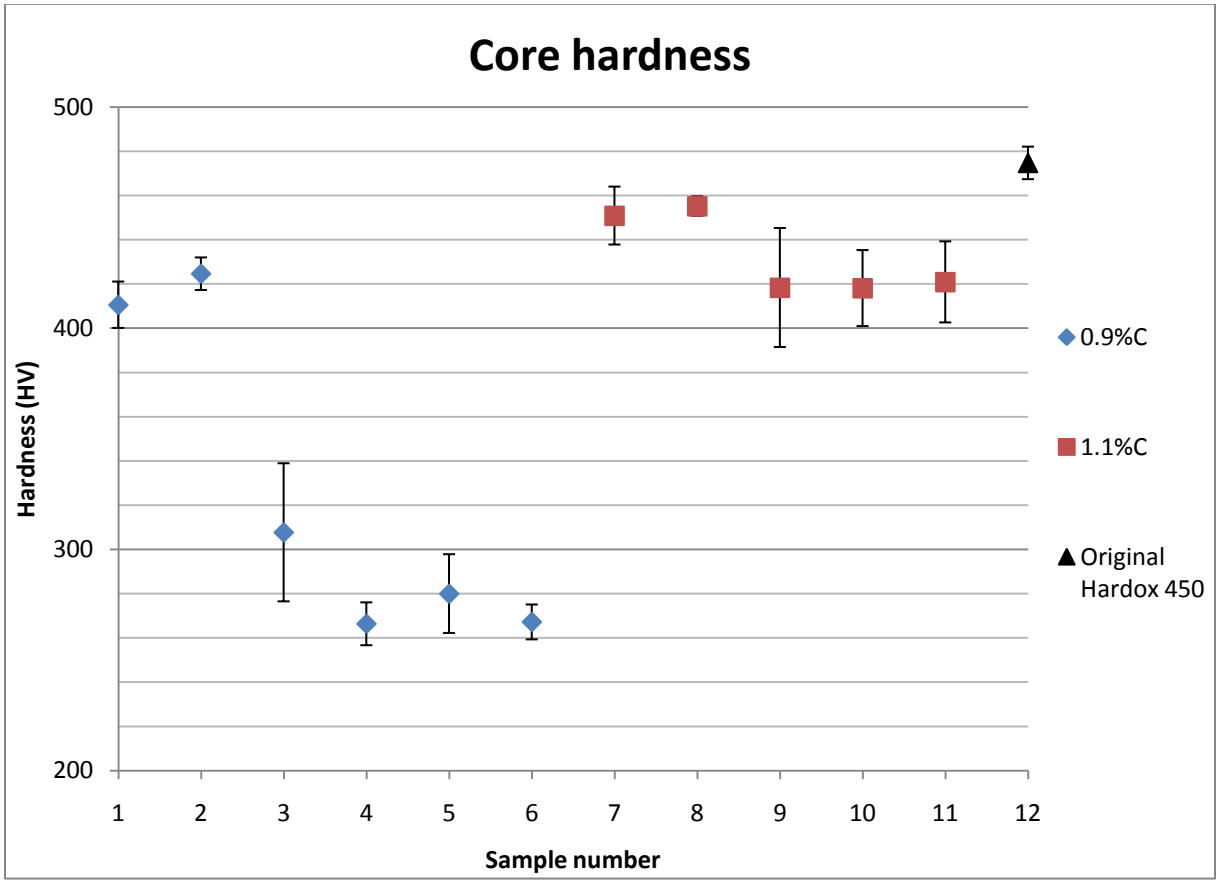

Figure 31. Core hardness of the case hardened samples (1-11) and the original Hardox 450 reference sample (12). The samples 1-6 were case hardened at 0.9% carbon potential, the samples 7-11 were case hardened at 1.1% carbon potential and the reference sample was not case hardened at all.

All case hardening courses gave a reduction in the core hardness compared to that of the reference sample, however, some was more reduced than others. Samples 1 and 2 had an average core hardness of 411 and 425 HV, respectively. The samples 3-6 experienced a significant reduction of hardness, down to approximately 265-310 HV. The case hardened samples with the highest core hardness were samples 7 and 8 with core hardness of 451 HV and 455 HV, respectively. Samples 9-11 had similar hardness values of 418, 418 and 421 HV,

respectively. The original Hardox 450 had an average hardness of 475 HV. This value was an average of only four measurements, as one of the measurements showed a hardness of only 395 HV, while the other four measurements ranged from 469 to 485, indicating that the lowest may be e.g. a soft particle or inclusion. The average value corresponds with hardness values measured before, in both the preliminary project and in Torseth's thesis. The five hardness values measured for each sample are given in Appendix C.

4.3.2 Surface hardness

The hardness profiles of the case hardened samples and the original Hardox 450 sample are displayed in Figure 32. The hardness of all the case hardened samples was gradually decreasing from the carburized surface and in towards the core. The samples 1, 3, 5 and 6, carburized at 0.9% carbon potential, had maximum hardness at the surface of 559 HV to 612 HV. The samples 2 and 4, also carburized at 0.9% carbon potential, had surface hardness of 661 HV and 702 HV, respectively. While the hardness of samples 1 and 2 was reduced to 411 and 425 HV at a distance of 2500 µm below the surface, the hardness of the samples 3-6 was only 266-308 HV at the same depth from the surface. The samples that were case hardened at 1.1% carbon potential varied in hardness from 684 HV to 735 HV at the surface, and all decreased gradually in hardness to values between 418 HV and 459 HV at a distance of 2500 µm from the surface. The original Hardox 450 reference sample had a low surface hardness of 263 HV, but it increased to 478 at a distance of 200 µm inside the metal. From there and inwards the hardness values ranged from 449 HV to 498 HV. Each curve is the average of three parallel hardness profile measurements, which can be found in Appendix D.

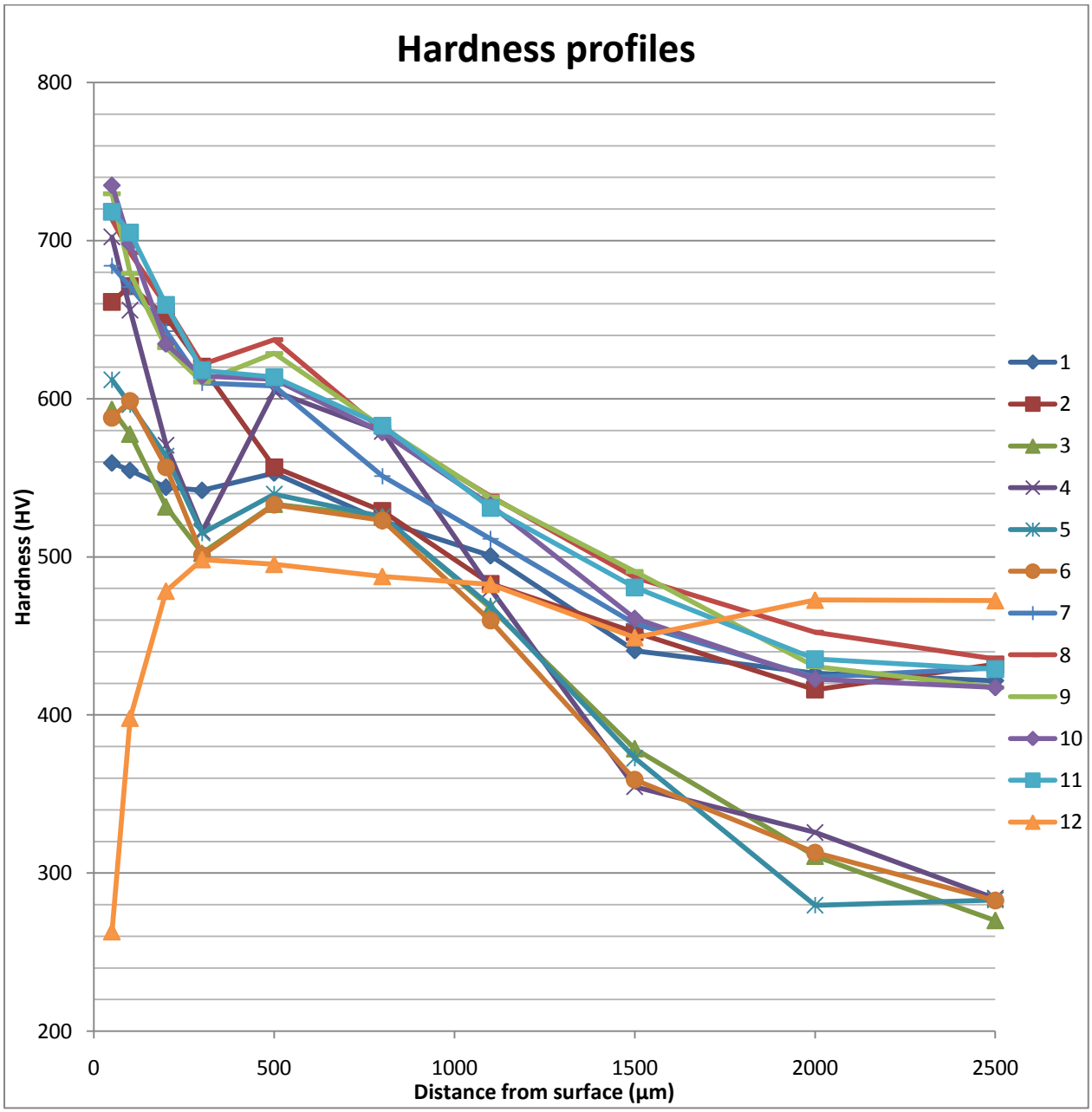

Figure 32. The hardness profiles of the case hardened samples (1-11) and the original Hardox 450 reference sample (12). The samples 1-6 were case hardened at 0.9% carbon potential, the samples 7-11 were case hardened at 1.1% carbon potential, and the reference sample was not case hardened at all.

4.3.3 Hardness integral

The integrals of the cross-section hardness profiles were calculated, and the values are given in Figure 33. Some assumptions were made:

- The hardness profiles of the surface was equal on both sides of the plate, i.e. the integral value was calculated for 0 µm to 6000 µm, and doubled to find the integral of the complete cross-section.
- The hardness value between two hardness measurement locations was set equal to the average of the hardness values at the two locations.
- The hardness at 0 µm was set equal to the hardness at 50 µm.
- The hardness at 6000 µm was set equal to the average core hardness value.

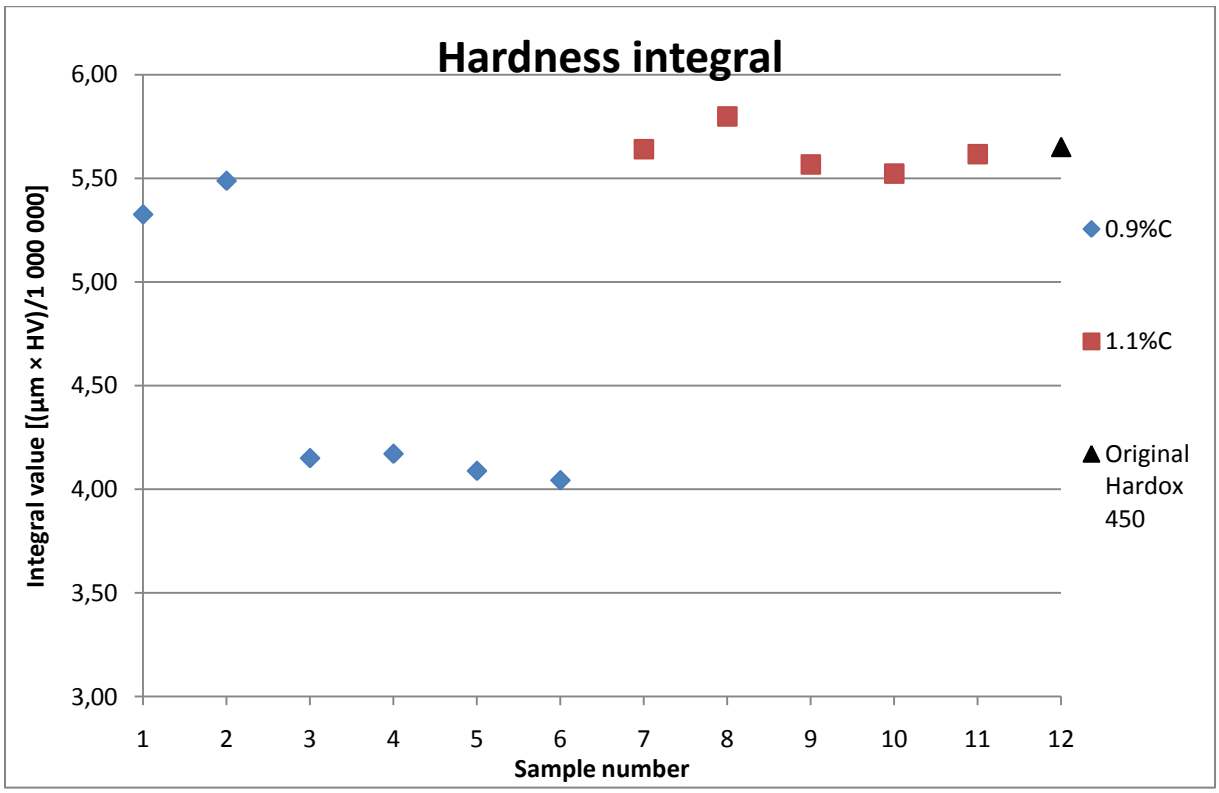

Figure 33. The hardness integral values of the case hardened samples (1-11) and the original Hardox 450 reference sample (12). The samples 1-6 were case hardened at 0.9% carbon potential, the samples 7-11 were case hardened at 1.1% carbon potential and the reference sample was not case hardened at all.

The integral values of the samples 3-6 were lower than the rest as expected. The hardness values of the samples 1, 2, 9 and 10 were somewhat lower than for the reference sample,

while samples 7 and 11 had similar values as the reference sample. Sample 8 had a significantly higher hardness integral value than the reference sample.

4.3.4 Microstructure

The carburization effect was clearly visible on low magnification images of the sample surfaces of samples 1-11, exemplified by sample 7 in Figure 34a. Note the darker color on the upper part of the steel. The original Hardox 450, Figure 34b, was not case hardened and showed no darkening effect, on the other hand, a narrow layer of brightened material is visible at the surface of the sample.

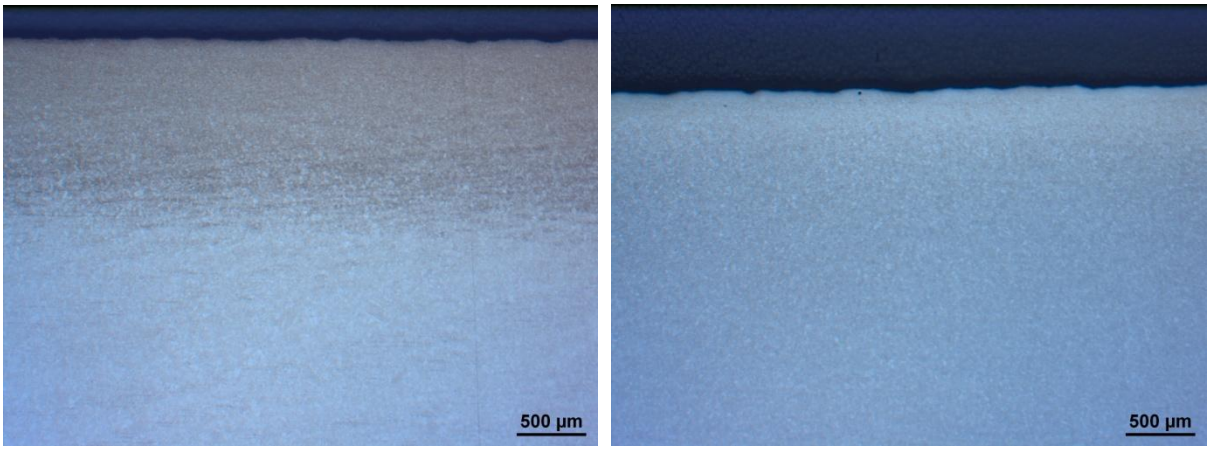

a) **b)**

Figure 34. Low magnitude images of sample 7 (a) and the reference sample (b). Etched in 2% nital.

The samples 1, 2 and 7-11 had similar microstructures, being a transition from high-carbon martensite at the surface to low-carbon martensite in the core. Figure 35 shows the microstructure of sample 1 at 200 µm, 600 µm, 1000 µm and 6000 µm from the surface. The core microstructure is the same as the core microstructure found in the carburized samples from the preliminary project. The samples were etched in nital to reveal the austenite grain boundaries. Corresponding images of samples 2 and 7-11 are shown in Appendix E.

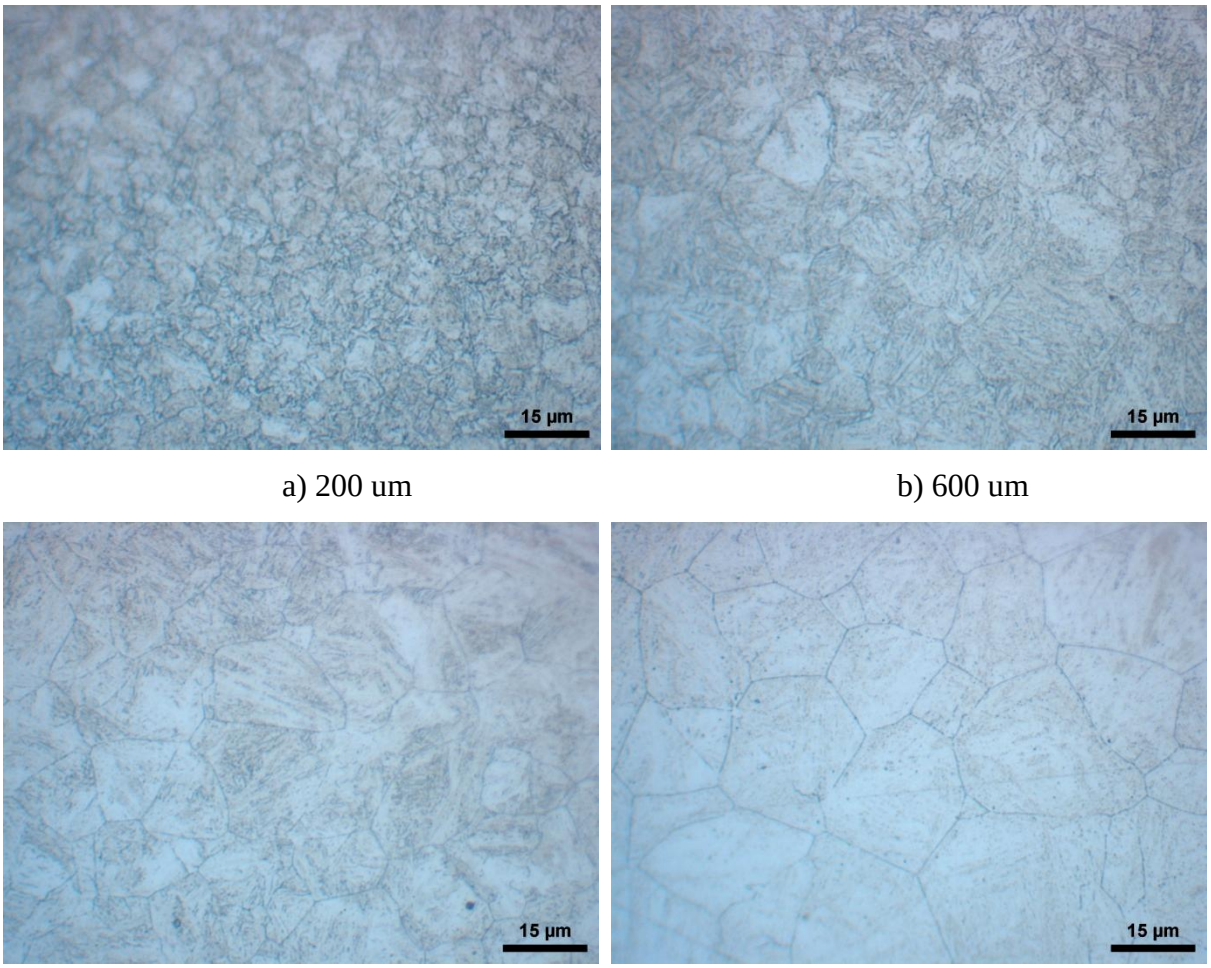

a) 200 um b) 600 um

c) 1000 um d) 6000 um

Figure 35. 100x magnification of sample 1 at 200 µm, 600 µm, 1000 µm and 6000 µm from the surface. Etched in 2% nital.

The samples 3-6 had a similar microstructure as 1, 2, 7-11, at the surface and till approximately 1000 µm below the surface, where the presence of bainite started. The microstructure of the sample core was almost fully bainitic. This is shown in the images of sample 5 in Figure 36. Images of samples 3, 4 and 6 are found in Appendix E. The bainitic microstructure indicates a slow rate of cooling during the final quenching step.

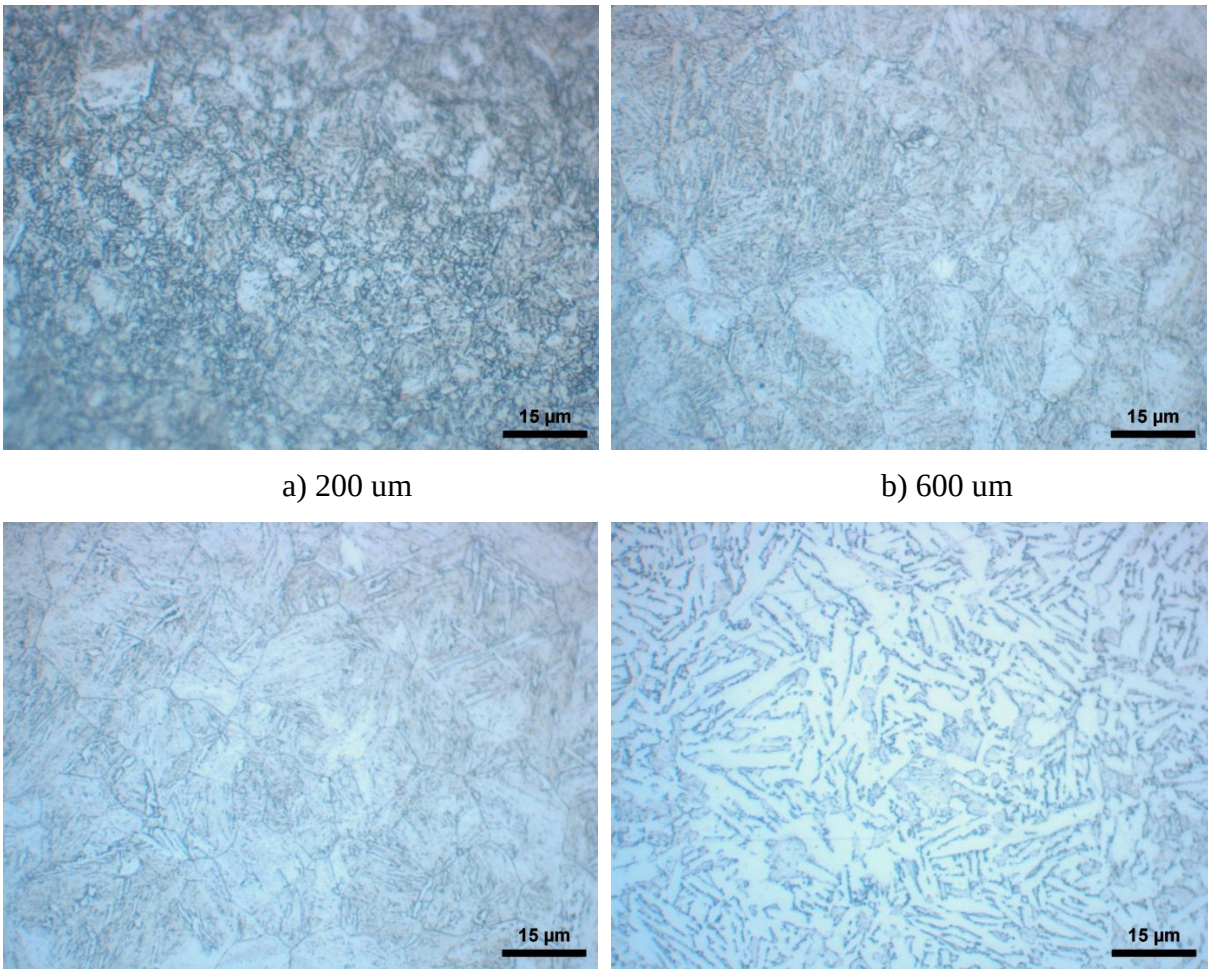

a) 200 um b) 600 um

c) 1000 um d) 6000 um

Figure 36. 100x magnification of sample 5 at 200 µm, 600 µm, 1000 µm and 6000 µm from the surface. Etched in 2% nital.

The microstructure of the original Hardox 450 sample is shown in Figure 37. The images show a transition from very low-carbon martensite at the surface to low-carbon martensite in the core. The very low-carbon microstructure near the surface, Figure 37a, indicates that decarburization had occurred during the processing of the steel plate.

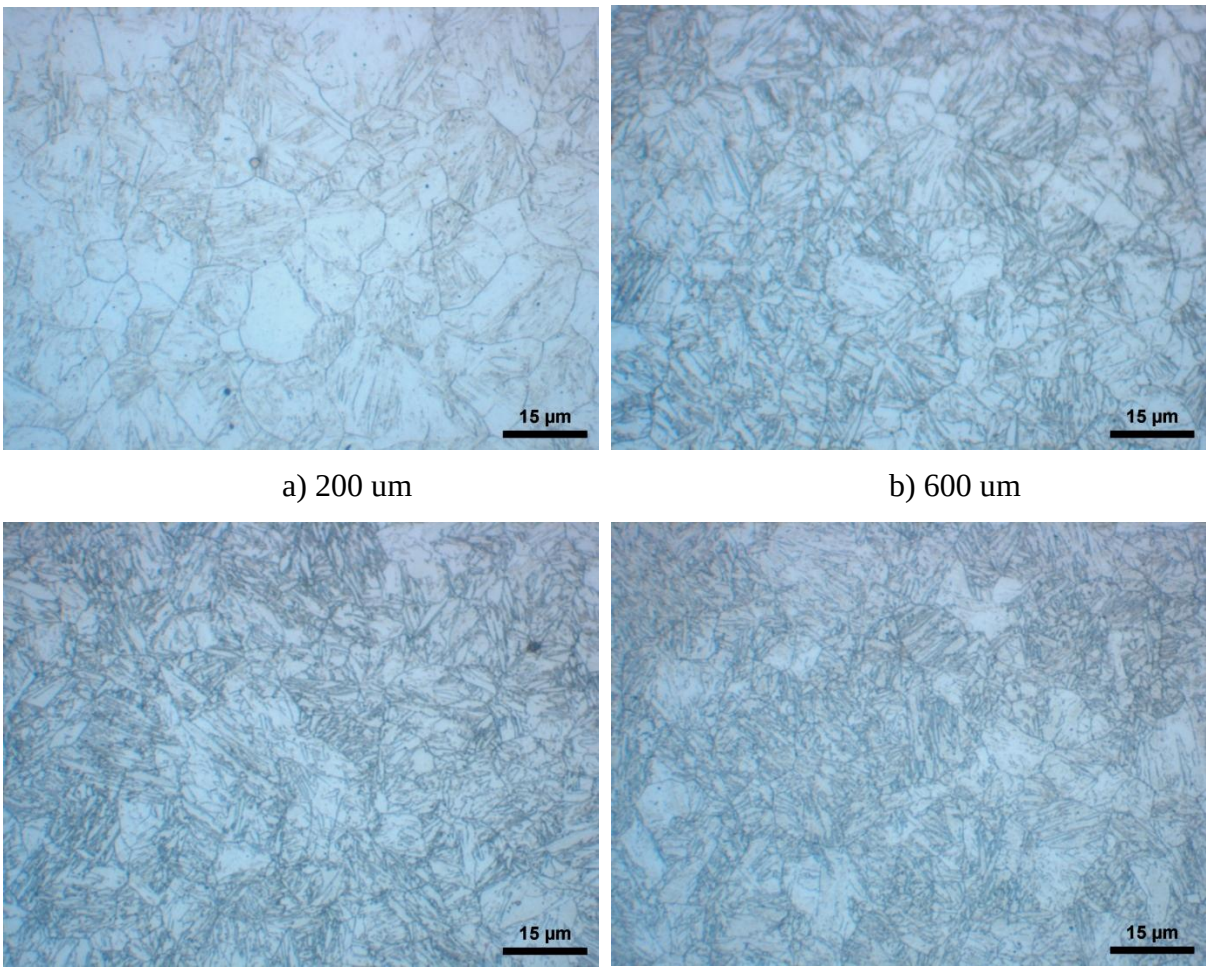

a) 200 um b) 600 um

c) 1000 um d) 6000 um

Figure 37. 100x magnification of the original Hardox 450 sample at 200 µm, 600 µm, 1000 µm and 6000 µm from the surface. Etched in 2% nital.

4.3.5 Grain size

The austenite grain sizes of the case hardened sample cores and the original Hardox 450 sample core are displayed in Figure 38.

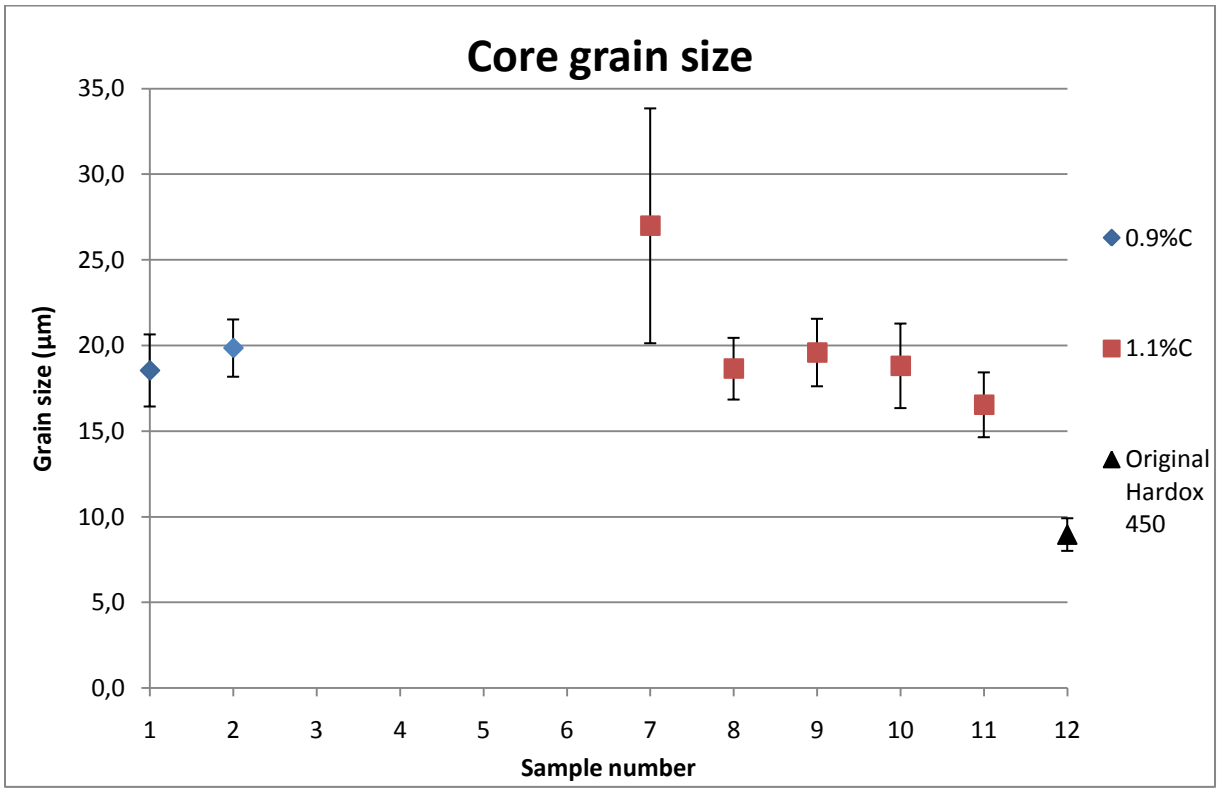

Figure 38. The core grain size of the case hardened samples (1-11) and the original Hardox 450 reference sample (12). The samples 1-6 were case hardened at 0.9% carbon potential, the samples 7-11 were case hardened at 1.1% carbon potential and the reference sample was not case hardened at all.

Samples 1, 2, 8, 9, 10 and 11 all have fairly similar grain sizes ranging from 17 to 20 µm, which was slightly lower than the average core grain sizes of the carburized samples from the preliminary project. The core grain size of the samples 3-6 could not be measured due to the bainitic microstructure. Sample 7 had a large scatter in the measured grain size, and the average grain size was 27 µm, which is significantly larger than the other measured values. The original Hardox 450 stood out from the case hardened samples, with an average grain size of 9.0 µm. The original Hardox 450 core grain size measured in the post-examinations of the preliminary project was 10.0 µm.

5 Discussion

Through this master's thesis and a preliminary project work, the present author has been trying to improve the work performed by Hans Magne Thorseth in his master's thesis, "Optimalisering av stål i beskyttelseskonstruksjoner" [11]. The aim of his work was to improve the ballistic strength of Hardox 450 steel by use of the case hardening process. The results were disappointing, though, as the ballistic strength (measured as ballistic limit velocity) was slightly reduced compared to that of the original Hardox 450. The suspected main contributors to the reduction of ballistic strength of the case hardened Hardox 450 was the too low increase of carbon in the metal surface, and thus too low surface hardness, and a reduction of core hardness from the heat treatment included in the case hardening process.

The objective in the preliminary project was to find optimum case hardening parameters in order to obtain the desired carburizing effect, with resulting hardening of the steel surface and at the same time retain the hardness of the core. Three different carbon potentials, 0.9%, 1.1% and 1.3%, respectively, were tested to see if the carbon content of the metal surface could be successfully increased. Different heat treatments were tested in an attempt to retain the core hardness. The results were split, as carburized layers with hardness of roughly 1000 HV was successfully produced, while the core hardness was reduced in all heat treatments, although some less than others.

However, some questions from the preliminary project work remained. These were answered through work in this master's thesis. EPMA measurements verified that the hardness increase of the metal surface was in fact from an increase in carbon content from the carburization. The microstructures of the carburized samples were identified as martensitic, high-carbon martensite near the surface and low-carbon martensite in the sample core. The uncarburized original Hardox 450 had a low-carbon martensite with significantly smaller grains in the core, which could explain the superior core hardness compared to the heat treated sample cores. Cracks from the surface and in towards the core were discovered on most of the carburized samples. The most and longest cracks were found in the samples that were carburized with 1.3% carbon potential, and therefore it was decided not to proceed with that carbon potential.

Based on information from the preliminary project work, a total of 11 different case hardening courses were selected. Six of the courses were carburized at 0.9% carbon potential, while the five remaining were carburized at 1.1% carbon potential. Of the courses at 0.9%C

potential, one sample was direct hardened, one was single hardened, two were double hardened and two were triple hardened. These samples were numbered 1, 2, 3, 4, 5 and 6 respectively. The single hardening (number 2) and one of the double hardening courses (number 4) were modified, i.e. the last hardening step was from above the A_3 temperature as opposed to traditional hardening where the last hardening step is from above the A_{cm} temperature, but still below the A_3 temperature. This was done as the modification would grain refine the whole cross-section of the metal instead of only the surface layer. All hardening courses, except one of the triple hardenings (number 6), included deep quenched at -72 °C after the last hardening step. The one triple hardened course did not include deep quenching to see whether the deep quenching made any difference. Of the courses at 1.1%C potential, one sample was direct hardened, one was single hardened, one was double hardened and two were triple hardened. These samples were numbered 7, 8, 9, 10 and 11, respectively. All hardening steps for these samples were modified, since the A_{cm} temperature at 1.1%C is approximately the same as the A_3 temperature, making it difficult to accomplish hardening between the two temperatures. Again, one of the triple hardenings (number 11) did not include deep quenching after the last hardening step, as opposed to the rest.

Due to capacity problems, the plates that were going to be case hardened were sandblasted to remove the corrosion resistant primer on the plates, instead of being ground as in the preliminary project. As the sandblasting would remove the allegedly carburization-preventing primer, this was seen as a satisfying solution. This would prove to be detrimental.

The core hardness measurements gave similar results as in the preliminary project, i.e. the original Hardox 450 had the highest hardness value, with an average of 475 HV. The results from the case hardened samples were divided. The samples 3-6 had core hardness values ranging from 266 HV to 308 HV, the samples 1, 2, 9-11 had core hardness values ranging from 411 HV to 425 HV, while the samples 7 and 8 had hardness values of 451 HV and 455, respectively. The low hardness values of the samples 3-6 was due to a bainitic microstructure, which will be discussed later. The samples 1, 2, 7-11 had hardness values a little lower than measured in the preliminary project, where the core hardness values varied between approximately 425 HV and 475 HV. The reason for this difference might be that in the preliminary project the samples were small, approximately 1 cm^3, and quenched in water at room temperature, in difference to in this thesis work where the samples were 30×30×1.2 cm^3 and quenched in oil at 70-80 °C. This would give a higher cooling rate in the preliminary project work experiments, and thus harder metal. Each hardening step was 30 minutes longer

in this thesis work than in the preliminary project, due to local practice at Bandak Raufoss. This might have had an effect on the hardness as well.

Low magnification microscopy of samples 1-11 clearly showed the carburized layers on the sample surfaces. High magnification showed a gradual transfer from high-carbon martensite at the surface to a low-carbon martensite in the core of the samples 1, 2, 7-11. The samples 3-6 had similar microstructures as samples 1, 2, 7-11 down to approximately 1000 µm below the surface. From there, bainite started to form, and in the core, the microstructure was almost fully bainitic. This explained the very low hardness values that were measured for these samples. The presence of bainite indicates a (too) slow rate of cooling. The reason for the slow cooling rate is unknown, however, no bainite was formed in the 1.1%C samples with similar hardening courses, which showed that the quenching at 70-80 °C before deep quenching at -72 °C was sufficient for martensite formation. High magnification of the original Hardox 450 reference sample showed a low-carbon martensite in the sample core. At the surface, the outer 100-200 µm was very light in color, suggesting decarburization, which was indicated by hardness measurements as well.

The core grain size of the samples 1, 2, 7-11 and the reference sample was measured. The core grain size of the samples 3-6 could not be measured due to the bainitic microstructure. The samples 1, 2, 8-11 had core grain sizes ranging from 17 µm to 20 µm, which was slightly lower than the core grain sizes measured in the preliminary project that ranged from 20 µm to 22 µm. Sample 7 (from this thesis), however, had very large grains compared to the other samples, with an average core grain size of 27 µm, and ranging from 16 µm to 39 µm. The reference sample clearly stood out from the case hardened samples with an average core grain size of 9 µm, which was similar to the preliminary project measurement of 10 µm. The importance of the grain size difference is unclear. Smaller austenite grains could give more ductile steel. However, this was examined by Torseth, and his experiments showed that heat treatments simulating direct case hardening at both 910 °C and 940 °C for 6 hours gave more ductile material than the original Hardox 450, despite larger grains [11]. The ductility was tested by normal tensile testing, though, and the ductility of a material may change with increasing strain rate, as in ballistic experiments. If the grain size is a key parameter, case hardening at 880 °C for 6 hours might be worth testing, as the grain growth at this temperature is far less than for 910 °C and 940 °C [11].

Hardness measurements of the case hardened metal surfaces revealed significantly lower hardness increases from the carburization than obtained in the preliminary project. The

hardest sample was sample 10 with a hardness value of 735 HV, followed by sample 9 with a hardness value of 730 HV. Sample 7 had the softest surface of the samples that were carburized at a carbon potential of 1.1% (7-11), its hardness value was 684 HV. In comparison, the sample that was carburized at 1.1%C in the preliminary project had hardness values over 1000 HV. The results from the samples that were carburized at 0.9% carbon potential were split, as samples 2 and 4 had hardness values of 661 HV and 702 HV, respectively, and the hardness values of the samples 1, 3, 5 and 6 were 559 HV, 593 HV, 612 HV and 588 HV, respectively. All these results represent significant reduction of hardness compared to the preliminary project, where the samples that were carburized at 0.9% carbon potential reached hardness values of almost 900 HV. However, hardening above the A_3 temperature might be positive for the hardening process, as indicated by the superior hardness of samples 2 and 4 compared to 1, 3, 5 and 6. Sample 1 was deep quenched from 940 °C, though, but as the hardening steps were carried out in carburizing atmosphere, the other samples were carburized for a longer time. This would apply for sample 7 as well. Also, sample 5 was somewhat harder than sample 6. Both these samples were triple hardened, and the only difference was that sample 6 was not deep quenched at -72 °. The same could be seen for the samples 10 and 11.This indicates that deep quenching might also be positive for the hardening process. The hardness values of samples 3-6 decreased to between 270-284 HV at a position 2500 µm below the surface due to the bainitic core. The hardness of samples 1, 2, 7-11 decreased to between 417 HV and 435 HV at a position 2500 µm into the material. The surface hardness of the original Hardox 450 reference sample was very low 50 µm below the surface, 263 HV. It increased to 478 HV at a depth of 200 µm below the surface, and from there the hardness value varied between 449-498 HV down to 2500 µm below the surface. The soft outermost parts of the surface could also indicate decarburization of the metal.

The reason for the far lower surface hardness increases in this work than in the preliminary project experiments is believed to be connected to the decarburization of the original Hardox 450. Surface hardness measurements performed by Torseth in his master's thesis also showed a drop in the hardness in the outer parts of the surface [11]. If the sample surfaces were decarburized prior to the case hardening, the carburizing gas had to "refill" the steel to its original carbon content, before starting the actual carburization, i.e. the real carburizing time would be less than the planned 6 hours. The grinding performed in the preliminary project work removed the decarburized layer, so that carburization above the original carbon contents would start at once and thus give the planned 6 hours of

carburization. With the desired carbon contents in the surface comes the desired hardness values, which were successfully obtained in the preliminary project.

The ballistic experiments gave disappointing results. The ballistic limit velocity of the original Hardox 450 target plate was calculated to be 797 m/s, while the highest ballistic limit velocity of the case hardened plates was calculated to be 787 m/s (improvement from Torseth's thesis) and the lowest was calculated to be 710 m/s. The core hardness seemed to be a key factor, as samples 3-6 with the soft bainitic core microstructure gave the lowest ballistic limit velocities, ranging from 710 m/s to 728 m/s. However, for samples 1, 2, 7 and 8, the core hardness did not seem decisive, as sample 1 had higher ballistic limit velocity, 779 m/s, than sample 2, 770 m/s, and at the same time sample 7 had higher ballistic limit velocity, 787 m/s, than sample 8, 767 m/s, although samples 2 and 8 had higher core hardness than samples 1 and 7. The results from samples 1 and 7, which went through the same treatment apart from the carburizing potential, suggest that carburizing at 1.1% carbon potential gives better ballistic properties than carburizing at 0.9% carbon potential, however, sample 7 had the highest core hardness of the two as well. Sample 10 had the second highest ballistic limit velocity of the case hardened samples despite the near equal core hardness to samples 2, 9 and 11, suggesting that a hard surface could be beneficial. Samples 1 and 7 (direct hardening, 0.9%C and 1.1%C) had the highest and the 3rd highest ballistic limit velocities, suggesting that direct hardening gave the best ballistic properties despite the relatively low surface hardness.

Examinations of the penetration zones after the ballistic experiments revealed another key discovery. The carburization of the rear side of the target plates seemed to have a negative effect as the carburized zones had a tendency to crack up, with crack propagation in the transition zone between carburized and uncarburized steel. This could explain why the direct hardened samples had better ballistic properties than the samples with additional hardening steps, as the direct hardened samples have relatively low surface hardness and thus less chance of cracking. This kind of cracking was not seen in the original Hardox 450 reference sample. From the projectile exit-holes it seems that samples 3-6 experienced radial fracture with possibly some ductile hole growth. Samples 1, 2, 7-11 seemed to have experienced radial fracture with considerable fragmentation. The reference sample showed signs of fragmentation only. By microscopy of the samples 1, 6, 10 and the reference sample, adiabatic shear bands (ASB) were found in all of them, with far more in 1, 10 and the

reference sample than in sample 6. This corresponds to the theory, as ductile materials have less chance of ASB development than harder materials.

When calculating the hardness profile integral values of all the samples, it turned out that the original Hardox 450 sample did not have the highest integral value. In fact, all of the samples 1, 2, 7-11 and the reference sample had integral values within ± 5% of each other. This does not correspond with the ballistic limit velocity calculations. However, the cracks of the case hardened samples could explain this because if the rear side of the target plate cracks before the projectile has completely perforated the plate, the projectile will actually have less distance to travel in the case hardened plates. This could explain why the direct hardened samples 1 and 7, with relatively low surface hardness, have the best and the 3rd best ballistic limit velocity as well. If removing the outermost 1 mm from the case hardened target plate rear side in the hardness integral calculations, the hardness integral of the reference sample will be significantly higher than that of the case hardened samples, and this corresponds well with the ballistic limit velocity calculations.

Summarized, a lot of factors proved to be important for the ballistic properties of the case hardened steel. Core hardness, surface hardness and the tendency to cracking seemed the most important. For further work it is strongly recommended to grind the target plates at least 200 µm on each side. This is particularly important for the front side where the projectile impacts. In addition, case hardening of the front side only is recommended, as this probably will reduce the cracking on the rear side. Most of the case hardening courses is recommended for further work, to determine the properties of the different hardening methods with the previously mentioned improvements. Case hardening at 880 °C to reduce grain size is also interesting for further testing.

6 Conclusion

The objective of this master's thesis has been to increase the ballistic properties of Hardox 450 by case hardening. The work is based on previous work done by other authors, as well as a preliminary project work by the present author.

From the preliminary project results it seemed possible to produce case hardened steel with surface hardness values over 1000 HV, and core hardness values around 470 HV, compared to the original Hardox 450 with surface and core hardness of approximately 475 HV. The changes introduced by the case hardening were believed to be sufficient to improve the ballistic limit velocity of the steel.

Based on the preliminary project results, 11 case hardening courses were selected for experiments. Six courses included a carbon potential of 0.9% and five courses employed a carbon potential of 1.1%. Different hardening courses were tested, including direct hardening, a modified single hardening process and traditional and modified versions of double and triple hardening. Prior to the case hardening, a corrosion-resistant primer on the original Hardox 450 was removed by sandblasting, instead of by grinding as in the preliminary project.

The ballistic experiments revealed reductions of the ballistic limit velocity of the case hardened samples compared to the original Hardox 450, as was also the case in Torseth's thesis. The reduction was from approximately 800 m/s for the original Hardox 450 to approximately 787 m/s for the best case hardened steel. This reduction was less than in Torseth's experiments, where approximately 770 m/s was the best ballistic limit velocity obtained.

The average core hardness of the original Hardox 450 plate was measured to be 475 HV. The core hardness measurements of the case hardened samples were in the range of 411-455 HV which is a decrease compared to the hardness value of the original Hardox 450 and also compared to most of the values obtained in the preliminary project. Four samples carburized at 0.9% carbon potential had indeed core hardness averages as low as 266-308 HV. This was due to bainite instead of martensite in the sample cores. The presence of bainite indicated a too slow rate of cooling for these four plates.

Hardness measurements of the case hardened steel surfaces revealed significantly lower hardness increases from the carburization than what was obtained in the preliminary project. The surface hardness values ranged from 588 HV to 735 HV, compared to hardness

values of over 1000 HV in the preliminary project. Surface hardness measurements and microscopy examinations revealed surface decarburization of the original Hardox 450. In contrary to in the preliminary project where this was ground away, the sandblasting did not remove the decarburized layer. Due to this, the case hardening did not have the desired effect on the steel surface, resulting in a too low surface hardness. Yet, some results seemed possible to extract from the experiments. The samples that were carburized at 1.1% carbon potential had somewhat higher surface hardness values than the samples carburized at 0.9% carbon potential. The modified hardness courses, where the final hardening step was at temperatures above the A_3 temperature seemed positive for the surface hardness increase. Deep quenching at -72 °C might also have a positive effect on the surface hardness increase, compared to quenching in oil at 70-80 °C alone.

However, the original Hardox 450 did not have the highest cross-section hardness integral value, despite the relatively low surface and core hardness values of the case hardened samples. Penetration zone examinations revealed cracks in the carburized layer on the rear side of the target plates. The cracks seemed to propagate in the transition area between carburized and uncarburized steel. The cracks were probably a result of the harder and thus more brittle steel caused by the carburization, as similar cracks was not seen in the original Hardox 450 reference plate. This might be the reason for the superior ballistic limit velocity of the original Hardox 450 compared to the case hardened samples, despite the similar cross-section integral value. If the rear side of the case hardened plates cracks in front of the projectile, the projectile will have less steel to travel through before perforation, and therefore the carburized layer will not lower the projectile velocity as much as the more intact original Hardox 450 plate.

Recommendations for further work include grinding of the Hardox 450 surface to remove the decarburized surface layer before case hardening. This will probably make sure the carburization goes as planned. No case hardening of the rear side of the target plate is recommended as this will probably limit the crack growth.

7 Acknowledgements

I would like to express my gratitude towards my supervisors, Professor Jan Ketil Solberg at the Department of Materials Science and Engineering and Professor II Tore Børvik at the Department of Structural Engineering.

I would also like to express my gratitude towards Pål Ulseth, from the Department of Materials Science and Engineering, Trond Auestad and Tore Wisth, both from the Department of Structural Engineering, for their aid during the semester.

The financial support of this work from the Centre for Research-based Innovation (CRI) is gratefully acknowledged.

8 References

[1] www.smallarmssurvey.org

[2] T. Børvik, S. Dey, A. H. Clausen, "Perforation resistance of five different high-strength steel plates subjected to small-arms projectiles", International Journal of Impact Engineering 36 (2009) 948-964, 2008.

[3] T. Børvik, A. H. Clausen, M. Eriksson, T. Berstad, O. S. Hopperstad, M. Langseth, "Experimental and numerical study on the perforation of AA6005-T6 panels", International Journal of Impact Engineering 32 (2005) 35-64, 2005.

[4] R. Klement, S. Rolc, R. Mikulikova, J. Krestan, "Transparent armour materials", Journal of the European Ceramic Society 28 (2008) 1091-1095, 2007.

[5] G. Cooper, P. Gotts, "Ballistics Protection", 2005.

[6] B. A. Gama, T. A. Bogetti, B. K. Fink, C. Yu, T. D. Klaar, H. H. Eifert, J. W. Gillespie Jr., "Aluminium foam integral armor: a new dimension in armor design", Composite Structures 52 (2001) 381-395, 2005.

[7] S. M. Walley, J. E. Field, P. W. Blair, A. J. Milford, "The effect of temperature on the impact behavior of glass/polycarbonate laminates", International Journal of Impact Engineering 30 (2004) 31-53, 2003.

[8] Howard E. Boyer, "Case Hardening of Steel", ASM INTERNATIONAL, Metals Park, Ohio, 1987.

[9] Jan Ketil Solberg, "TEKNOLOGISKE METALLER OG LEGERINGER", Kompendium, kap. 1.15, Department of Materials Science and Engineering, Norwegian University of Science and Technology, Trondheim, 2008.

[10] D. C. Lou, J. K. Solberg, T. Børvik, "Surface strengthening using a self-protective diffusion paste and its application for ballistic protection of steel plates", Materials and Design 30 (2009) 3525-3536, 2009.

[11] Hans Magne Thorseth, "Optimalisering av stål i beskyttelseskonstruksjoner", Department of Materials Science and Engineering, Norwegian University of Science and Technology, Trondheim, 2010.

[12] Johnson JB, Daniels S. "Process of manufacture of armour plate", US patent, No. 1563420, 1925.

[13] Karst DA, Pawlowski KFR, Warren WA., "Case-hardened plate armour and method of making", US patent, No. 4857119, 1989.

[14] www.ssab.com/en/Brands/Hardox/Products-2/

[15] T. Børvik, "Ballistic penetration and perforation of steel plates", Dr. ing. Thesis, Department of Structural Engineering, Norwegian University of Science and Technology, Trondheim, 2000.

[16] J. Zukas (Editor), "Impact Dynamics", John Wiley and Sons, Inc., 1982.

[17] M. E. Backman, W. Goldsmith, "The mechanics of penetration of projectiles into targets", International Journal of Engineering Science 16 1-99, 1978.

[18] M. E. Backman, Naval Weapons Center, NWC TP 578, 1976.

[19] Tor Arne Buberg, "Case hardening of Hardox 450 steel for increased ballistic strength", Project report, Department of Materials Science and Engineering, Norwegian University of Science and Technology, 2010.

[20] http://www.ipsen.de/en/Heattreatment-Products/AtmosphereTechnology/Atmosphere-furnace-TQ2.htm

Appendix

A. EPMA results from the preliminary project work

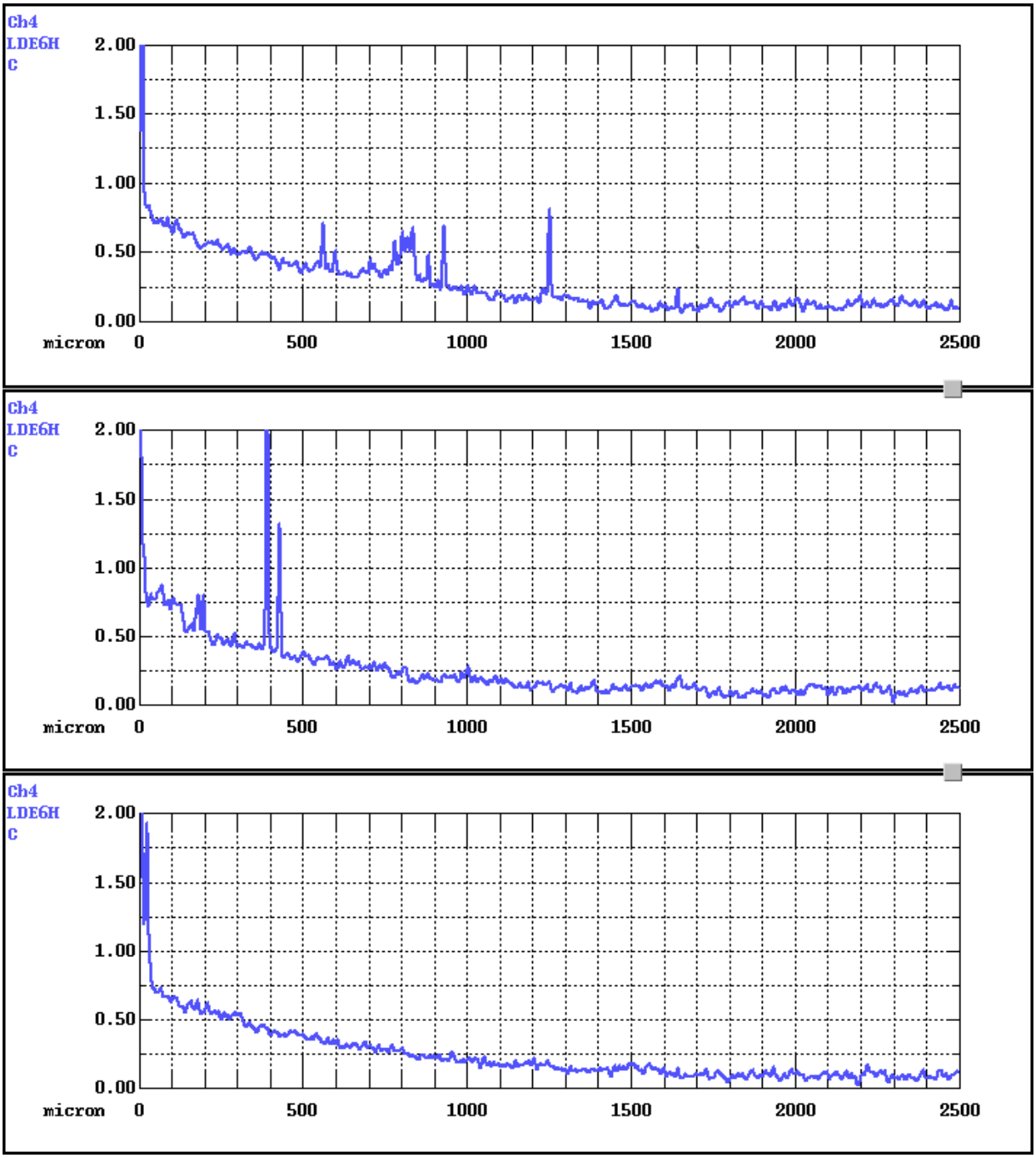

Figure A. The results from the EPMA examination of sample 0.9A. Three parallels line analyses were carried out. The x-axis shows the distance from the sample surface in µm. The y-axis shows the carbon content in atomic%.

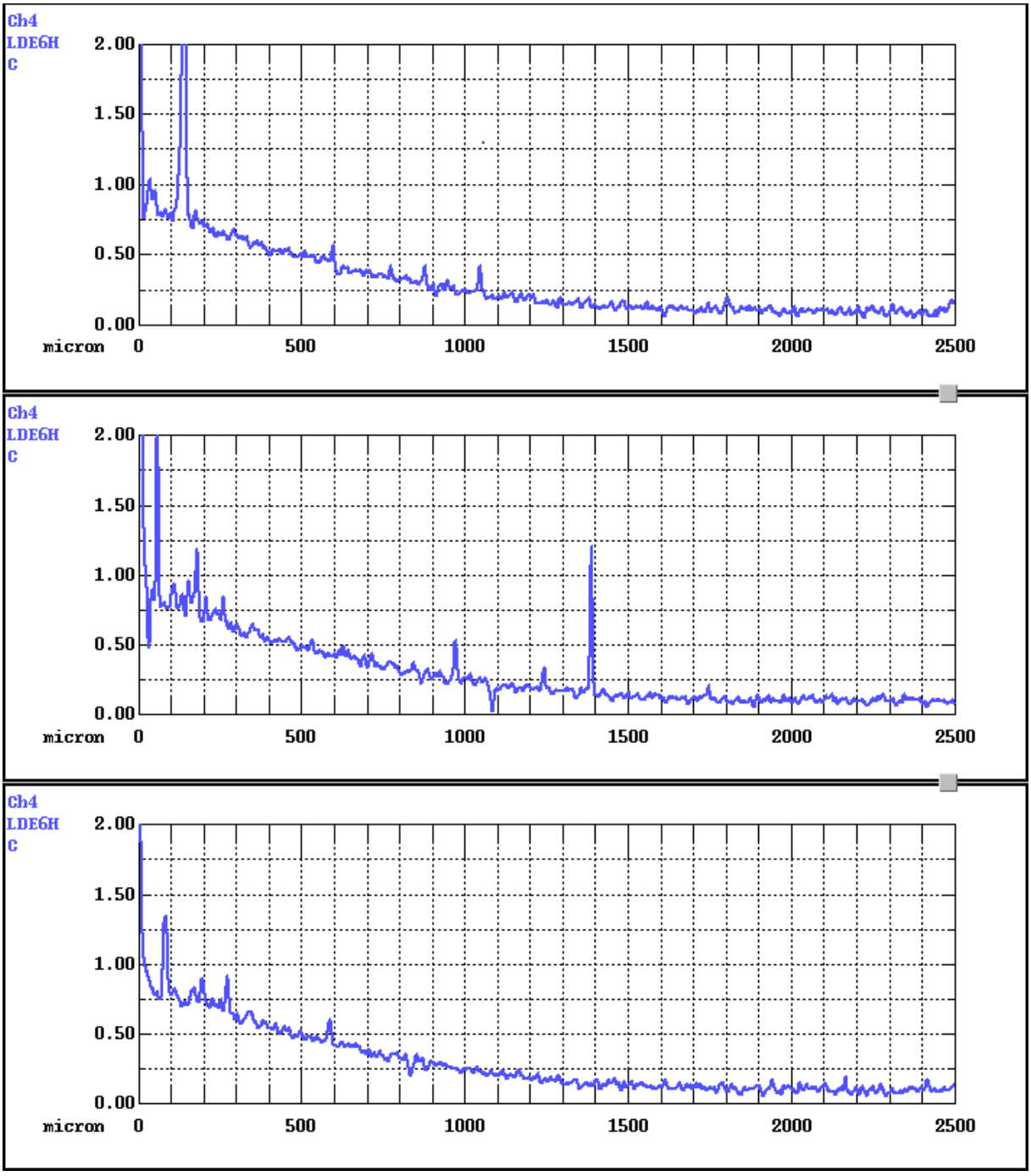

Figure B. The results from the EPMA examination of sample 0.9B. Three parallels line analyses were carried out. The x-axis shows the distance from the sample surface in µm. The y-axis shows the carbon content in atomic%.

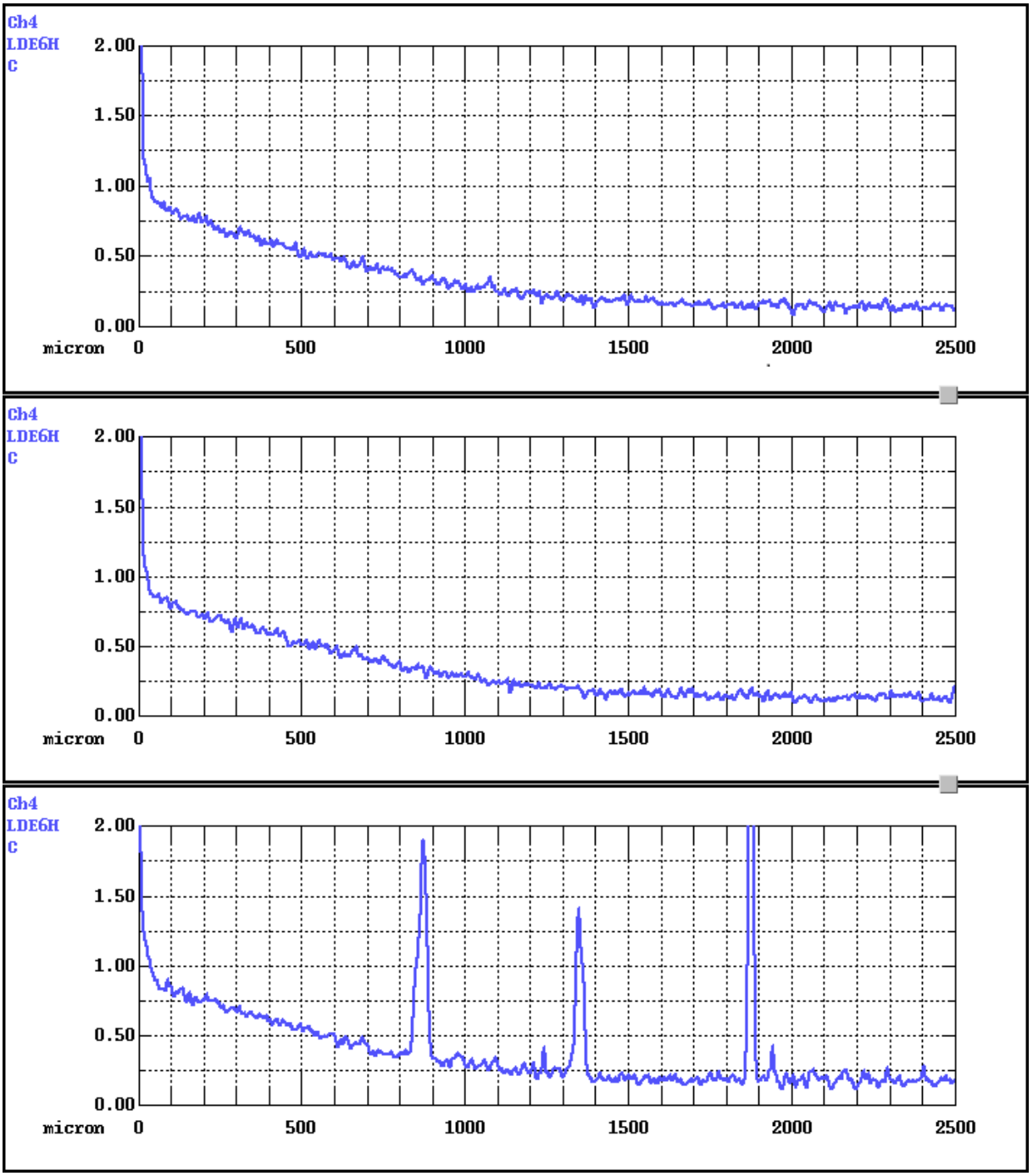

Figure C. The results from the EPMA examination of sample 0.9C. Three parallels line analyses were carried out. The x-axis shows the distance from the sample surface in µm. The y-axis shows the carbon content in atomic%.

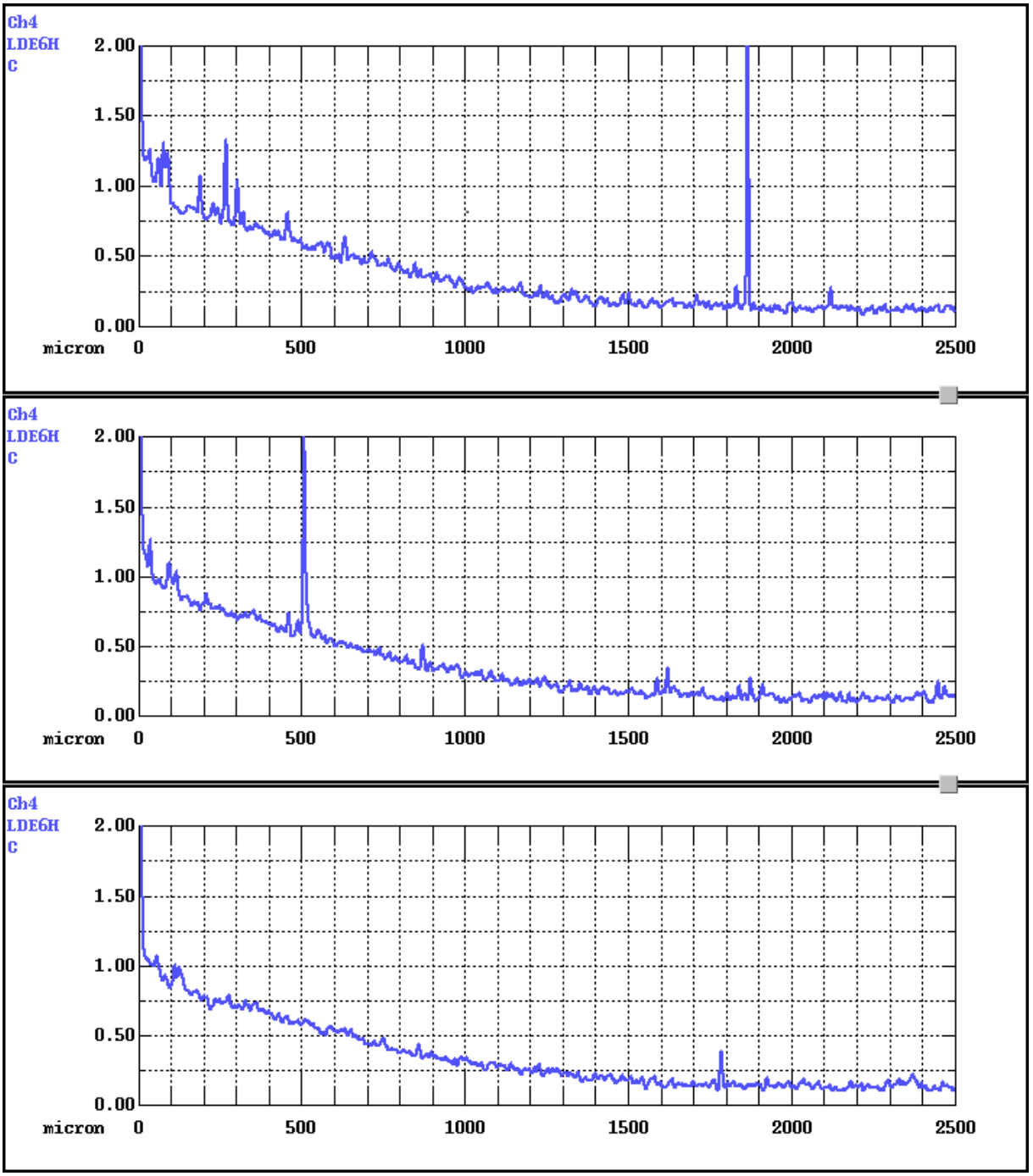

Figure D. The results from the EPMA examination of sample 1.1. Three parallels line analyses were carried out. The x-axis shows the distance from the sample surface in µm. The y-axis shows the carbon content in atomic%.

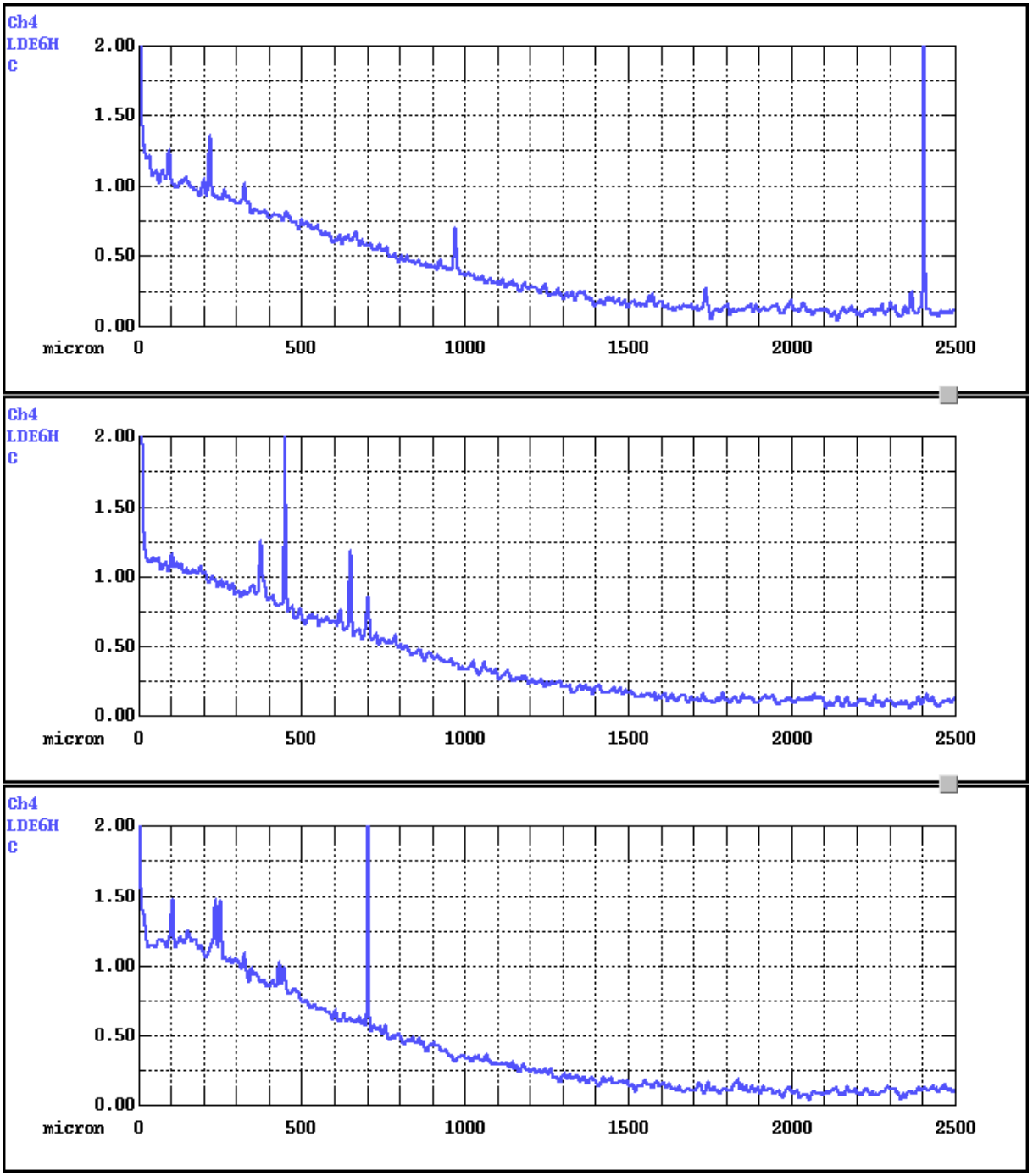

Figure E. The results from the EPMA examination of sample 1.3A. Three parallels line analyses were carried out. The x-axis shows the distance from the sample surface in µm. The y-axis shows the carbon content in atomic%.

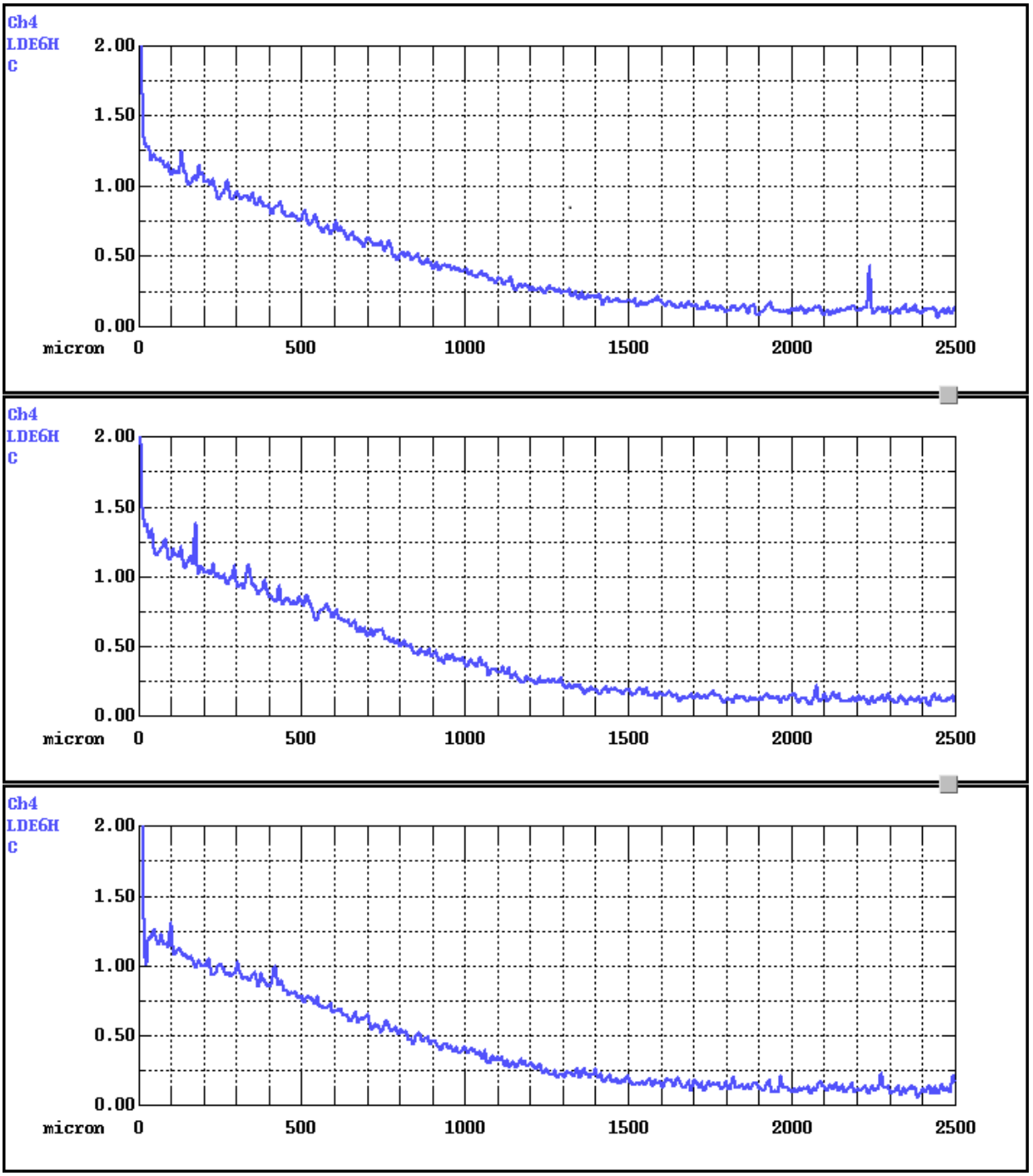

Figure F. The results from the EPMA examination of sample 1.3B. Three parallels line analyses were carried out. The x-axis shows the distance from the sample surface in µm. The y-axis shows the carbon content in atomic%.

B. Projectile entry and exit holes of the target plates

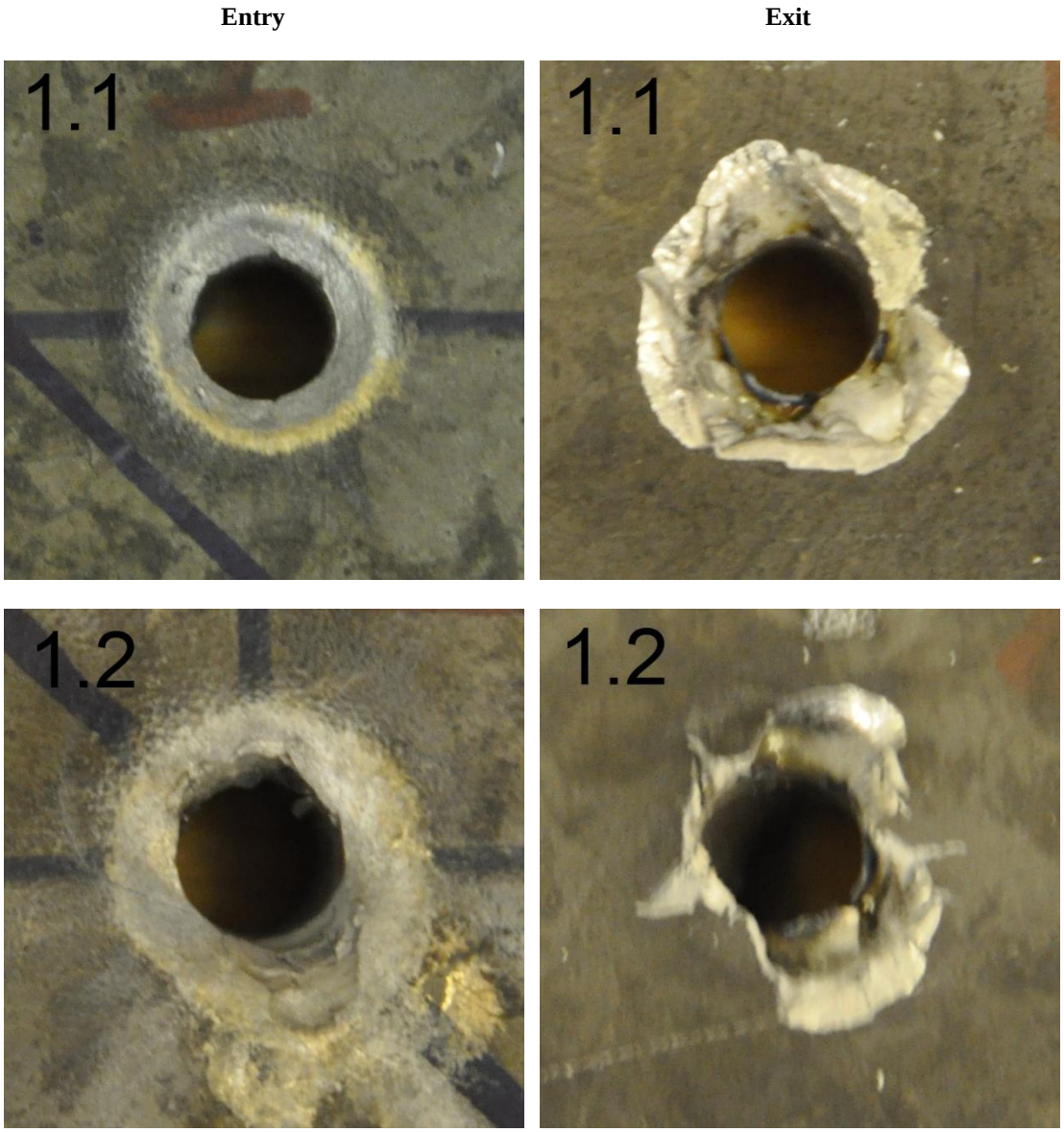

Figure G. Projectile entry and exit holes for shots 1 and 2 on sample 1

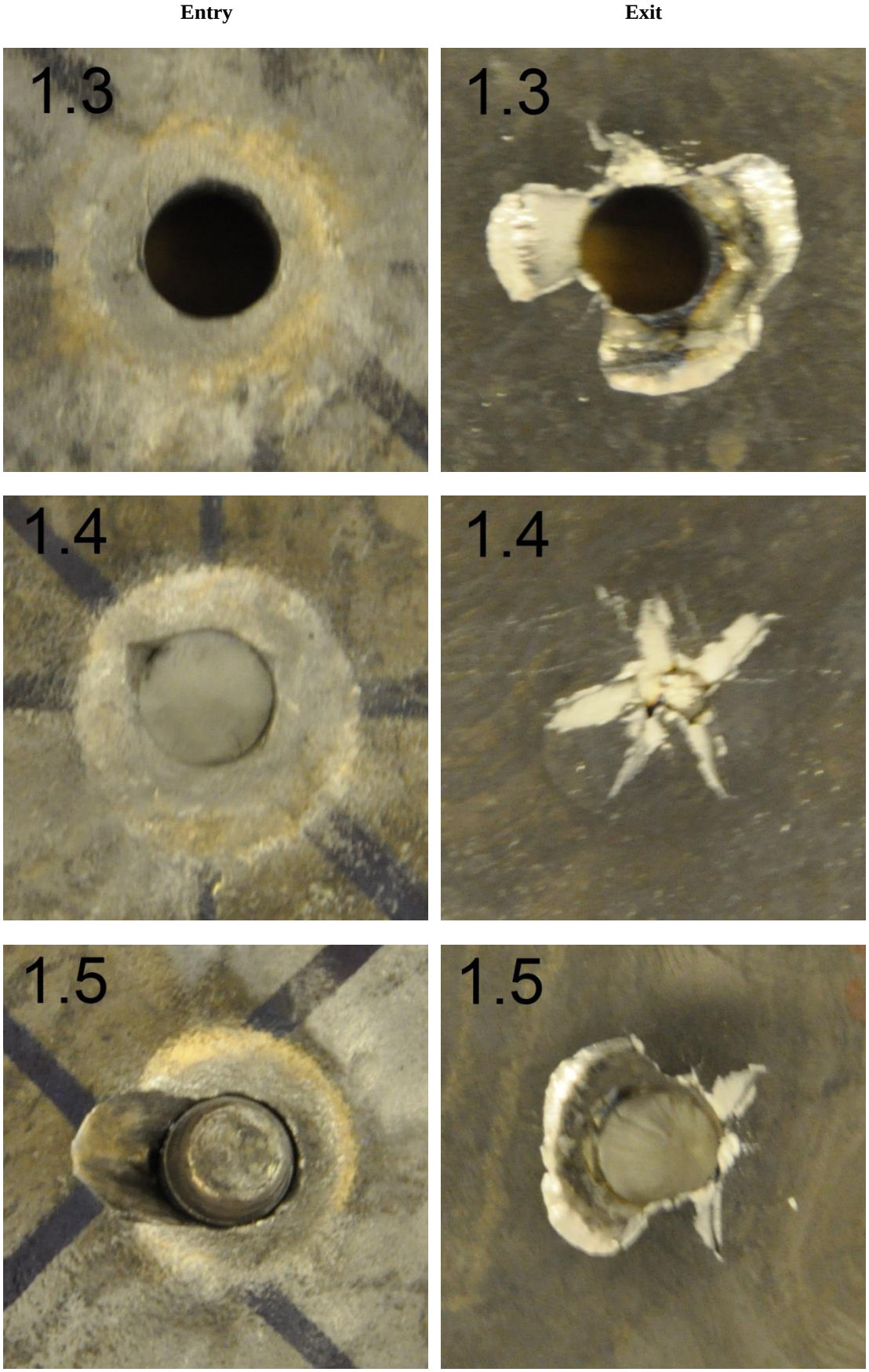

Figure H. Projectile entry and exit holes for shots 3, 4 and 5 on sample 1.

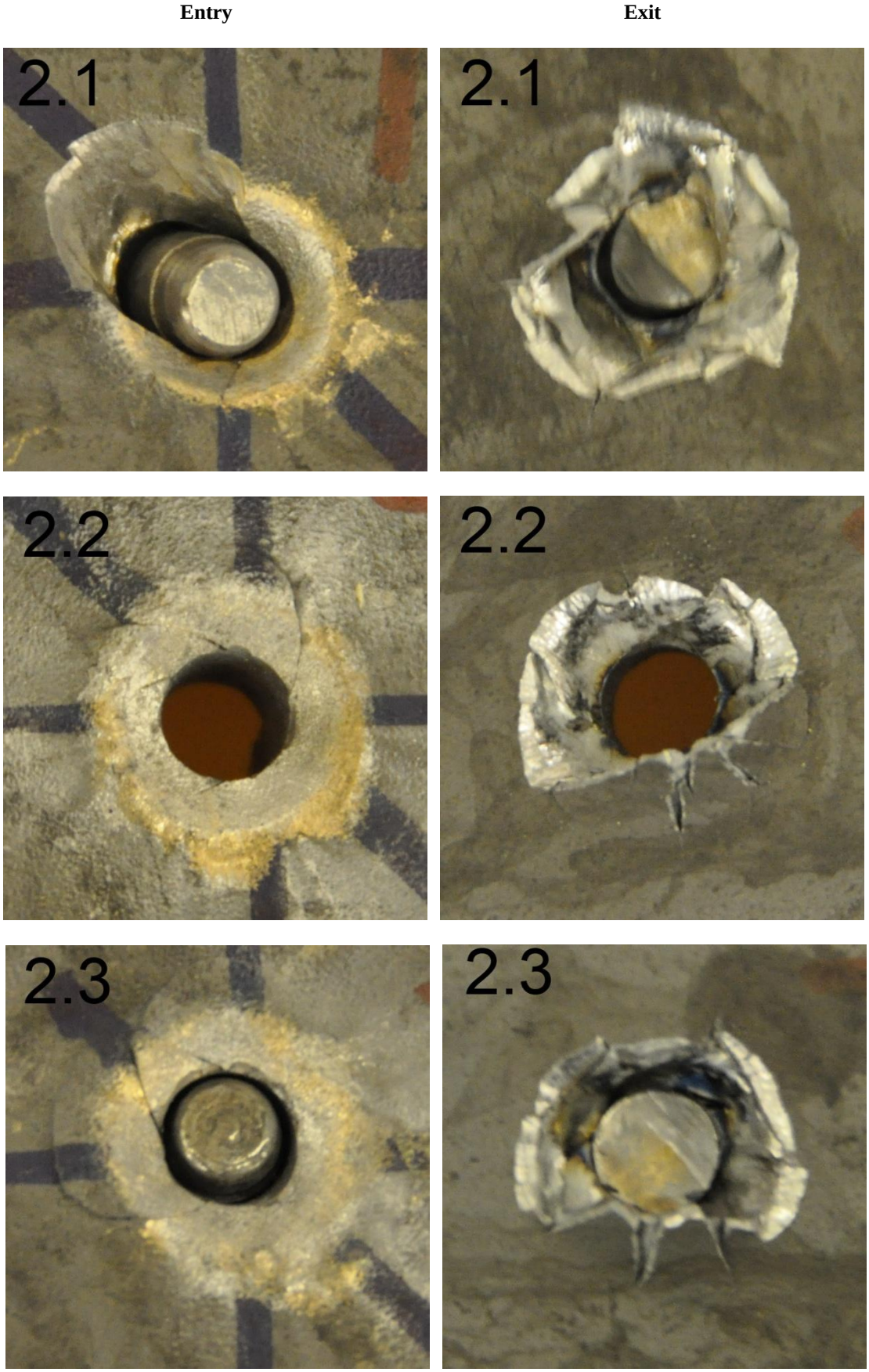

Figure I. Projectile entry and exit holes for shots 1, 2 and 3 on sample 2.

Entry **Exit**

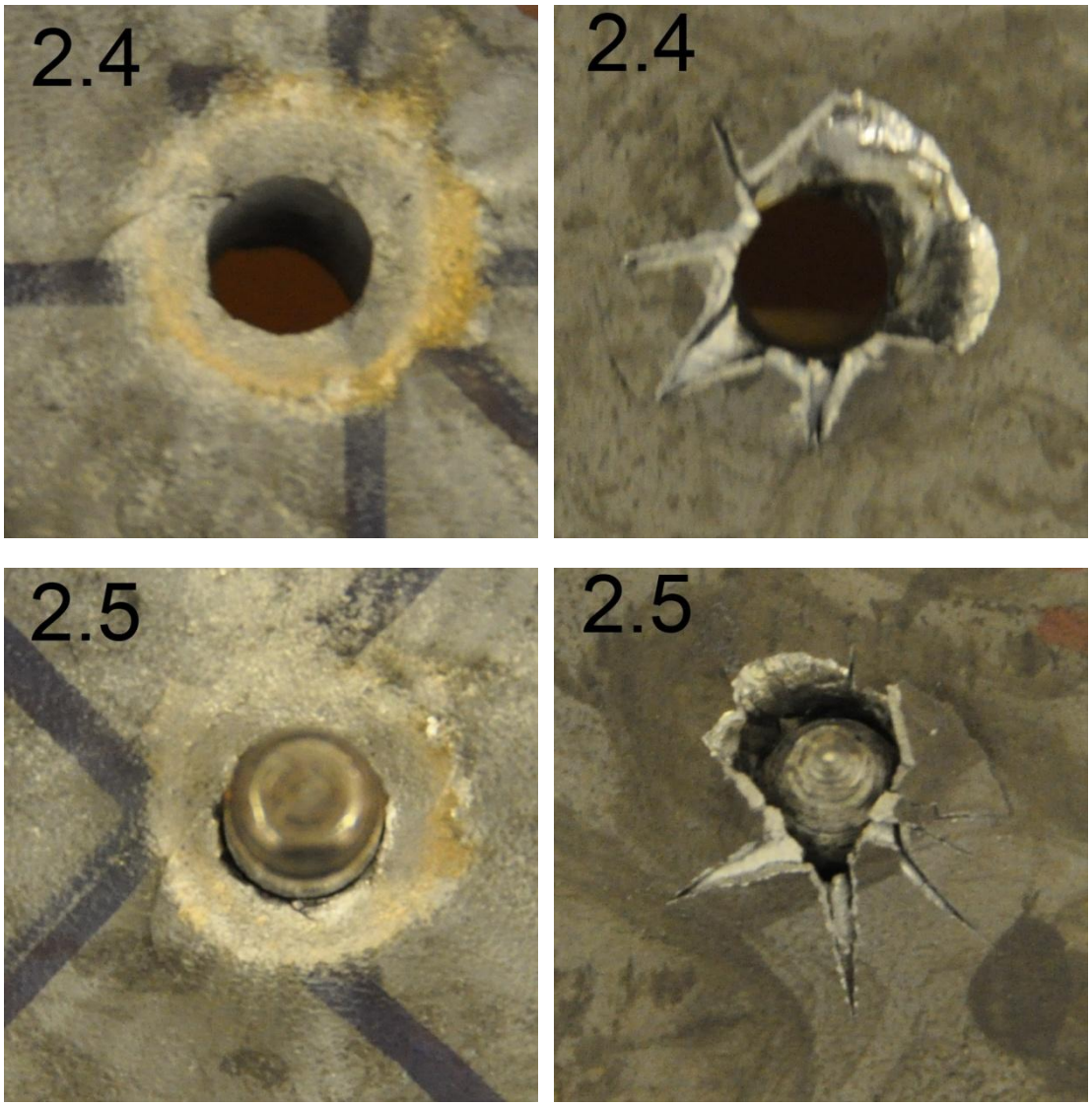

Figure J. Projectile entry and exit holes for shots 4 and 5 on sample 2.

Entry **Exit**

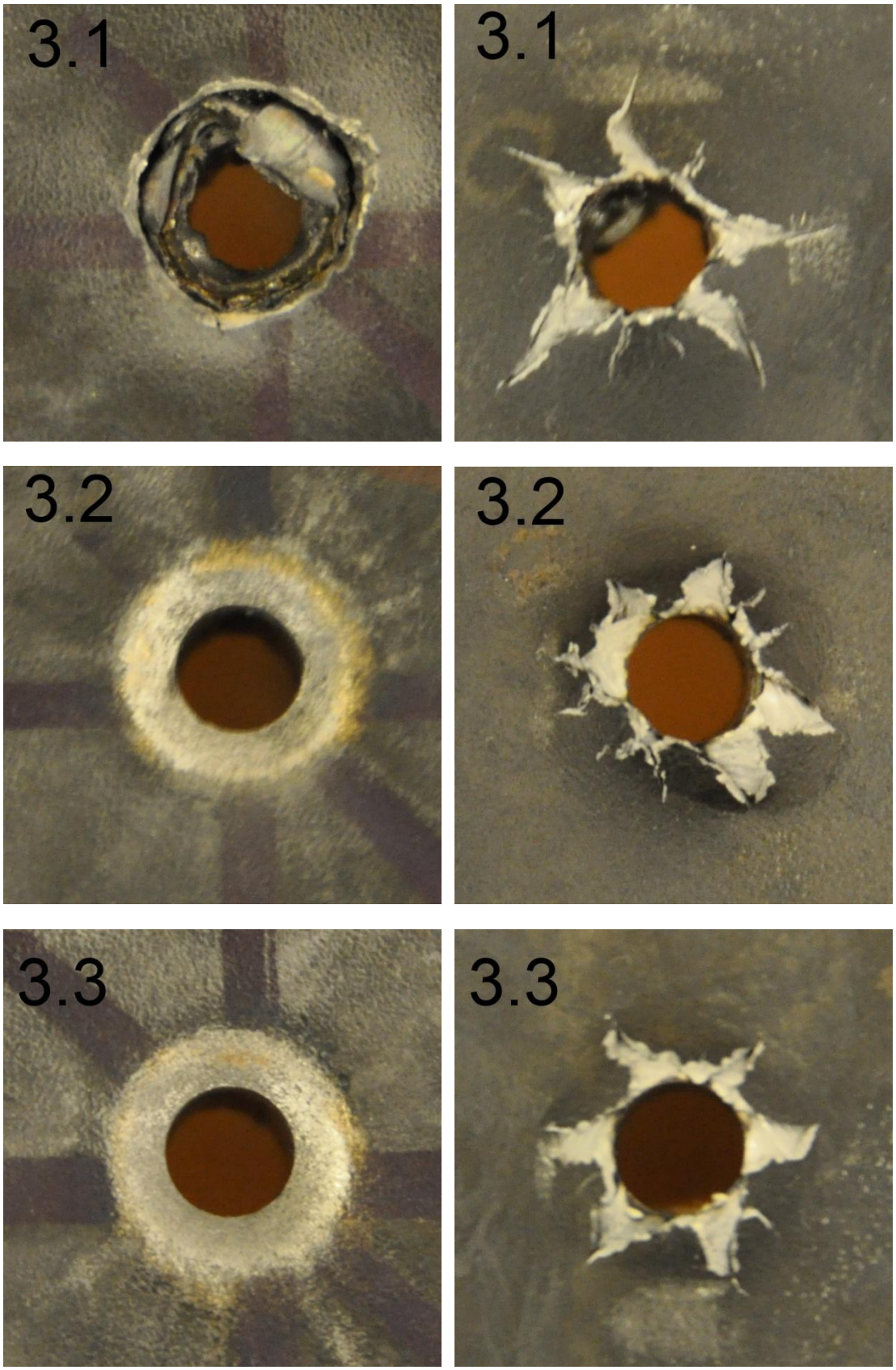

Figure K. Projectile entry and exit holes for shots 1, 2 and 3 on sample 3.

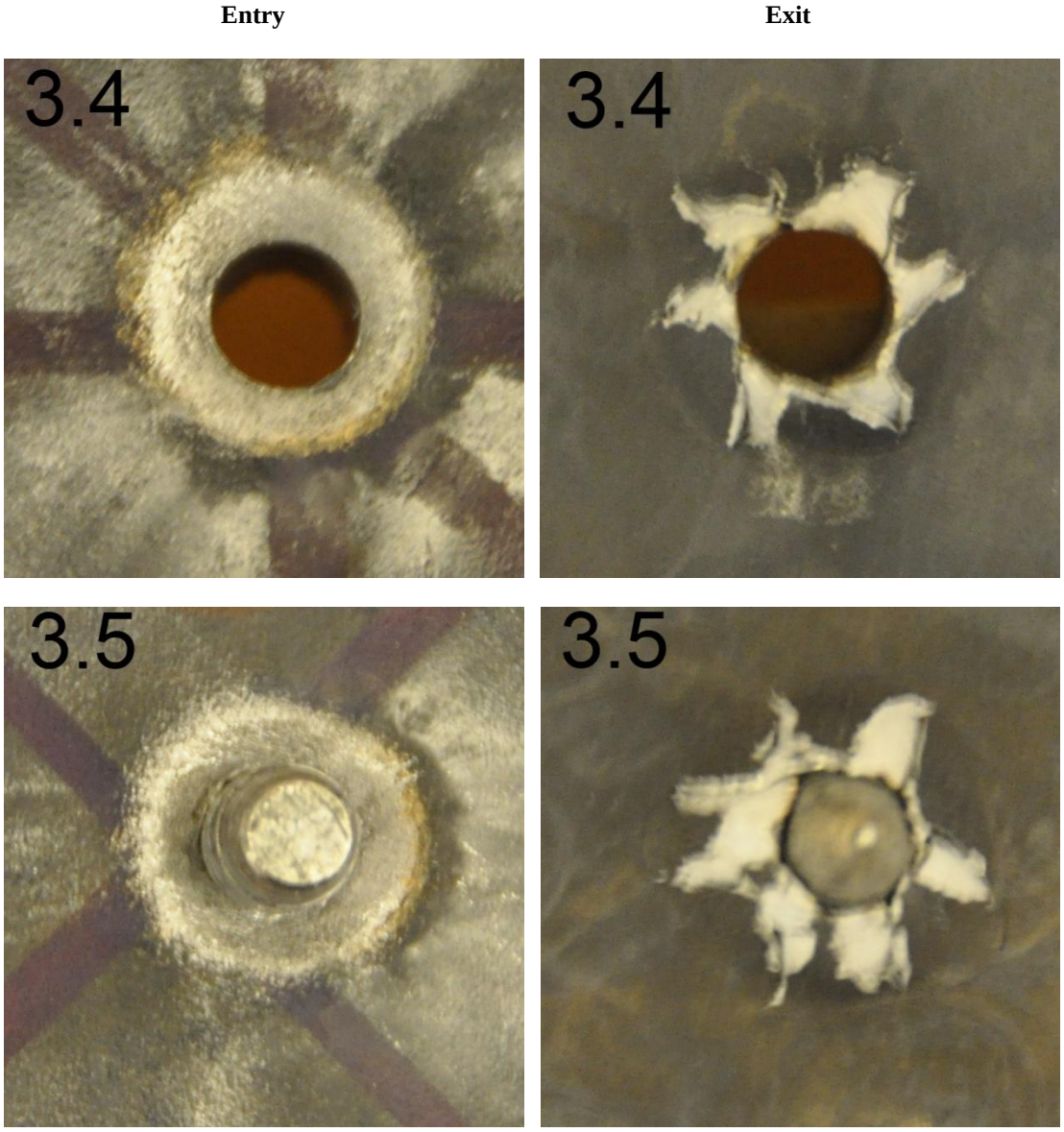

Figure L. Projectile entry and exit holes for shots 4 and 5 on sample 3.

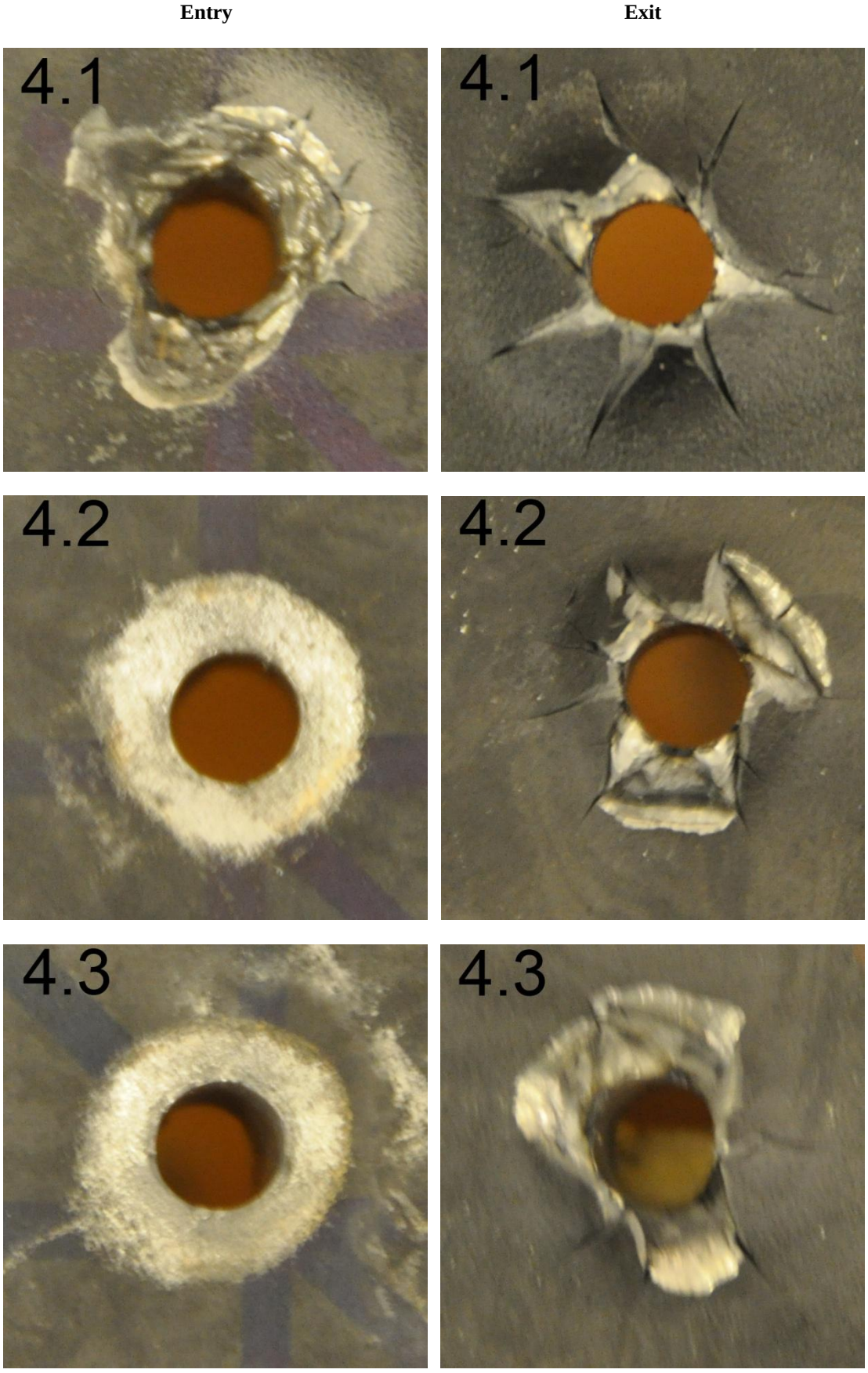

Figure M. Projectile entry and exit holes for shots 1, 2 and 3 on sample 4.

Entry **Exit**

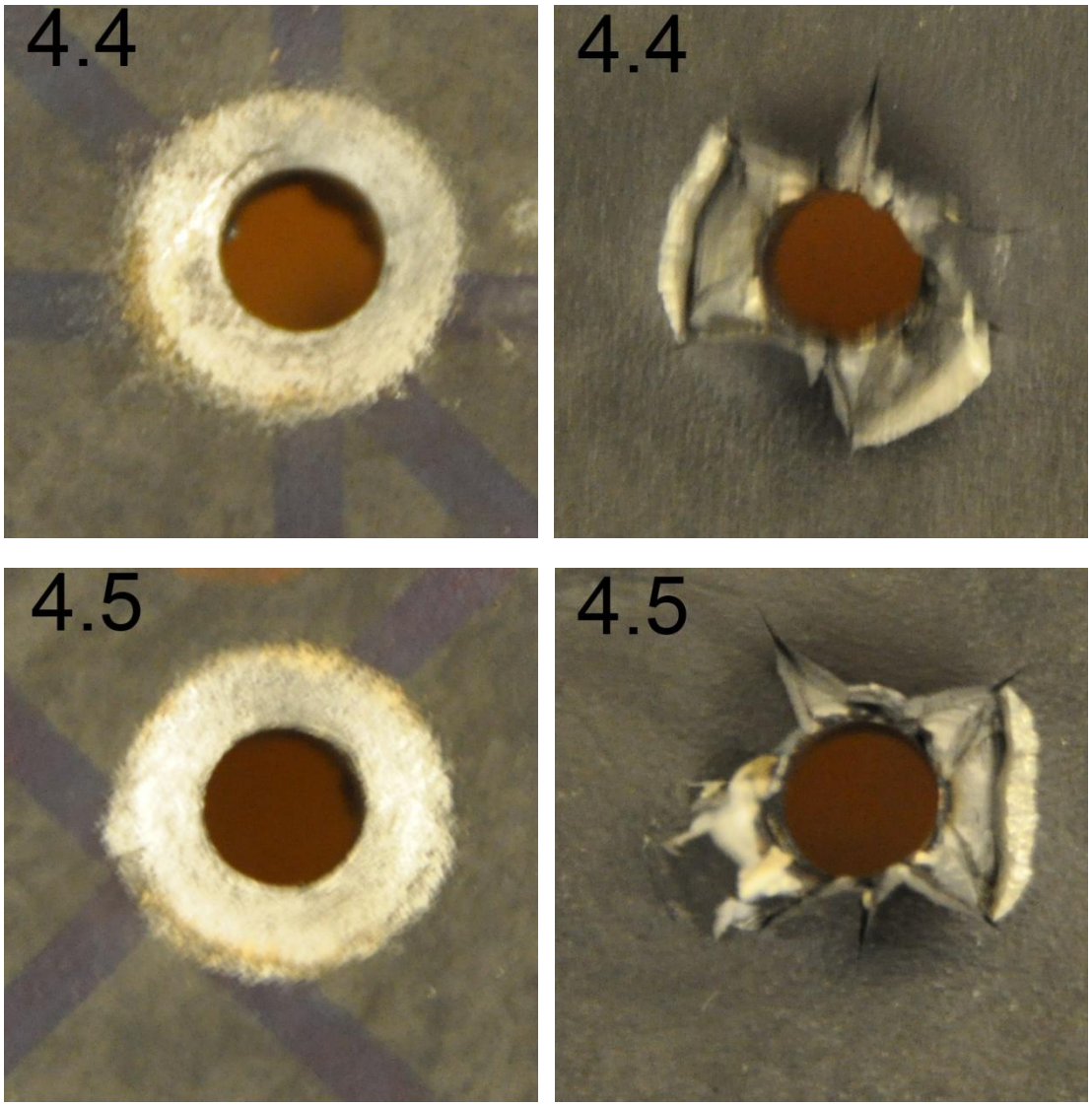

Figure N. Projectile entry and exit holes for shots 4 and 5 on sample 4.

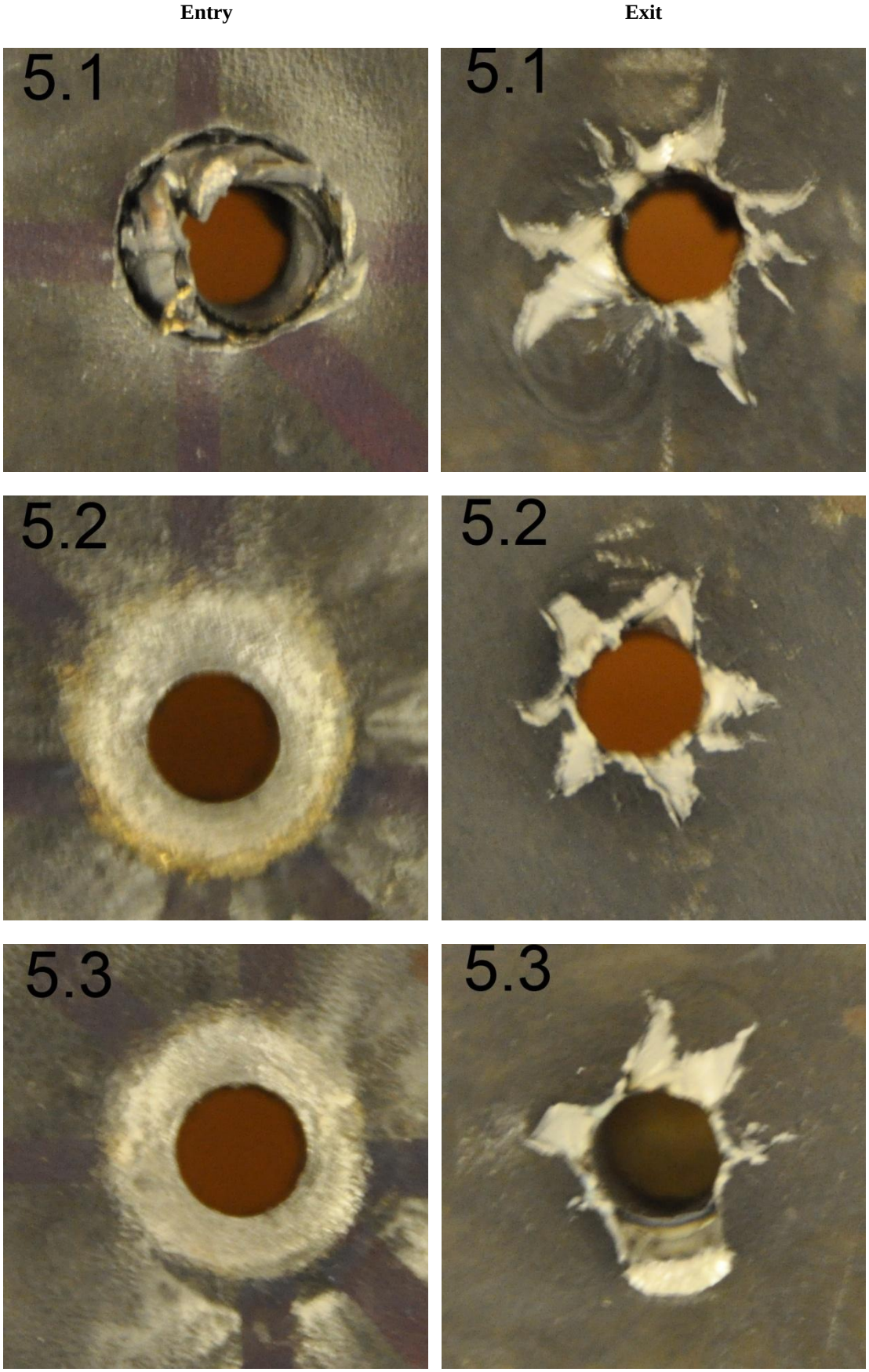

Figure O. Projectile entry and exit holes for shots 1, 2 and 3 on sample 5.

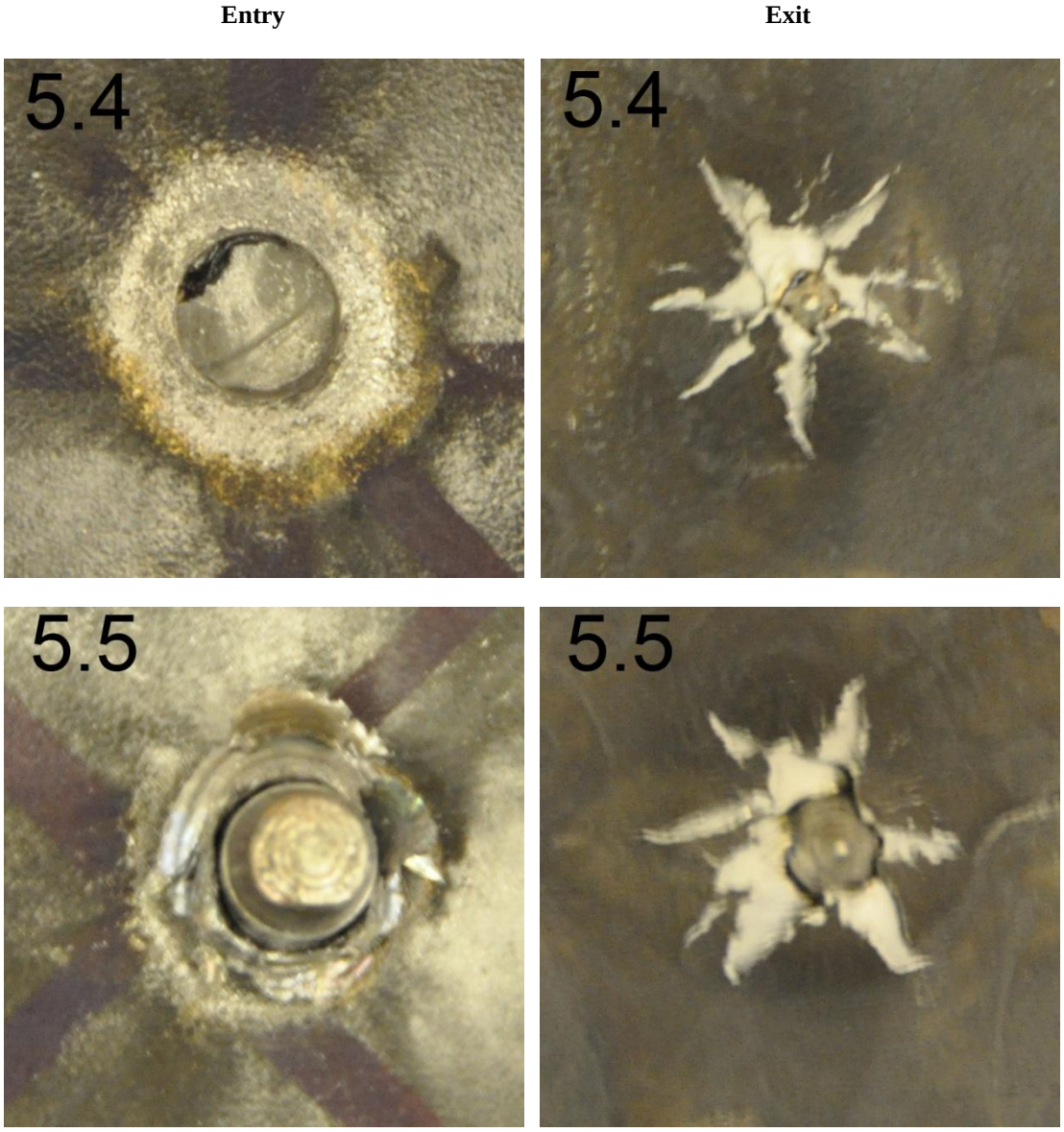

Figure P. Projectile entry and exit holes for shots 4 and 5 on sample 5.

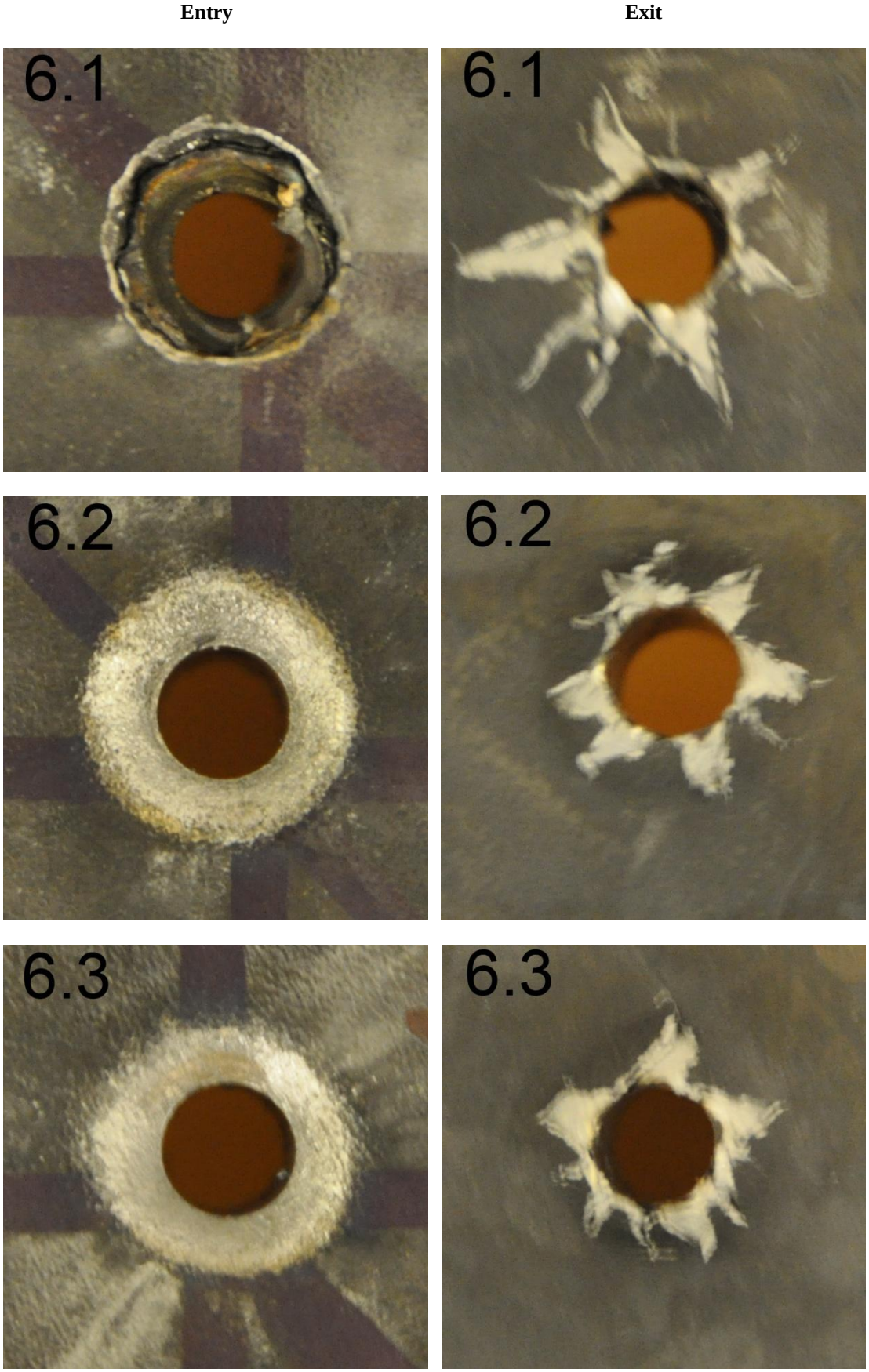

Figure Q. Projectile entry and exit holes for shots 1, 2 and 3 on sample 6.

Entry **Exit**

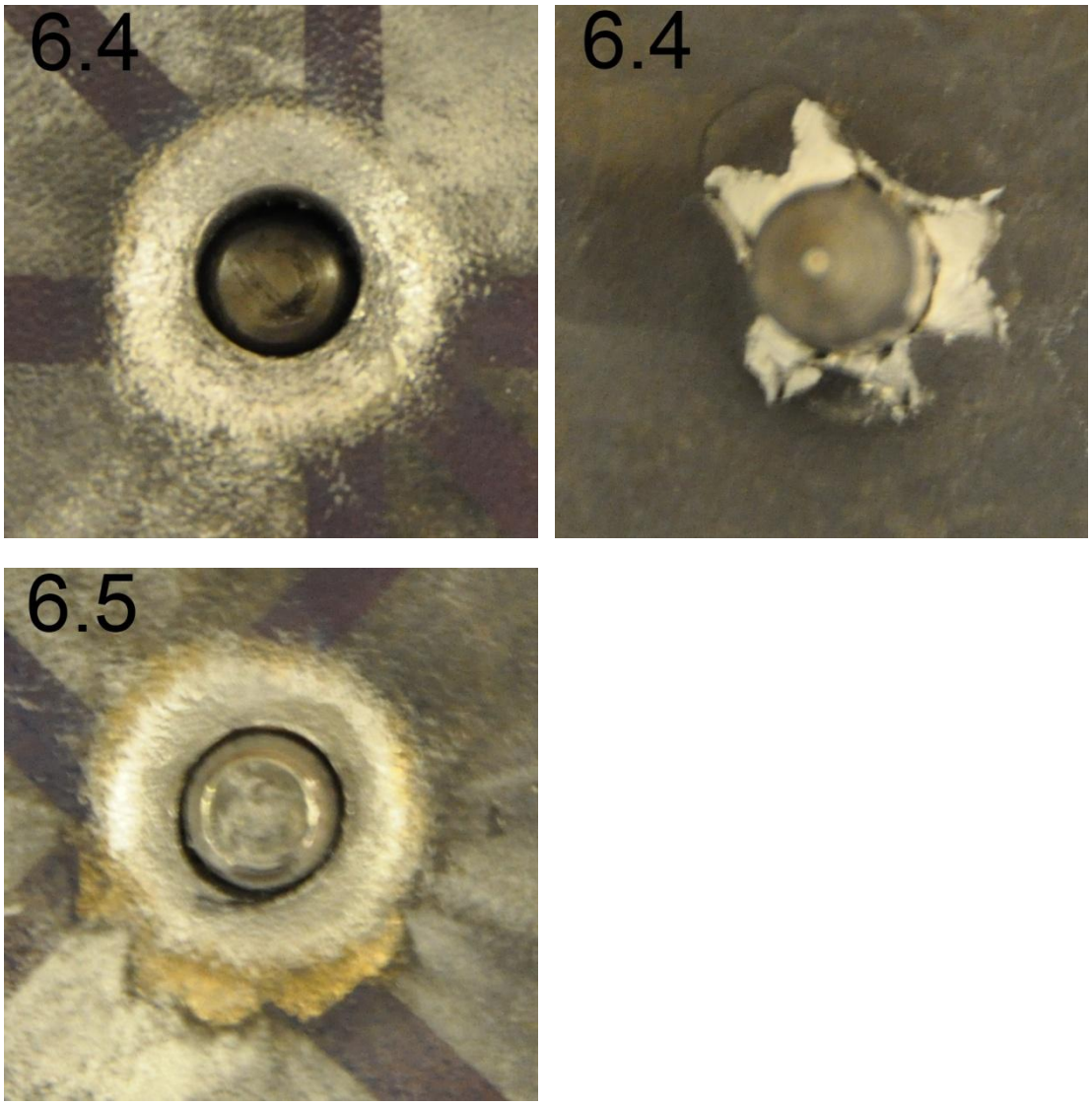

Figure R. Projectile entry and exit holes for shot 4 and entry hole for shot 5 on sample 6. Exit hole for shot 5 was not photographed.

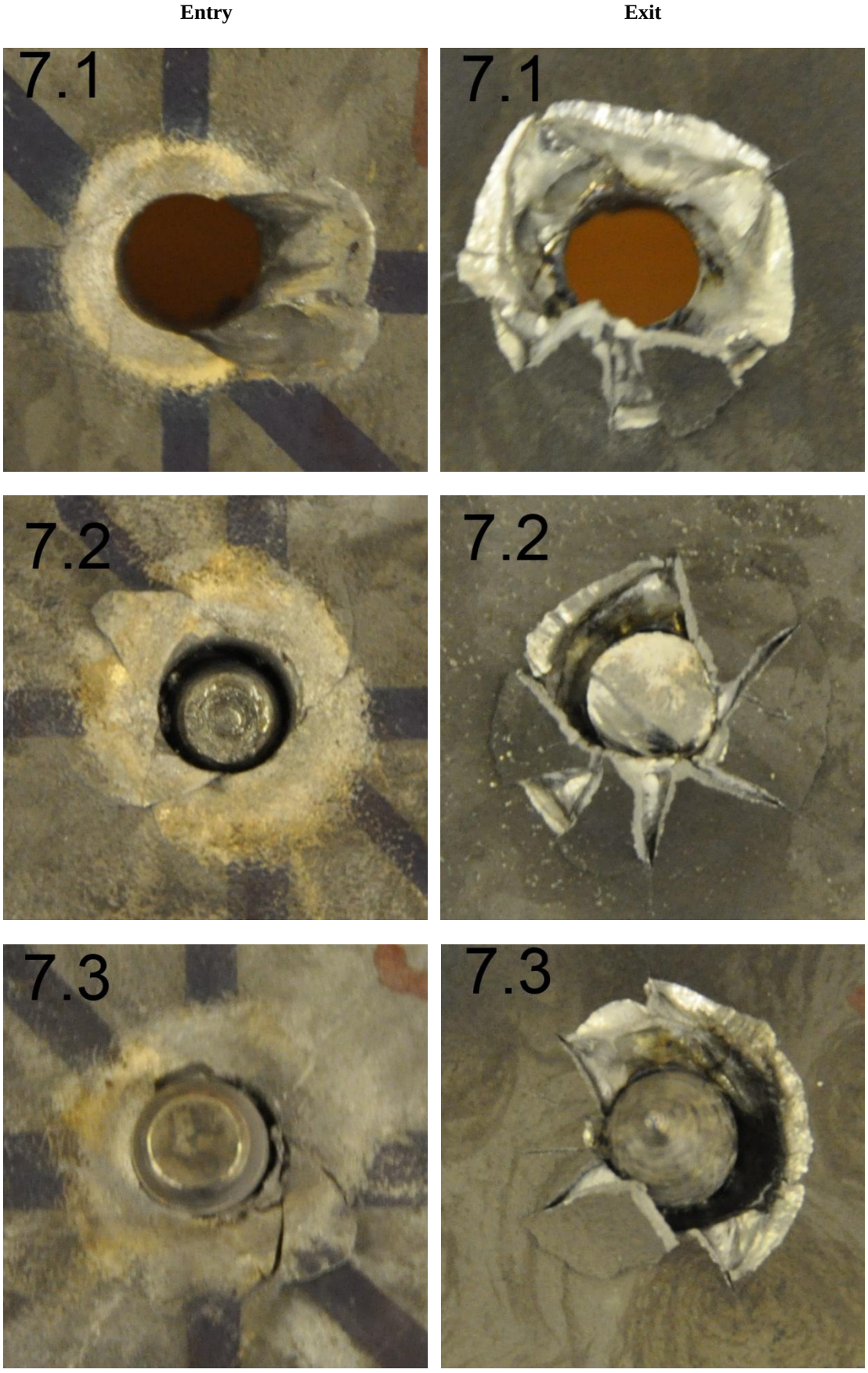

Figure S. Projectile entry and exit holes for shots 1, 2 and 3 on sample 7.

Entry **Exit**

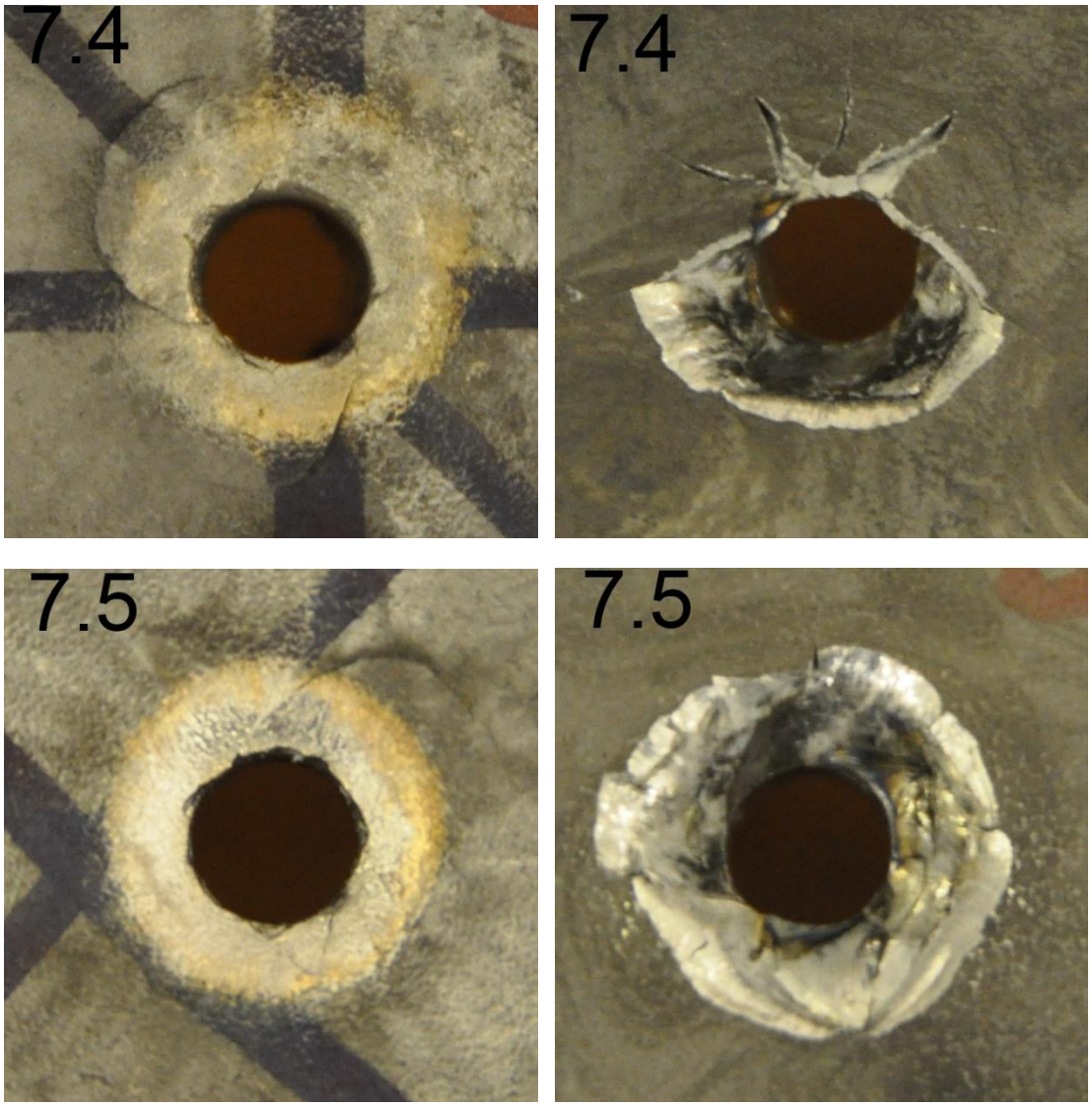

Figure T. Projectile entry and exit holes for shots 4 and 5 on sample 7.

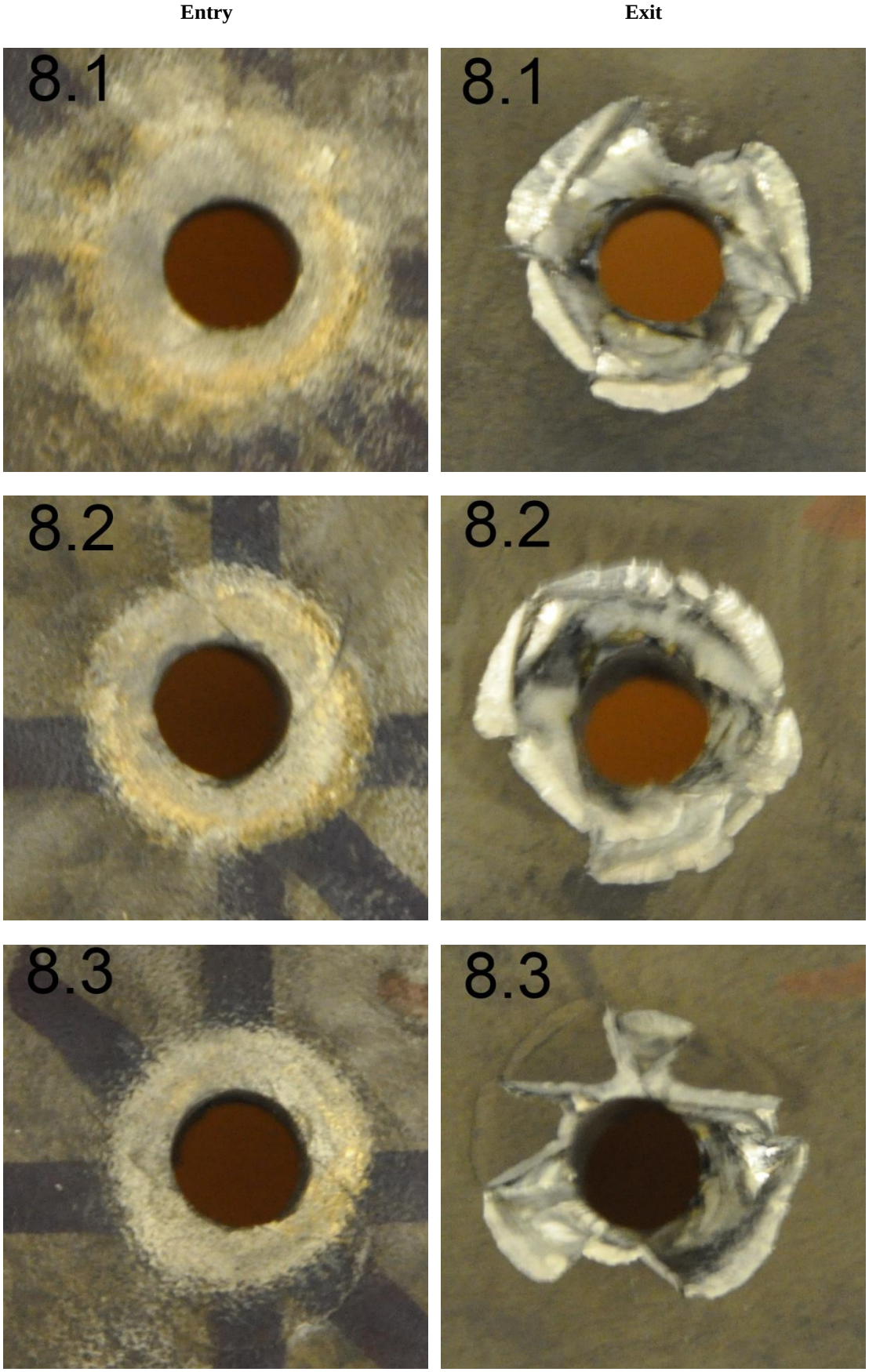

Figure U. Projectile entry and exit holes for shots 1, 2 and 3 on sample 8.

Entry **Exit**

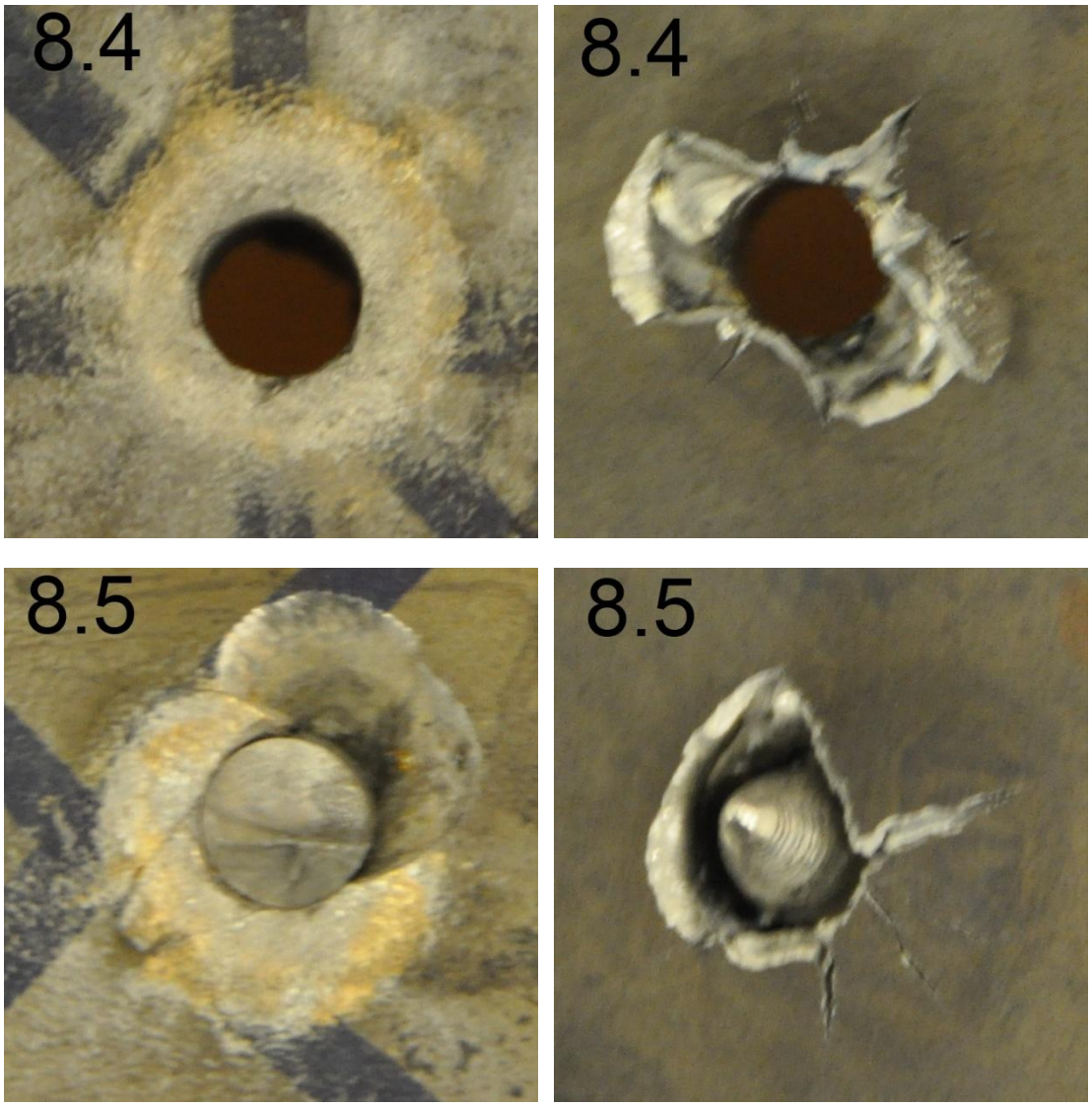

Figure V. Projectile entry and exit holes for shots 4 and 5 on sample 8.

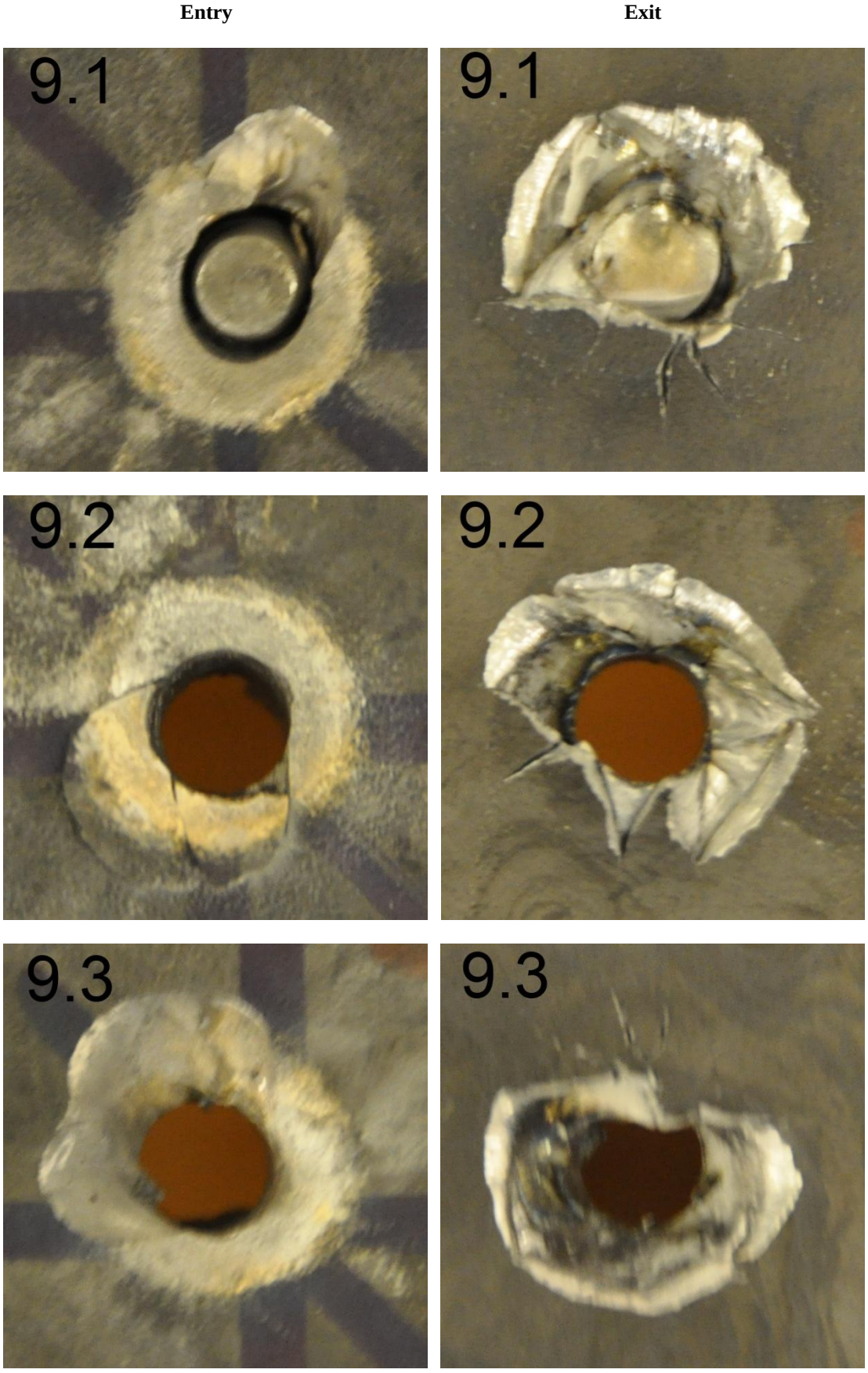

Figure W. Projectile entry and exit holes for shots 1, 2 and 3 on sample 9.

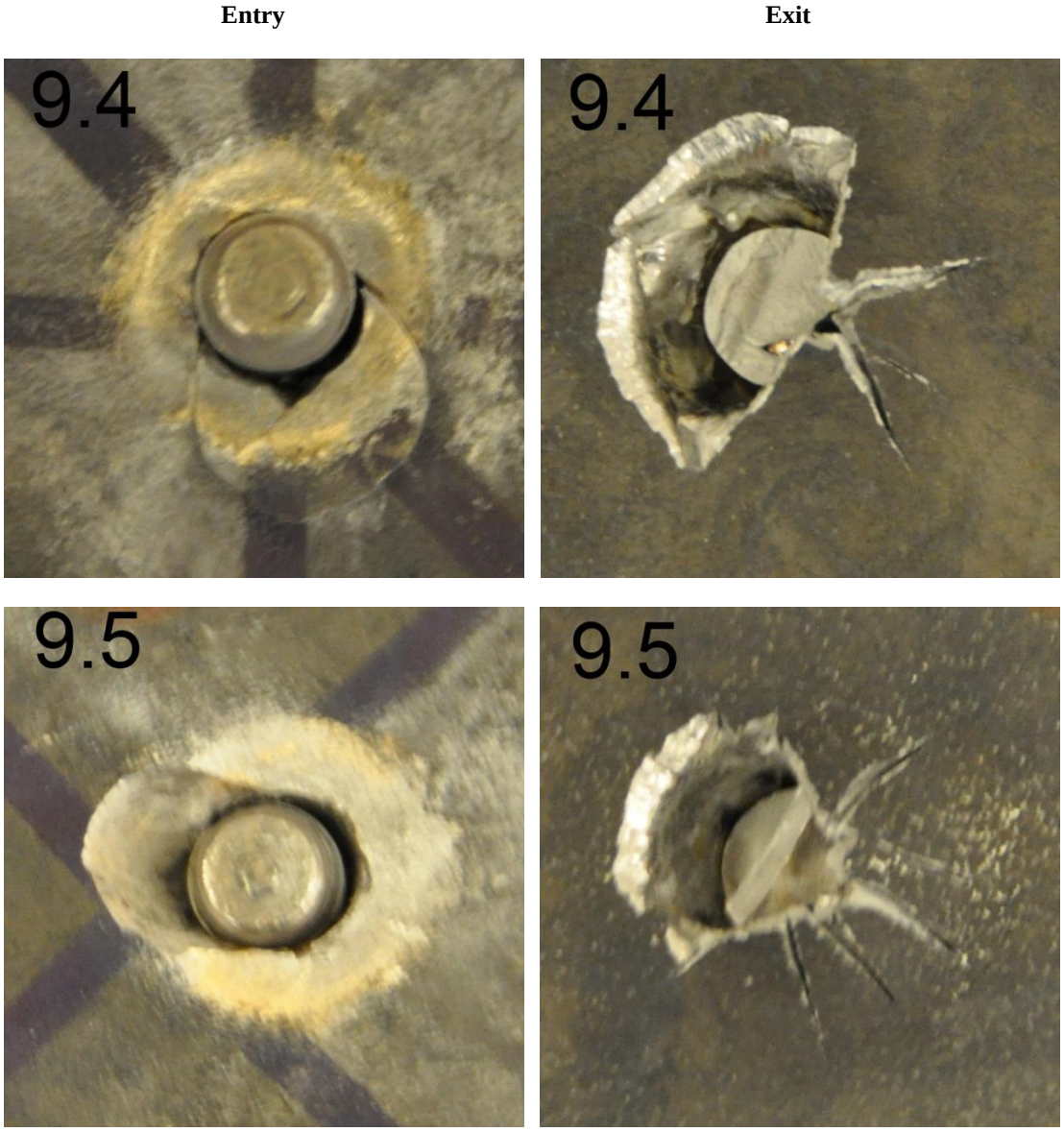

Figure X. Projectile entry and exit holes for shots 4 and 5 on sample 9.

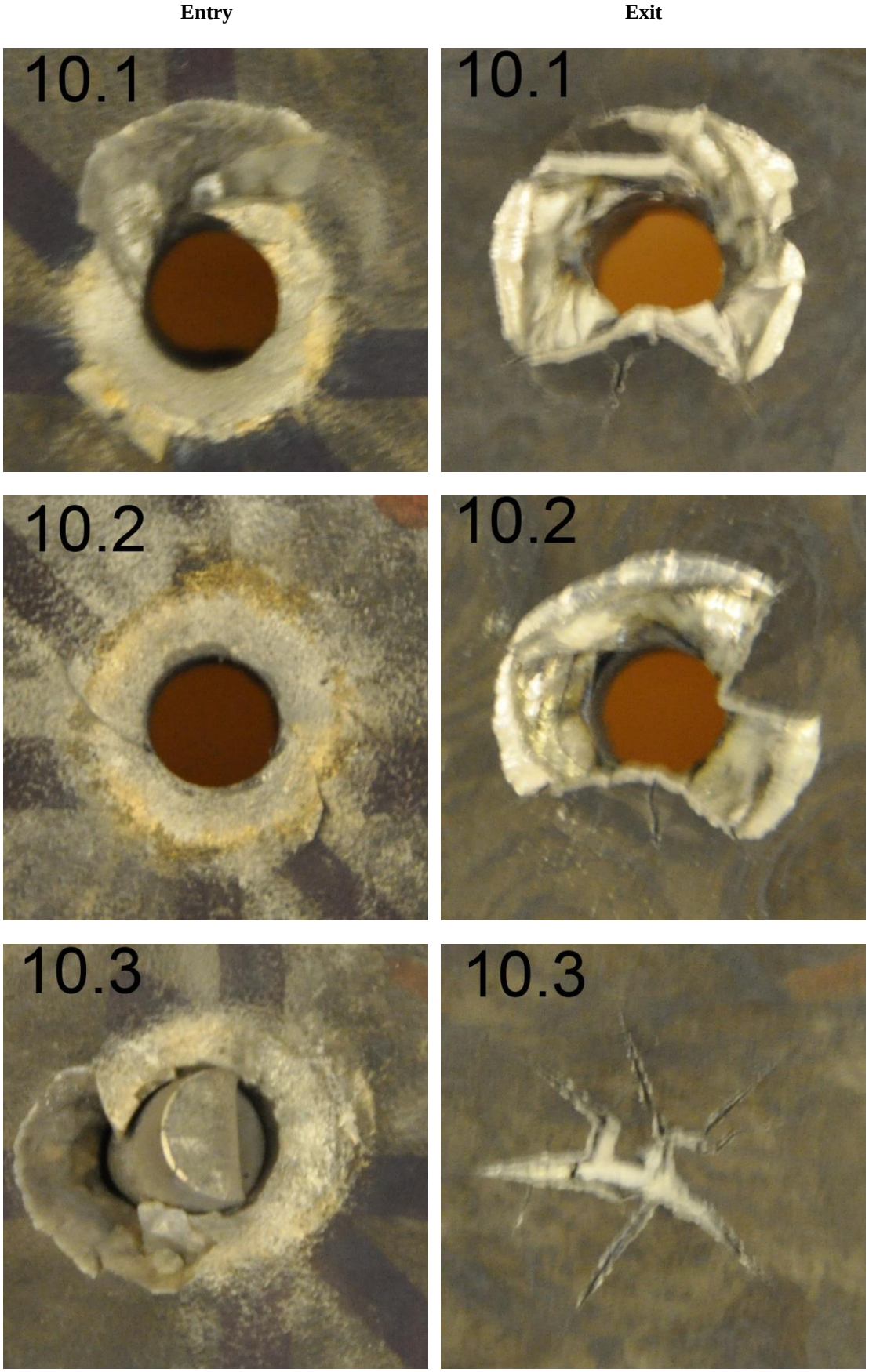

Figure Y. Projectile entry and exit holes for shots 1, 2 and 3 on sample 10.

Entry **Exit**

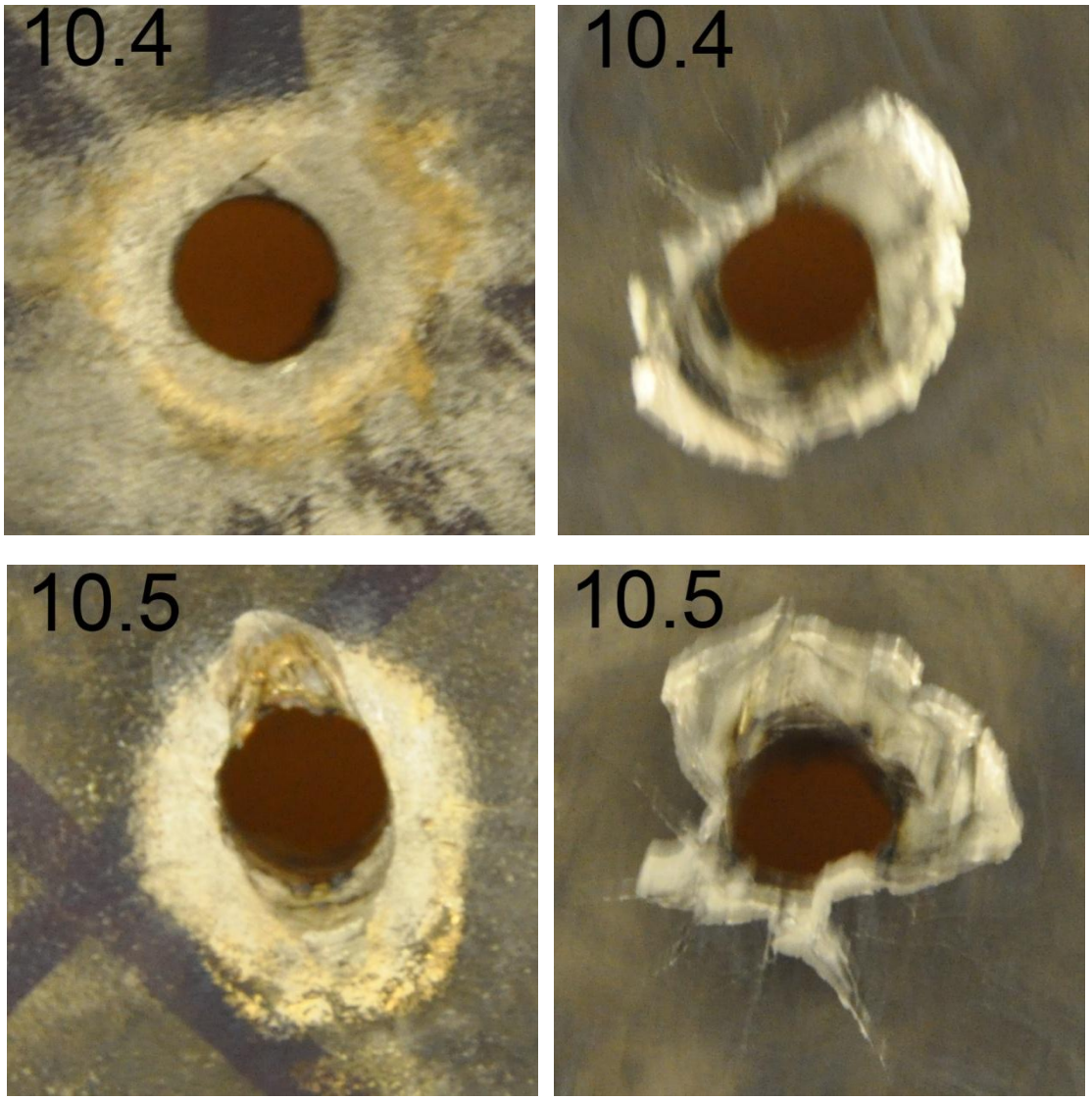

Figure Z. Projectile entry and exit holes for shots 4 and 5 on sample 10.

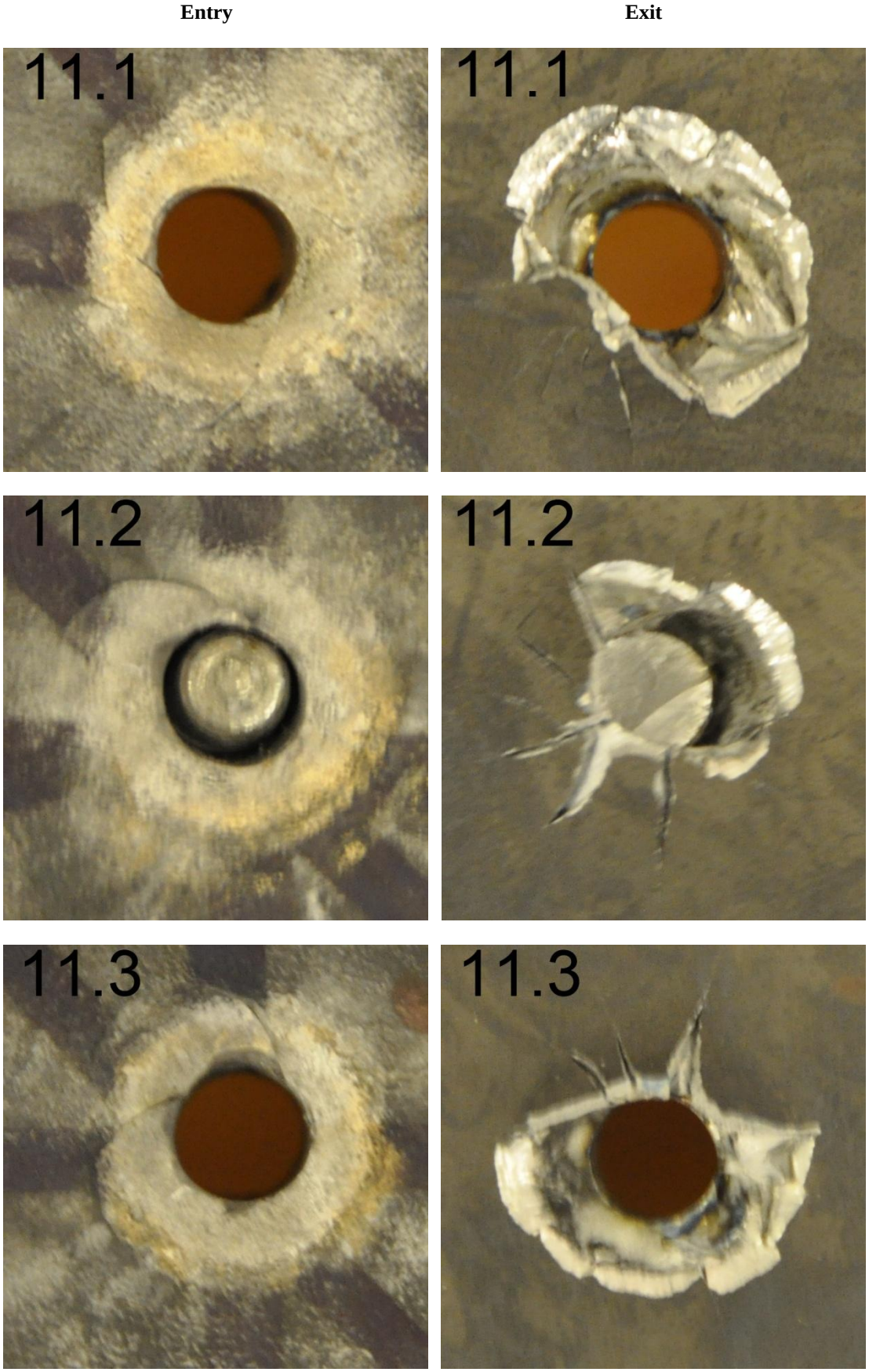

Figure AA. Projectile entry and exit holes for shots 1, 2 and 3 on sample 11.

Entry **Exit**

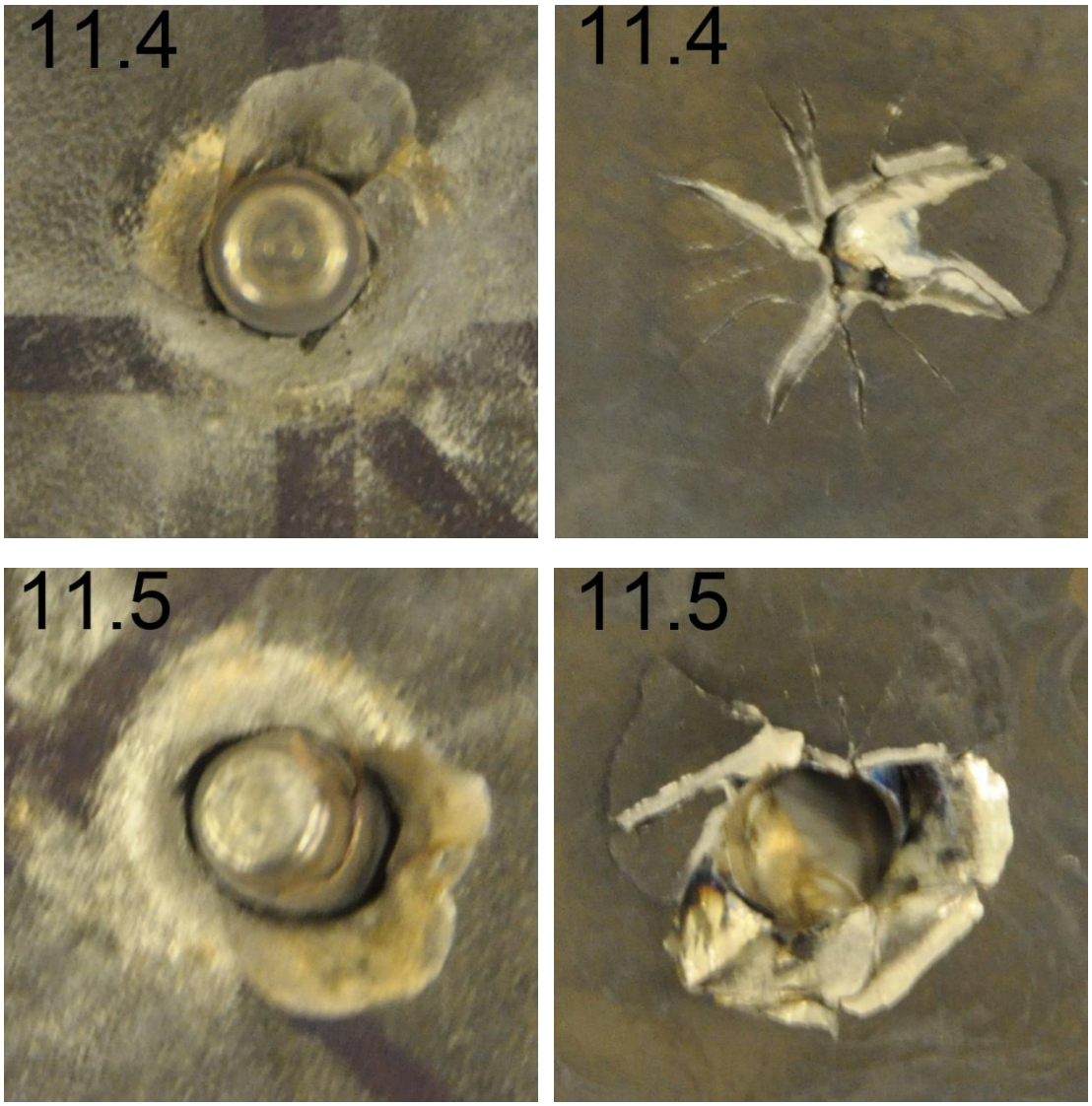

Figure AB. Projectile entry and exit holes for shots 4 and 5 on sample 11.

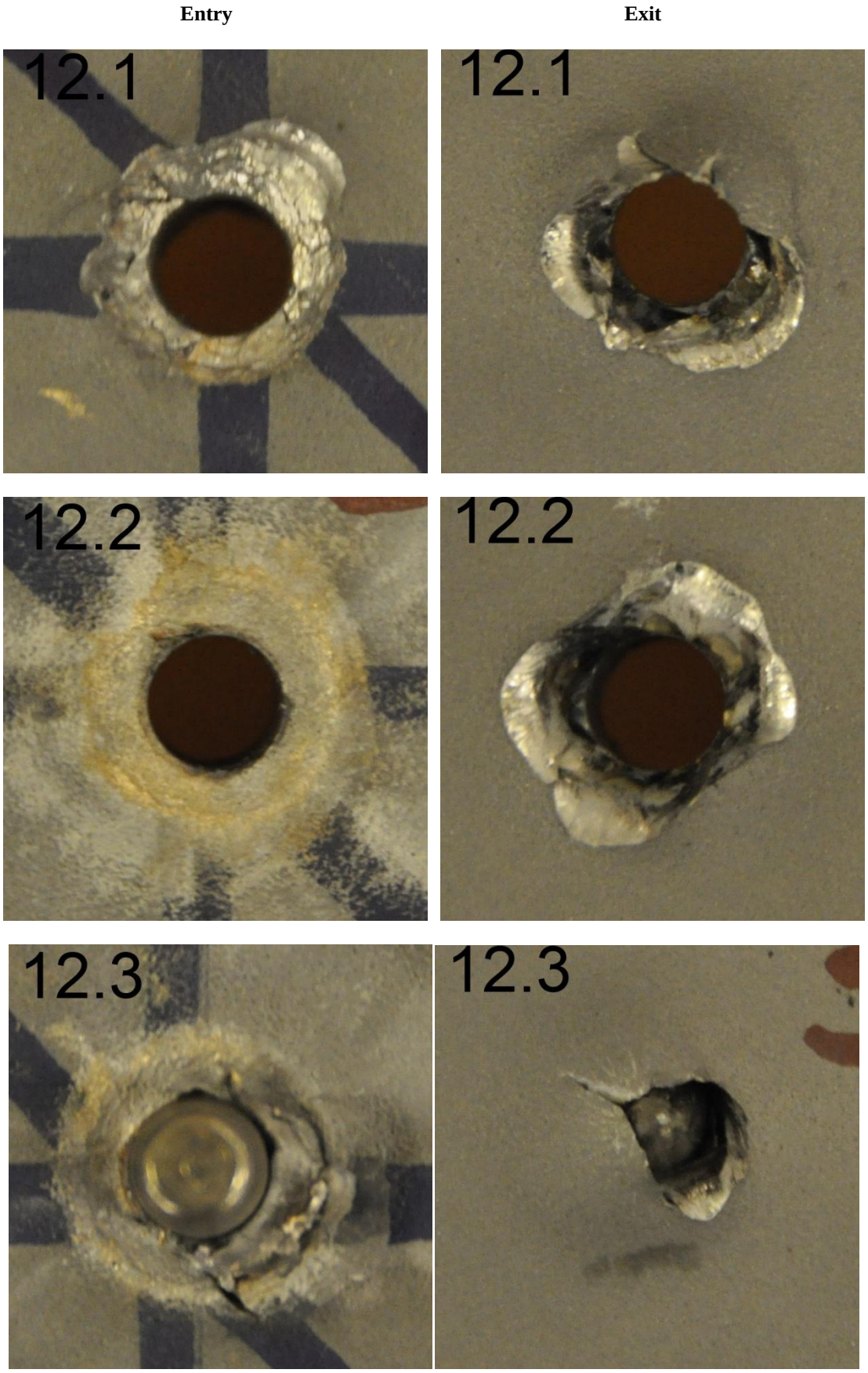

Figure AC. Projectile entry and exit holes for shots 1, 2 and 3 on the original Hardow 450 reference sample.

Entry **Exit**

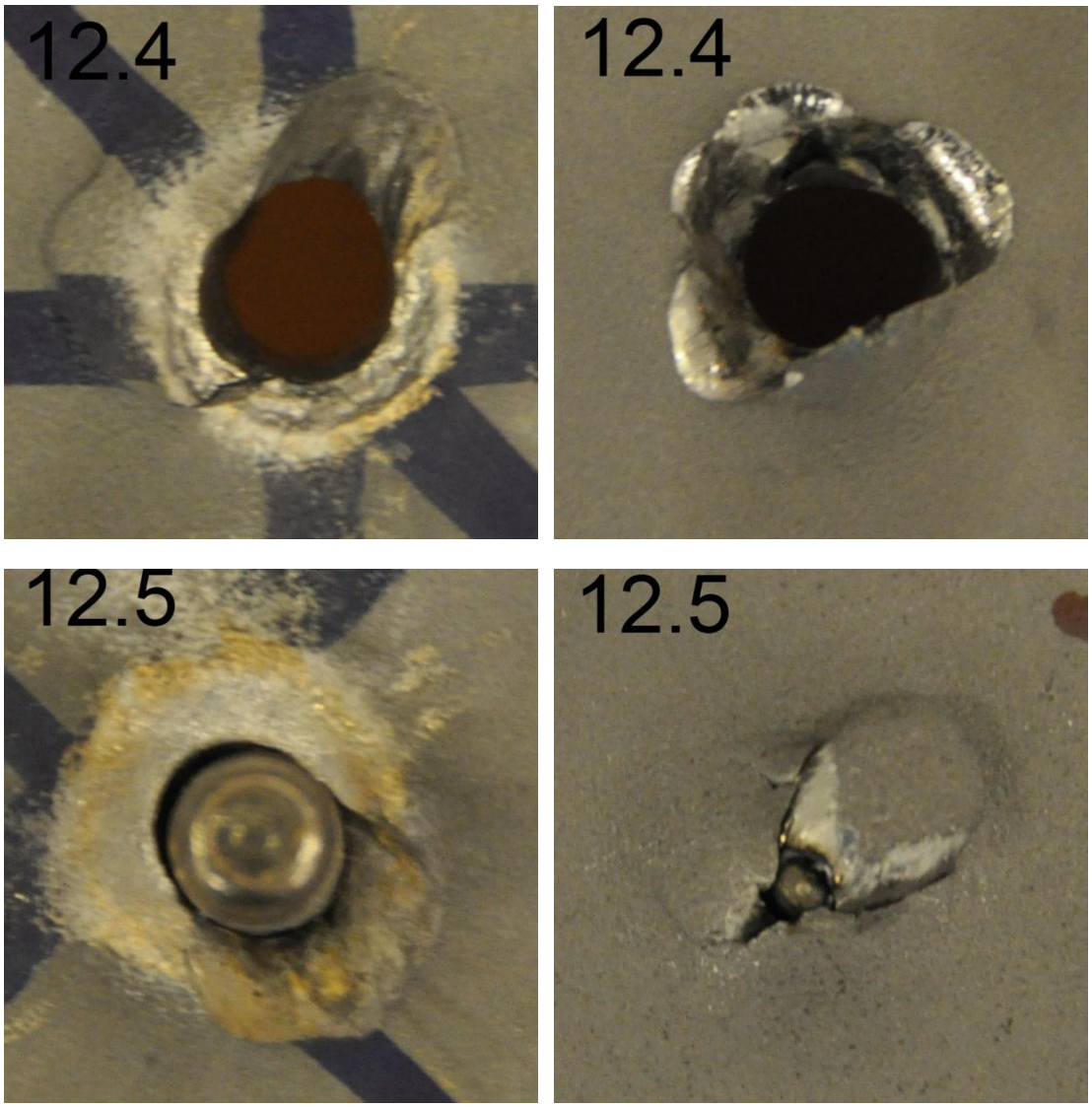

Figure AD. Projectile entry and exit holes for shots 4 and 5 on the original Hardox 450 reference sample.

C. Core hardness measurements of the samples

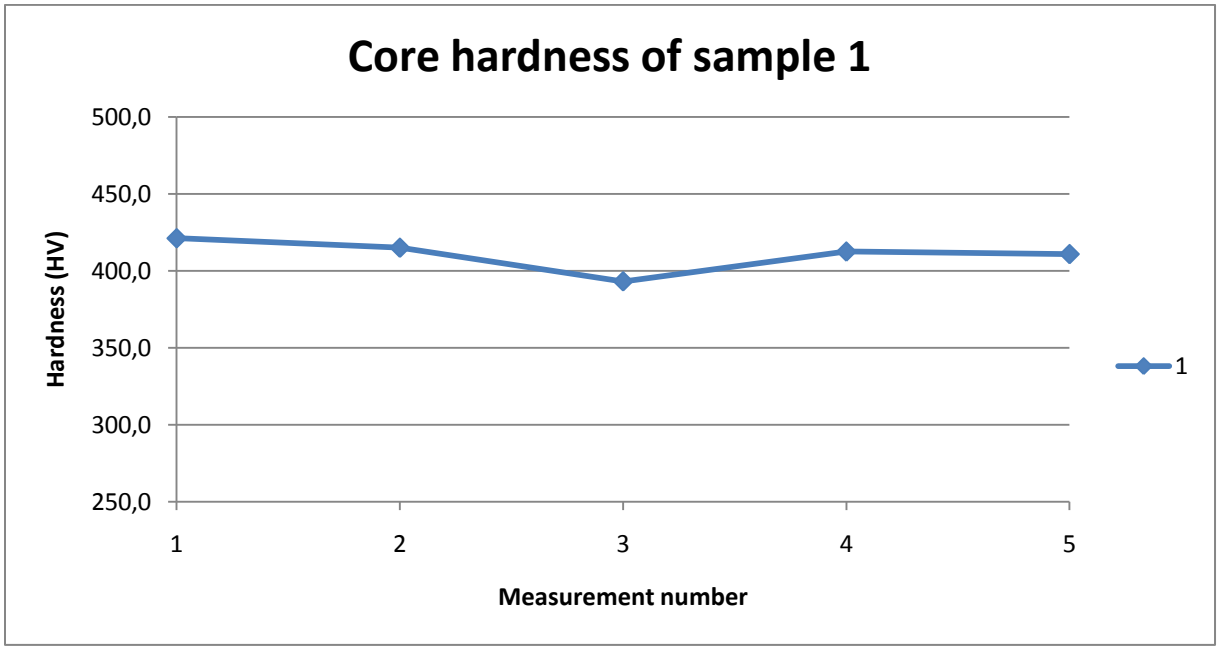

Figure AE. The five core hardness measurements of sample 1.

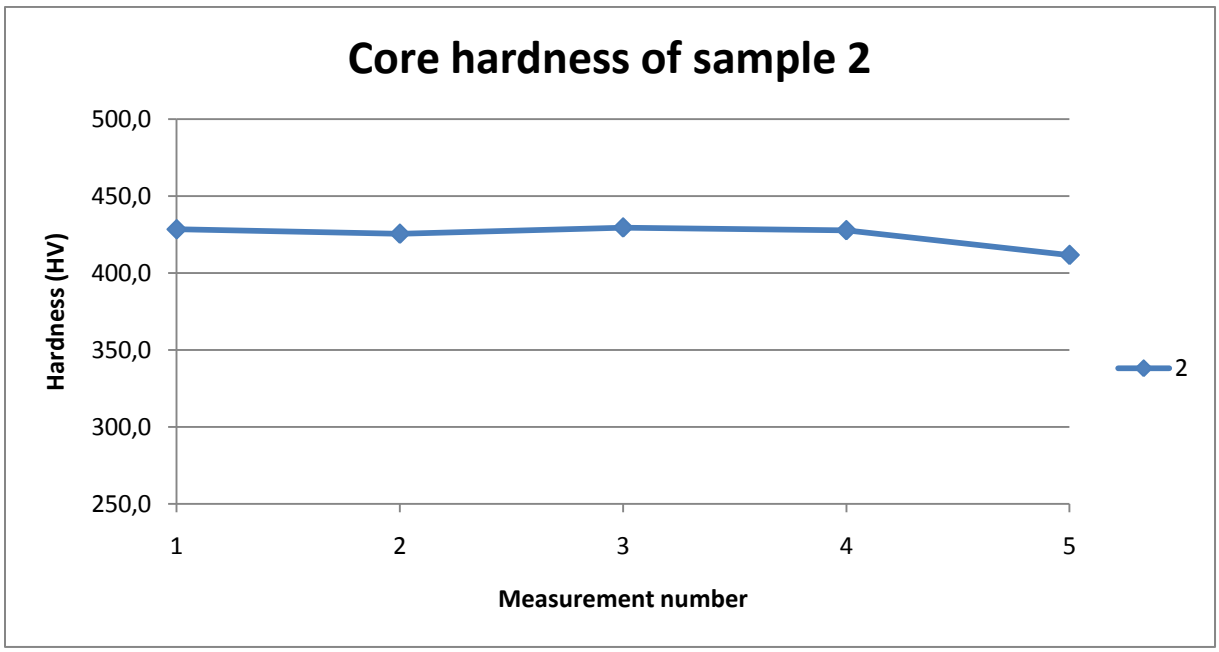

Figure AF. The five core hardness measurements of sample 2.

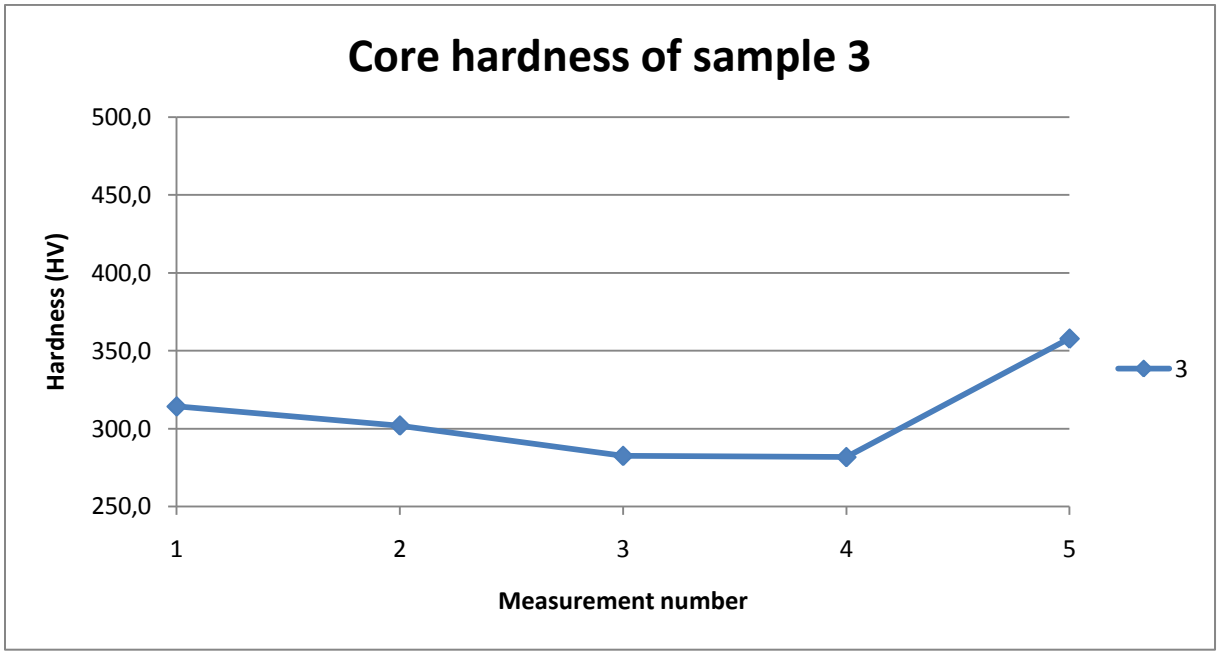

Figure AG. The five core hardness measurements of sample 3.

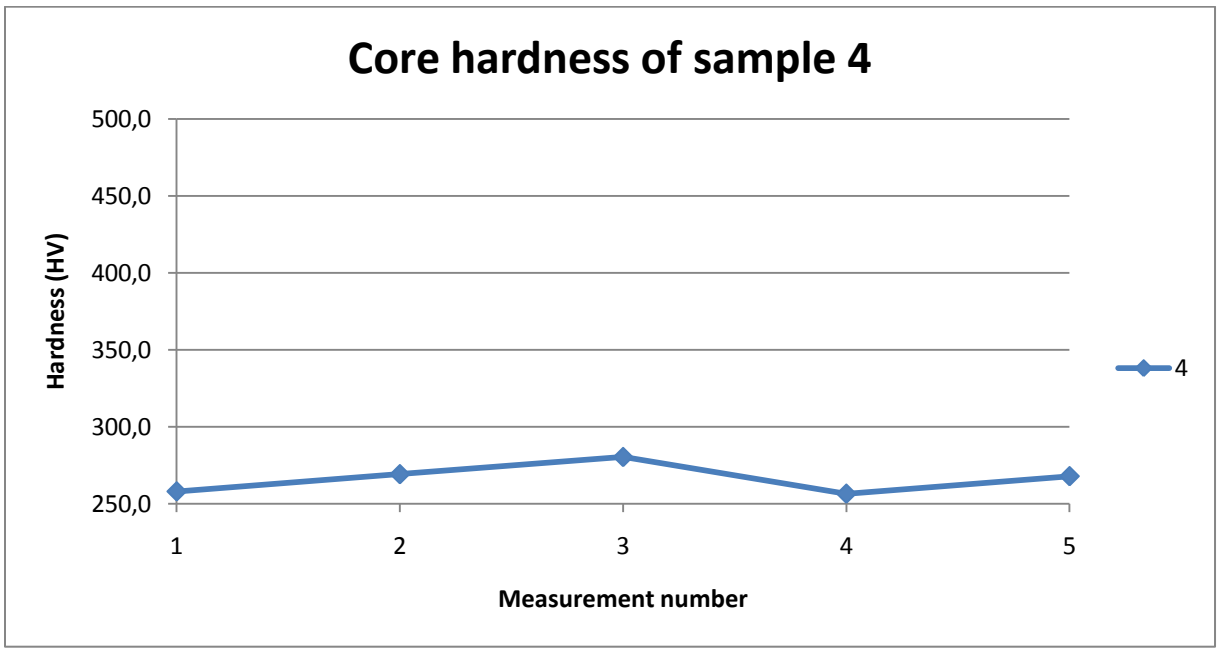

Figure AH. The five core hardness measurements of sample 4.

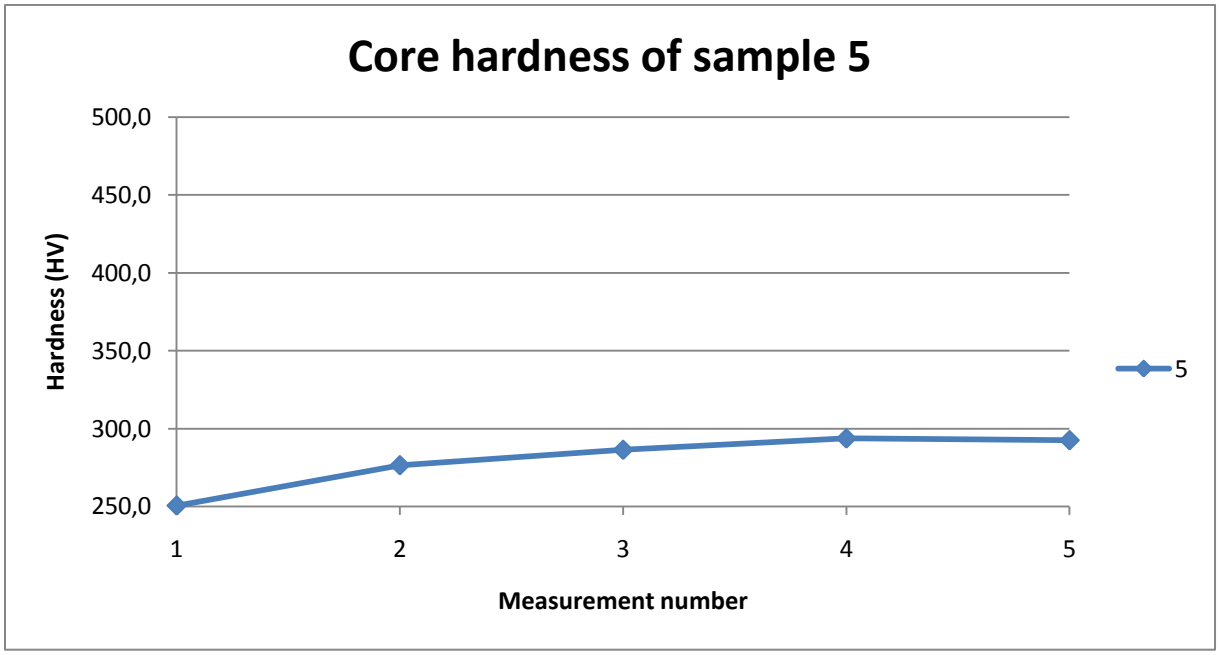

Figure AI. The five core hardness measurements of sample 5.

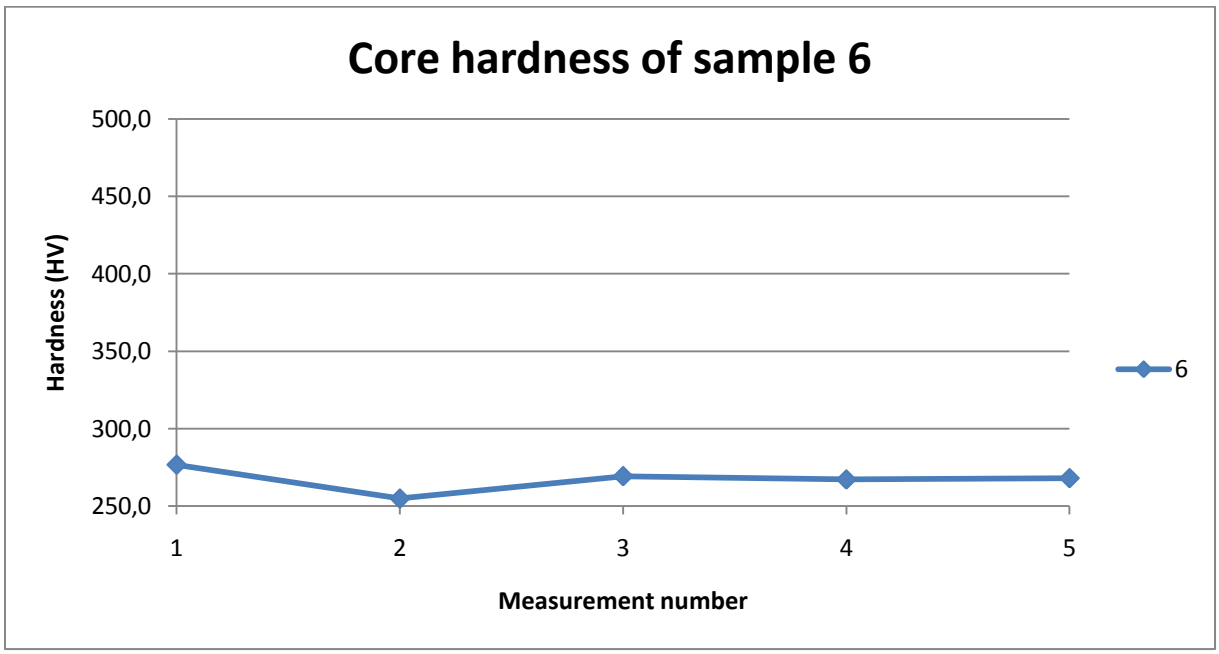

Figure AJ. The five core hardness measurements of sample 6.

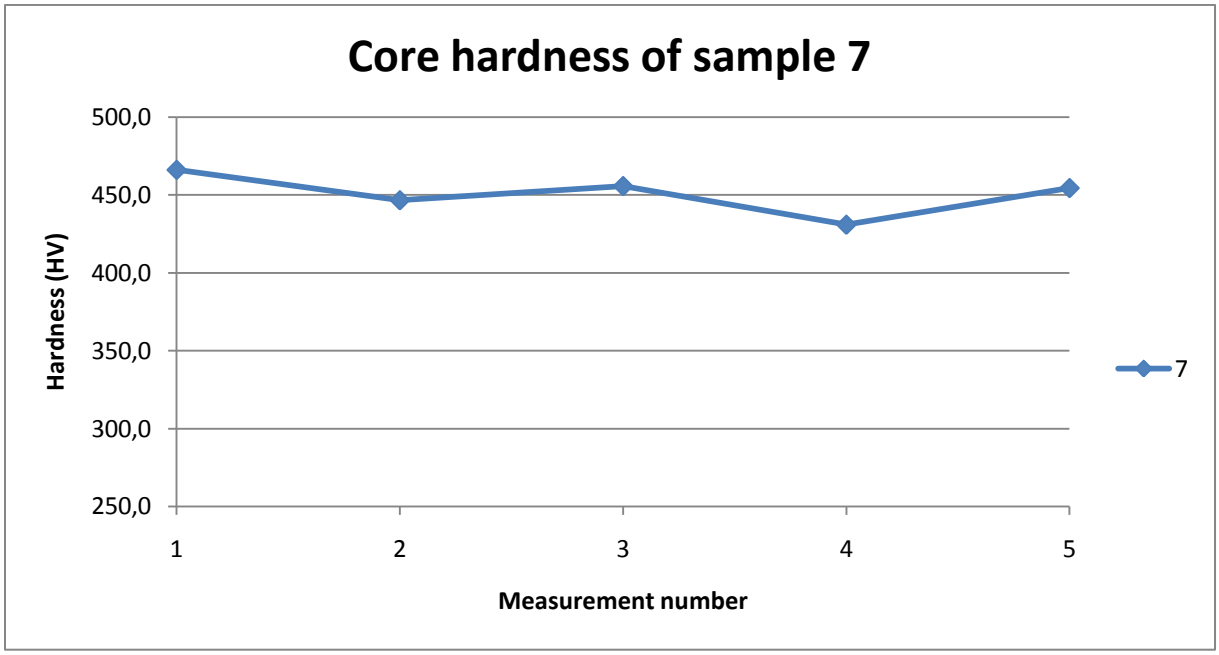

Figure AK. The five core hardness measurements of sample 7.

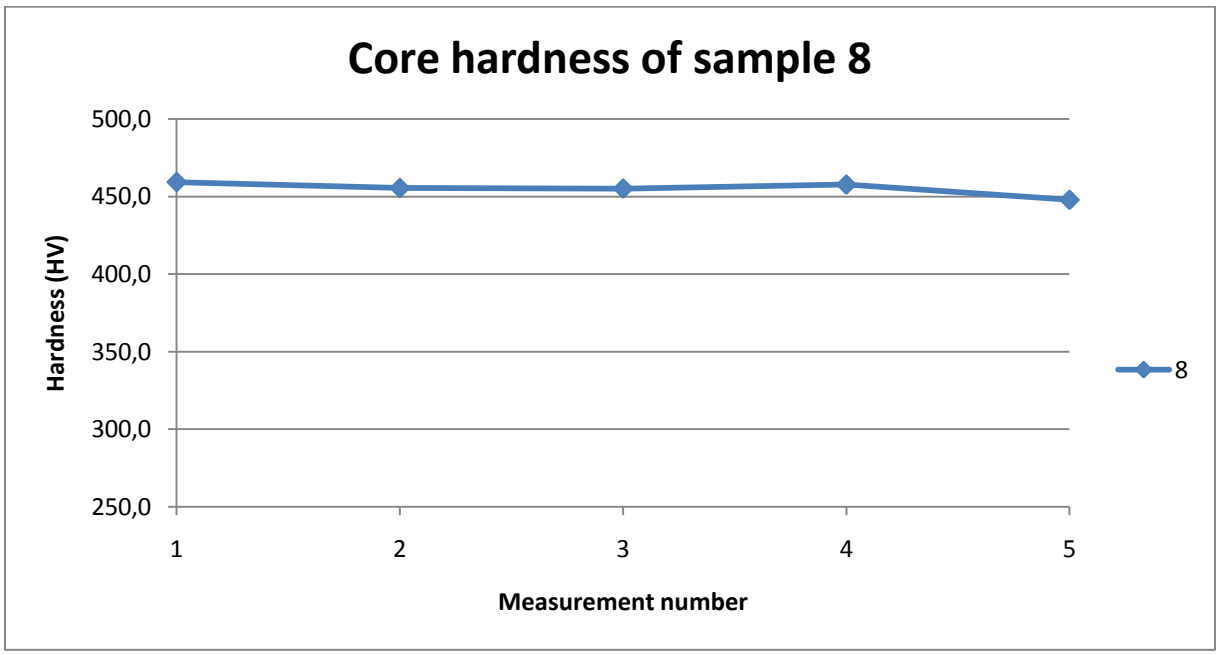

Figure AL. The five core hardness measurements of sample 8.

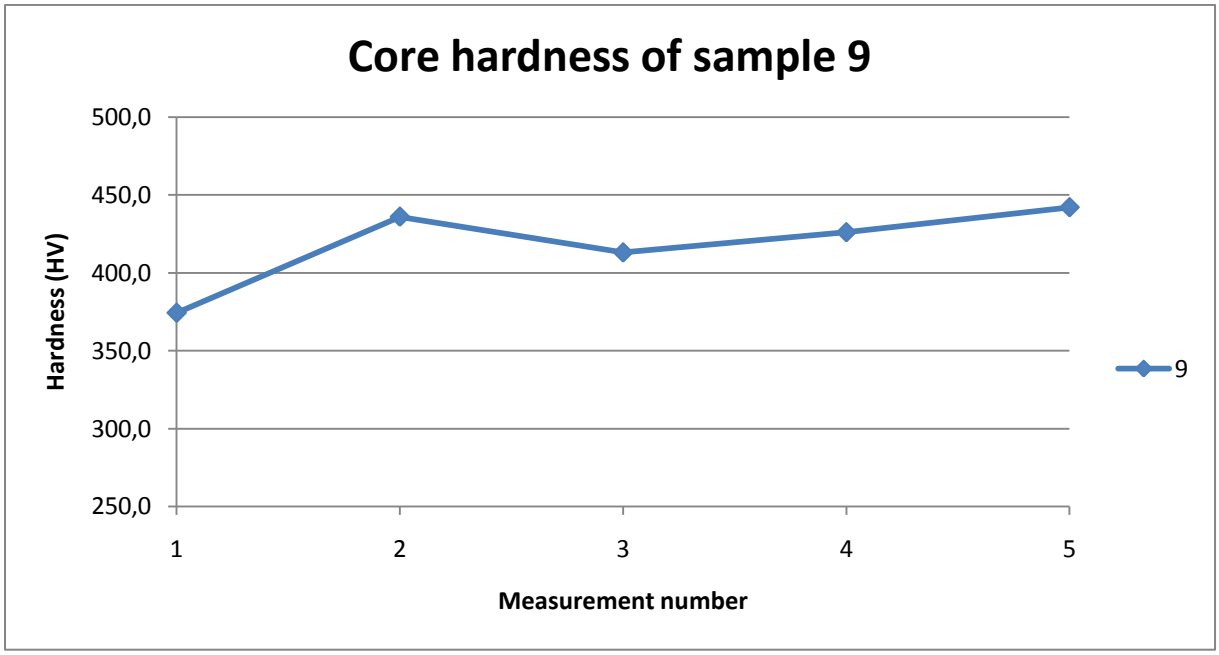

Figure AM. The five core hardness measurements of sample 9.

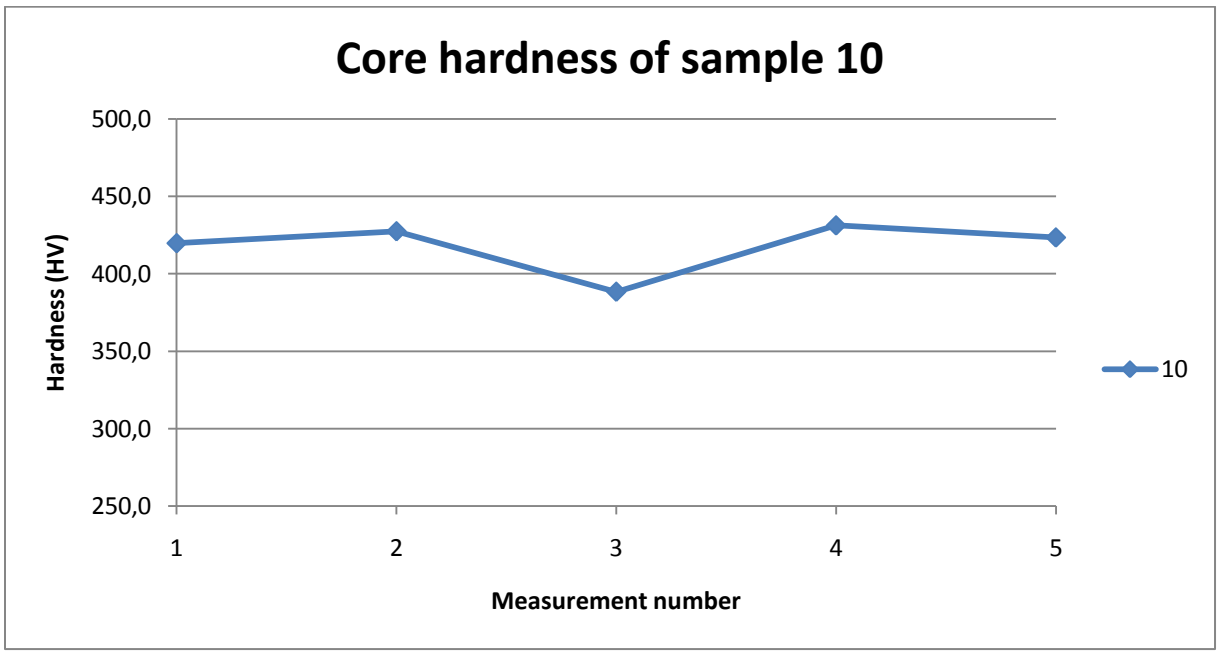

Figure AN. The five core hardness measurements of sample 10.

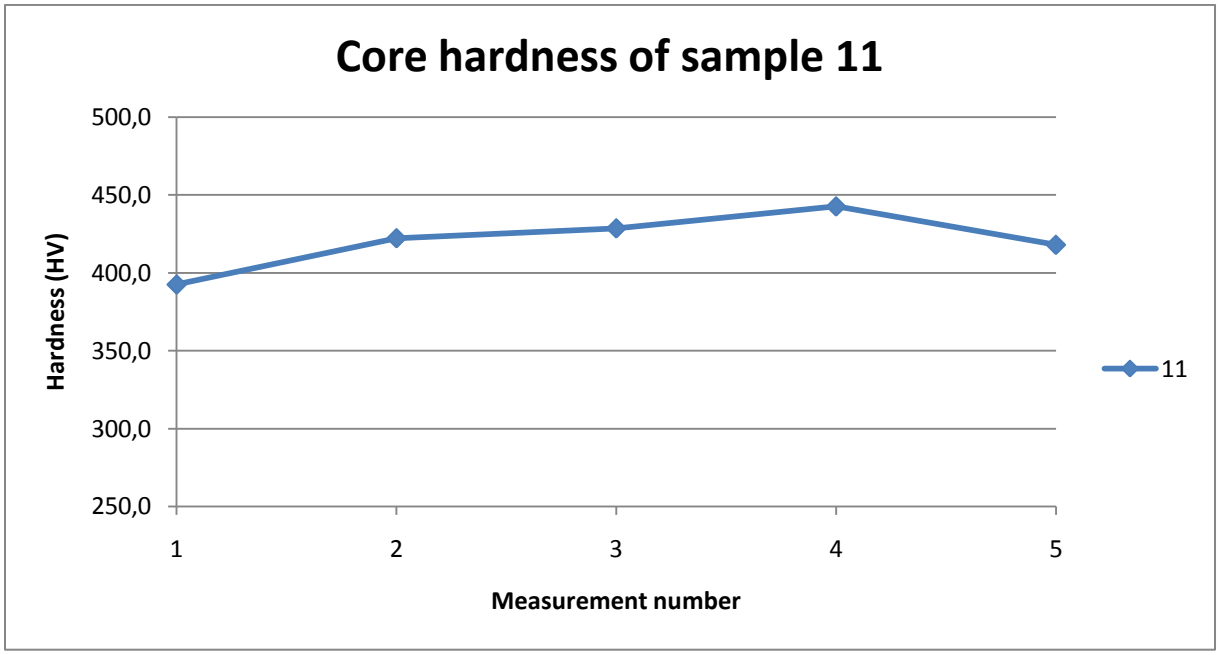

Figure AO. The five core hardness measurements of sample 11.

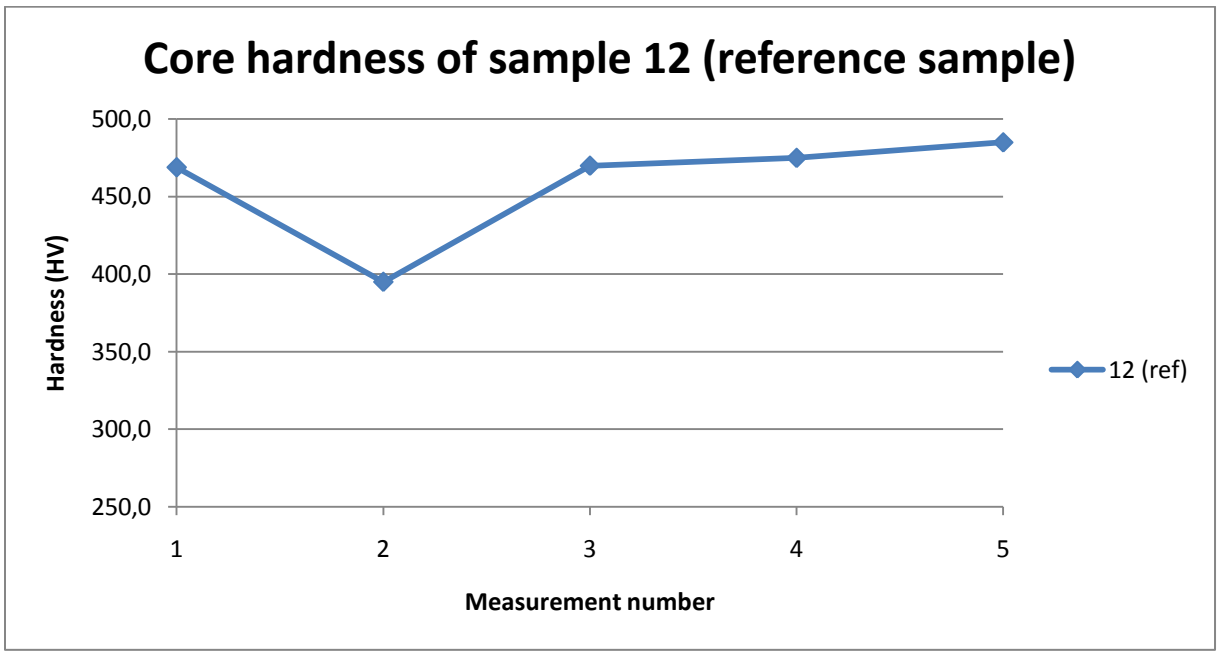

Figure AP. The five core hardness measurements of the original Hardox 450 reference sample.

D. Surface hardness measurements of the samples

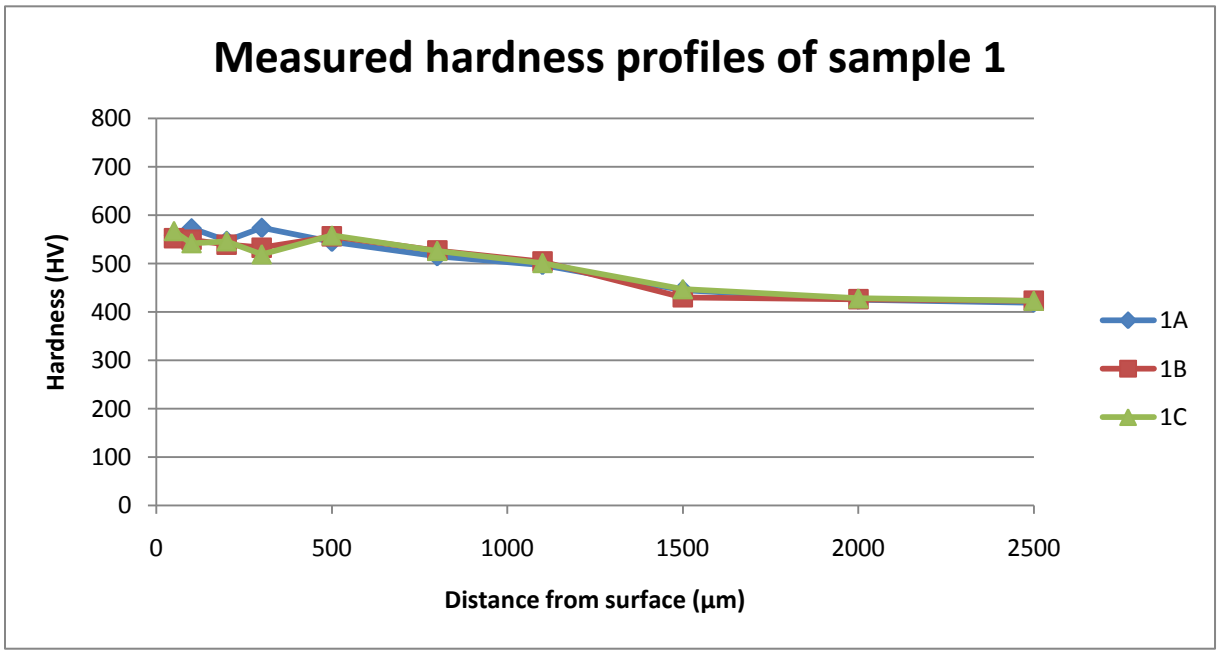

Figure AQ. The three parallel surface hardness profiles of sample 1.

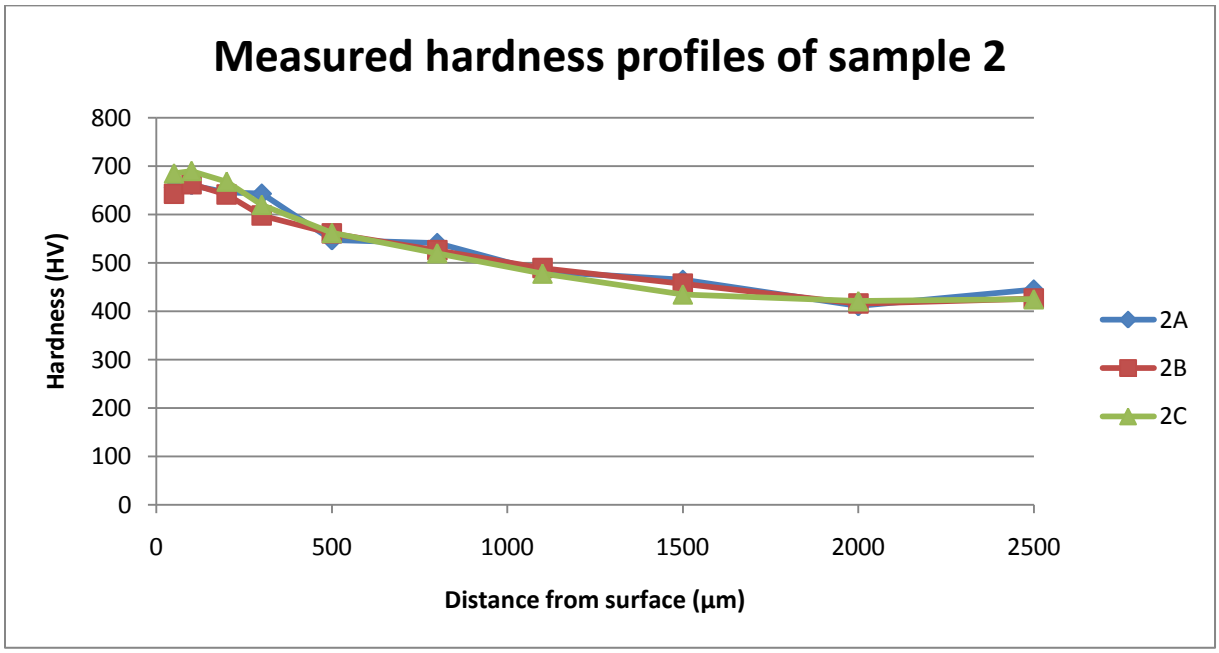

Figure AR. The three parallel surface hardness profiles of sample 2.

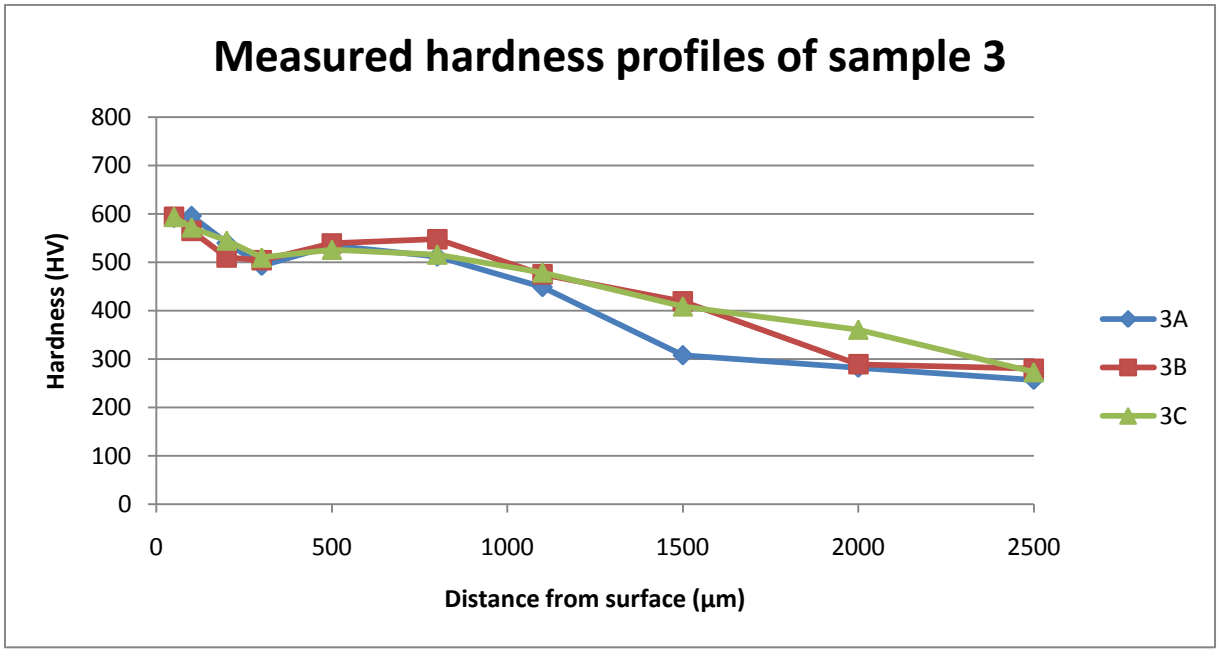

Figure AS. The three parallel surface hardness profiles of sample 3.

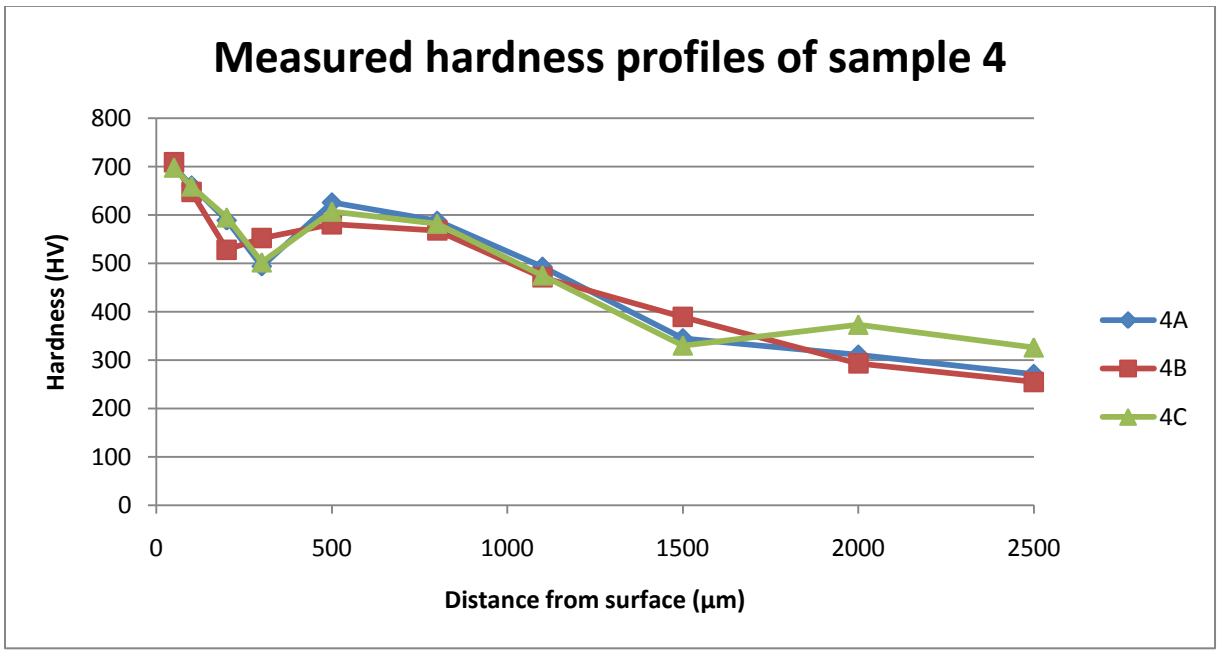

Figure AT. The three parallel surface hardness profiles of sample 4.

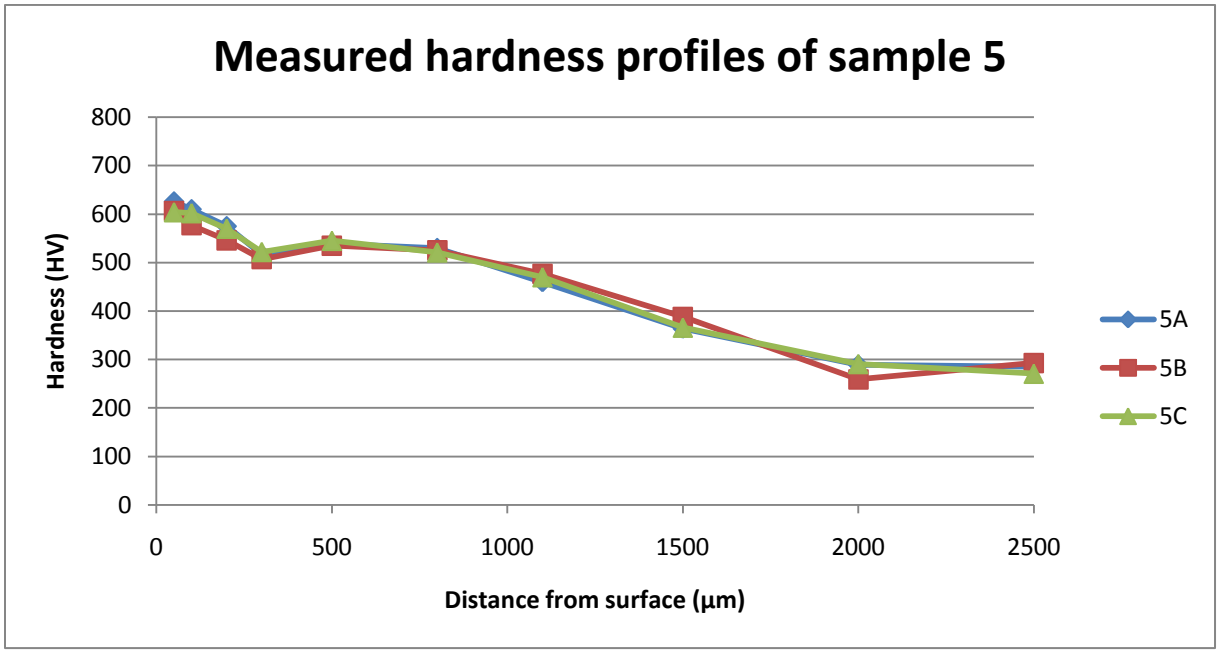

Figure AU. The three parallel surface hardness profiles of sample 5.

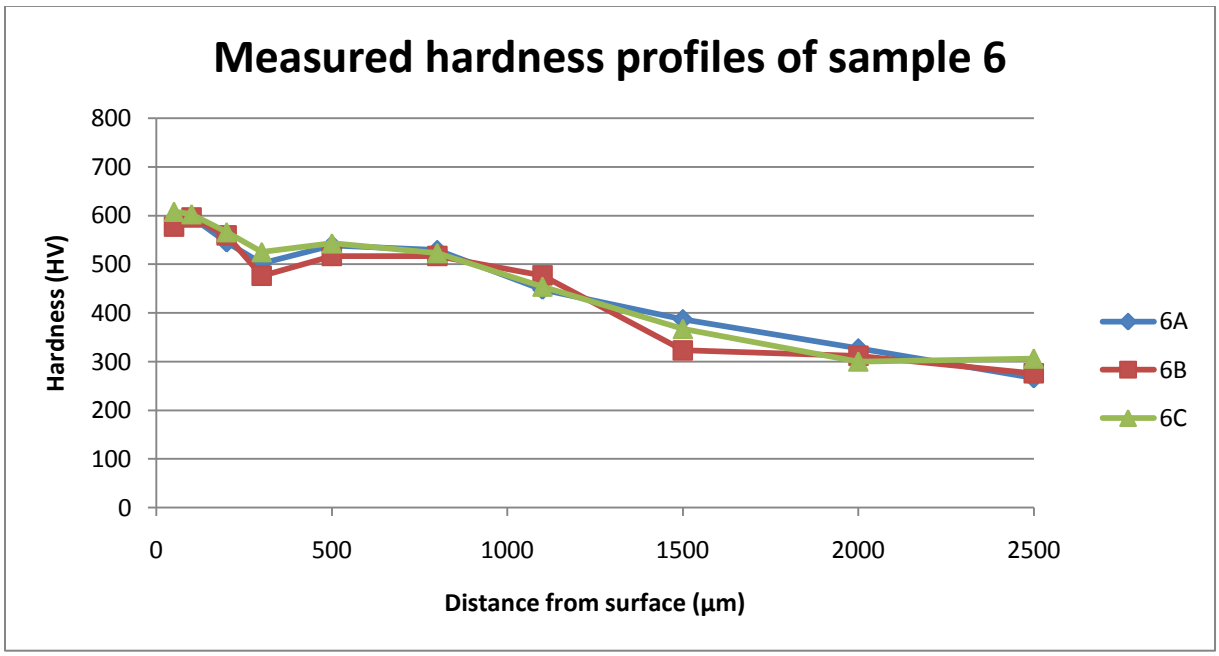

Figure AV. The three parallel surface hardness profiles of sample 6.

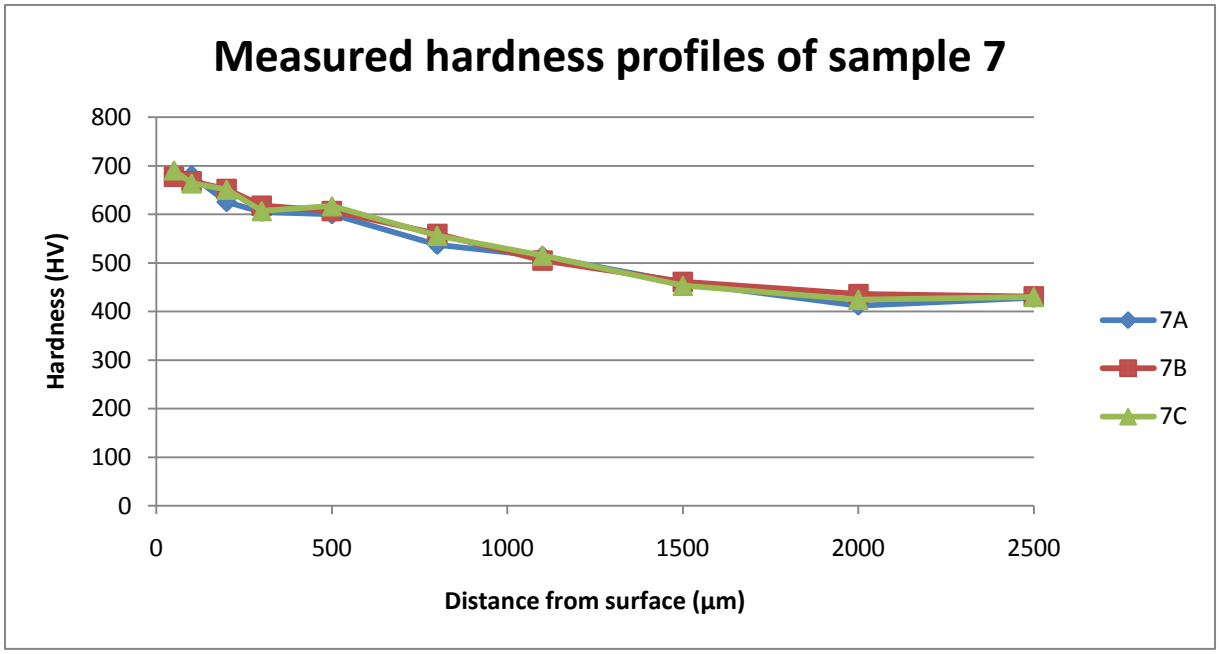

Figure AW. The three parallel surface hardness profiles of sample 7.

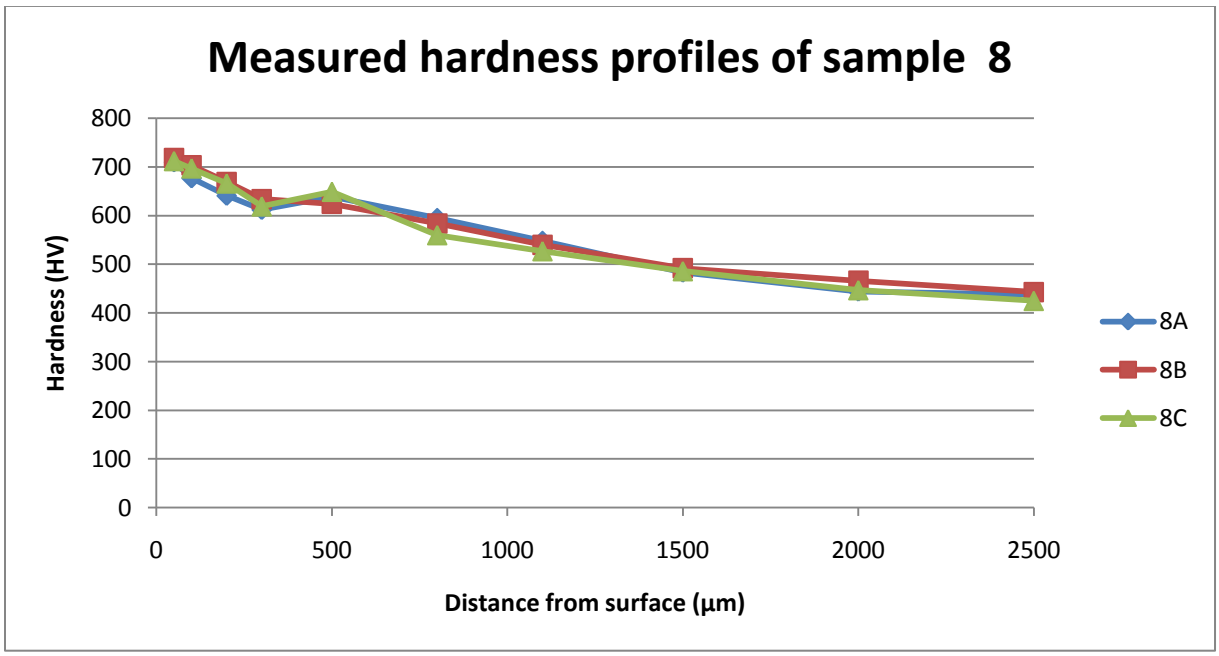

Figure AX. The three parallel surface hardness profiles of sample 8.

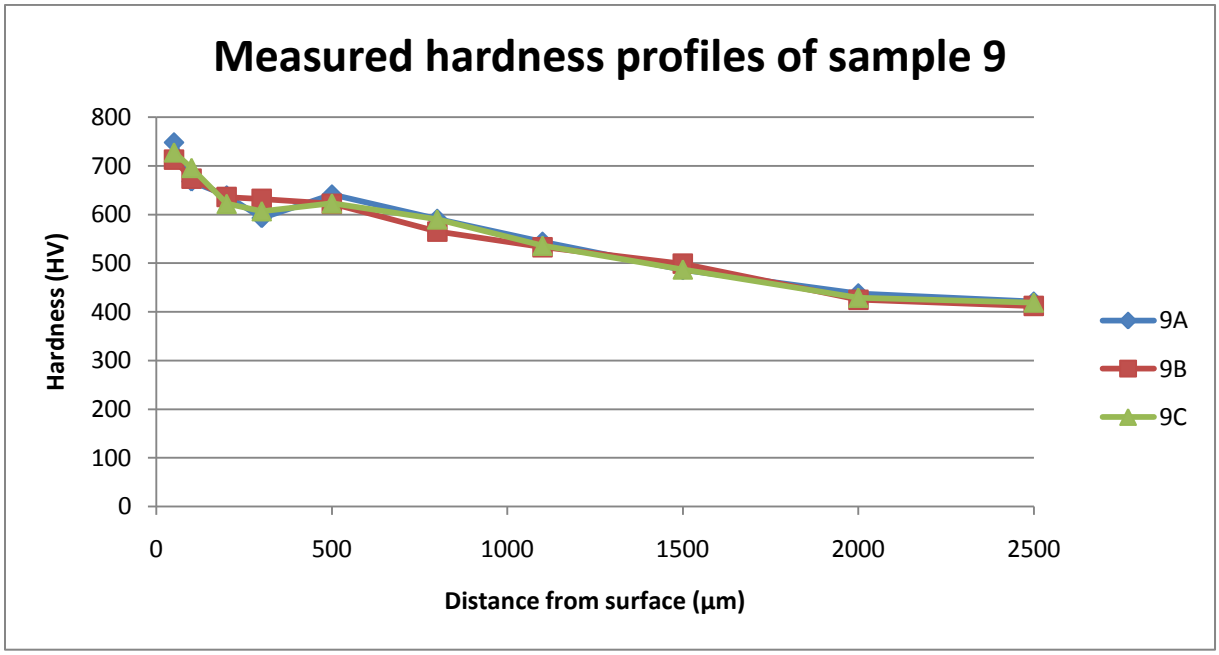

Figure AY. The three parallel surface hardness profiles of sample 9.

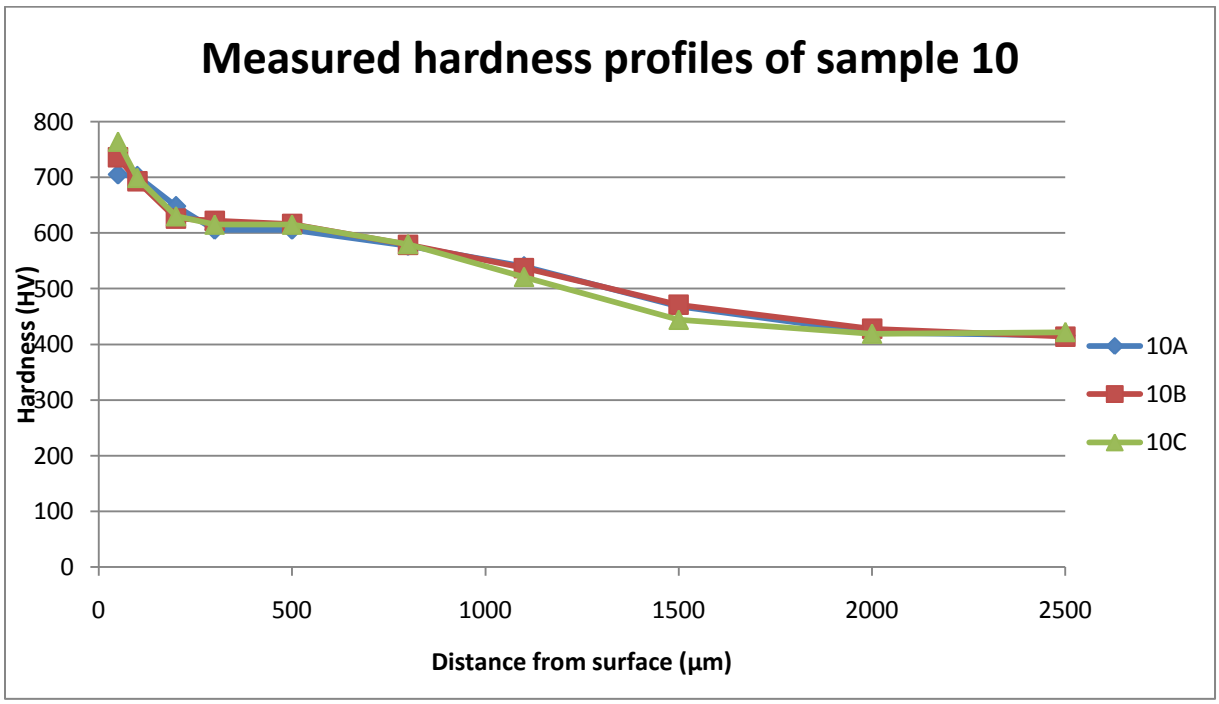

Figure AZ. The three parallel surface hardness profiles of sample 10.

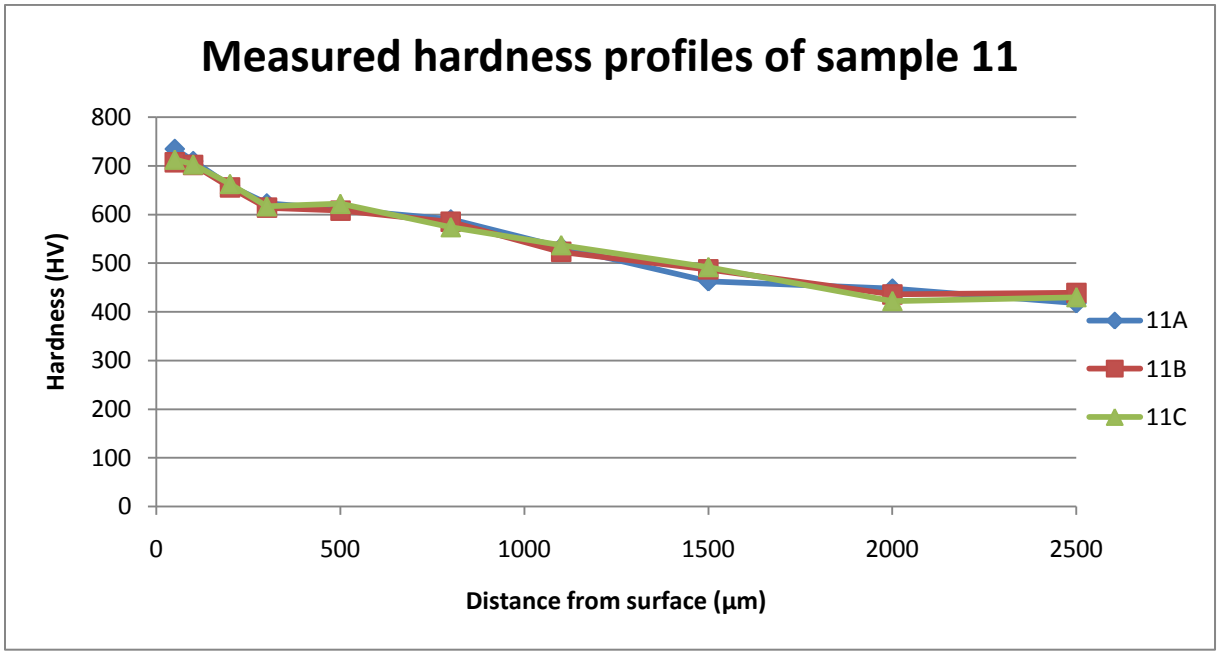

Figure BA. The three parallel surface hardness profiles of sample 11.

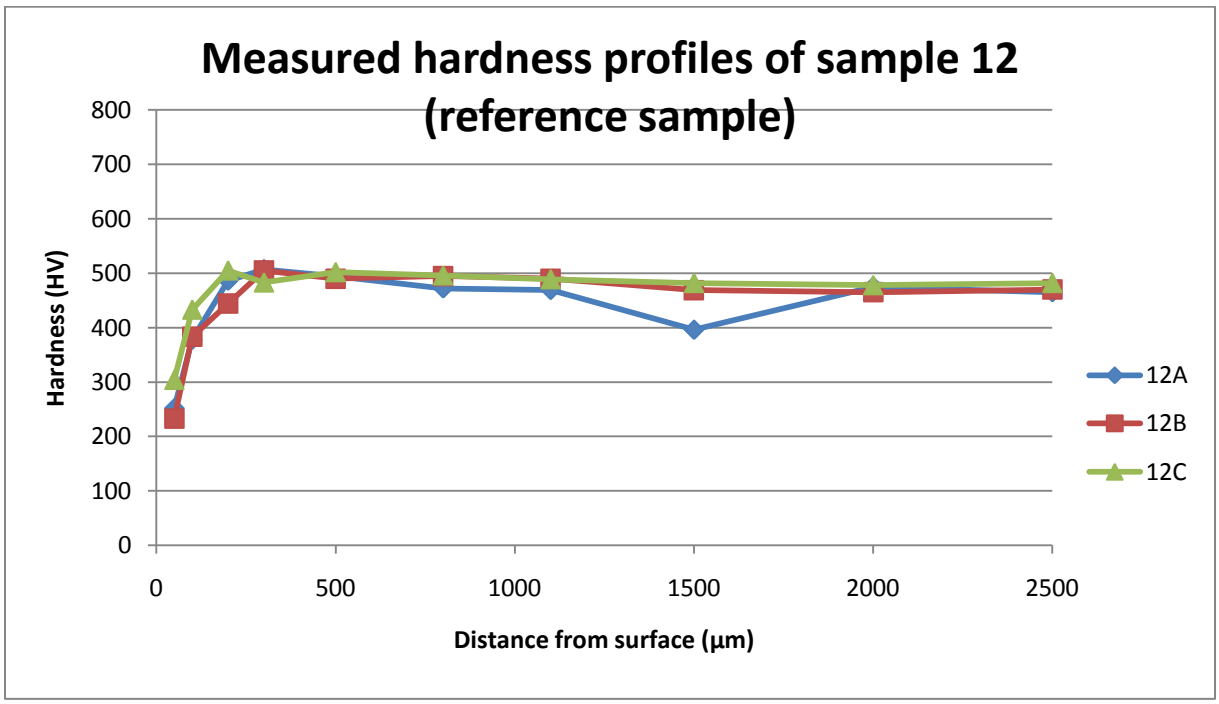

Figure BB. The three parallel surface hardness profiles of the original Hardox 450 reference sample.

E. Microstructure of the samples

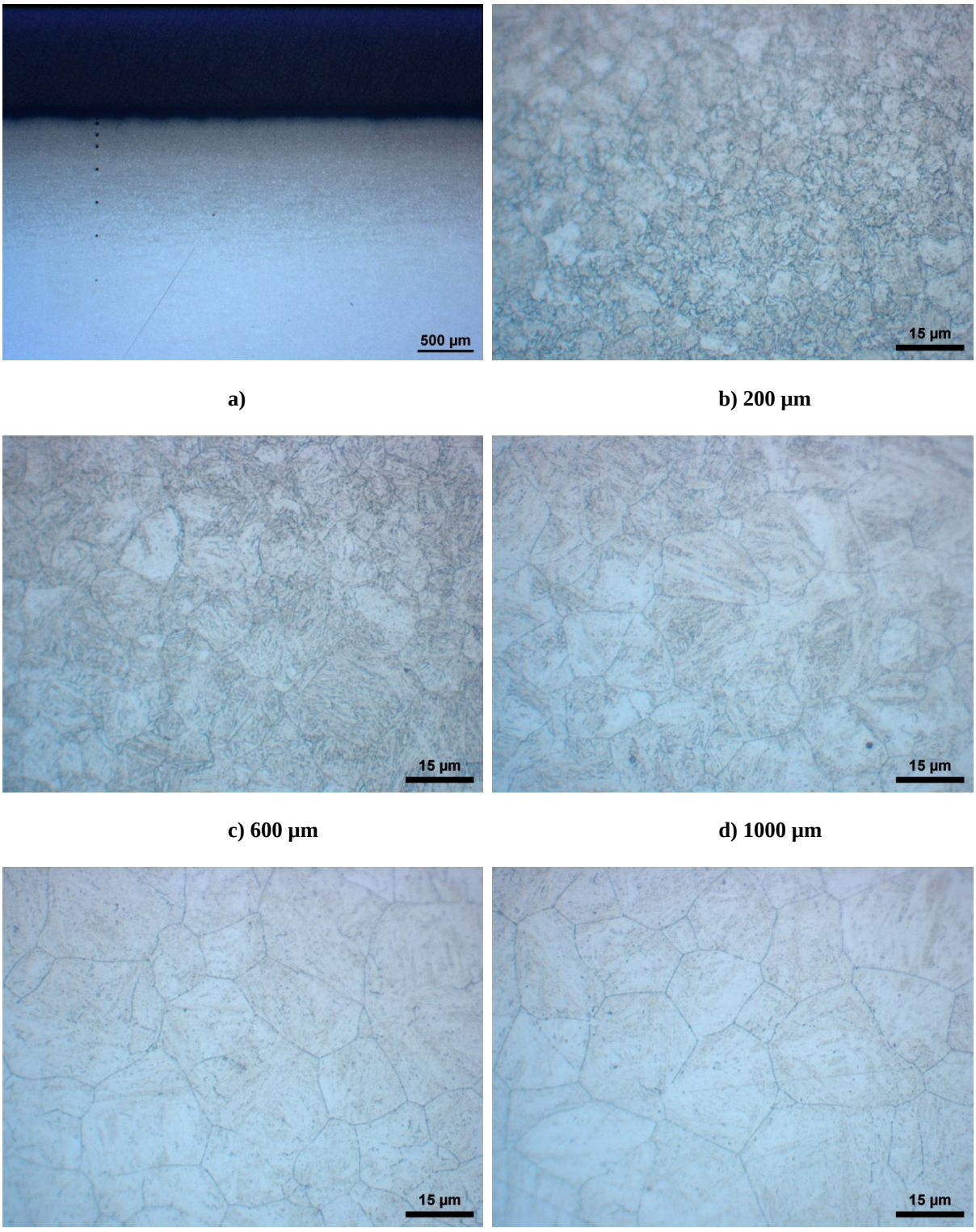

a) **b) 200 µm**

c) 600 µm **d) 1000 µm**

e) 2000 µm **f) 6000 µm**

Figure BC. Microstructure of sample 1. a): Low magnification of the sample surface. b)-f): Microstructure at different distances below the sample surface.

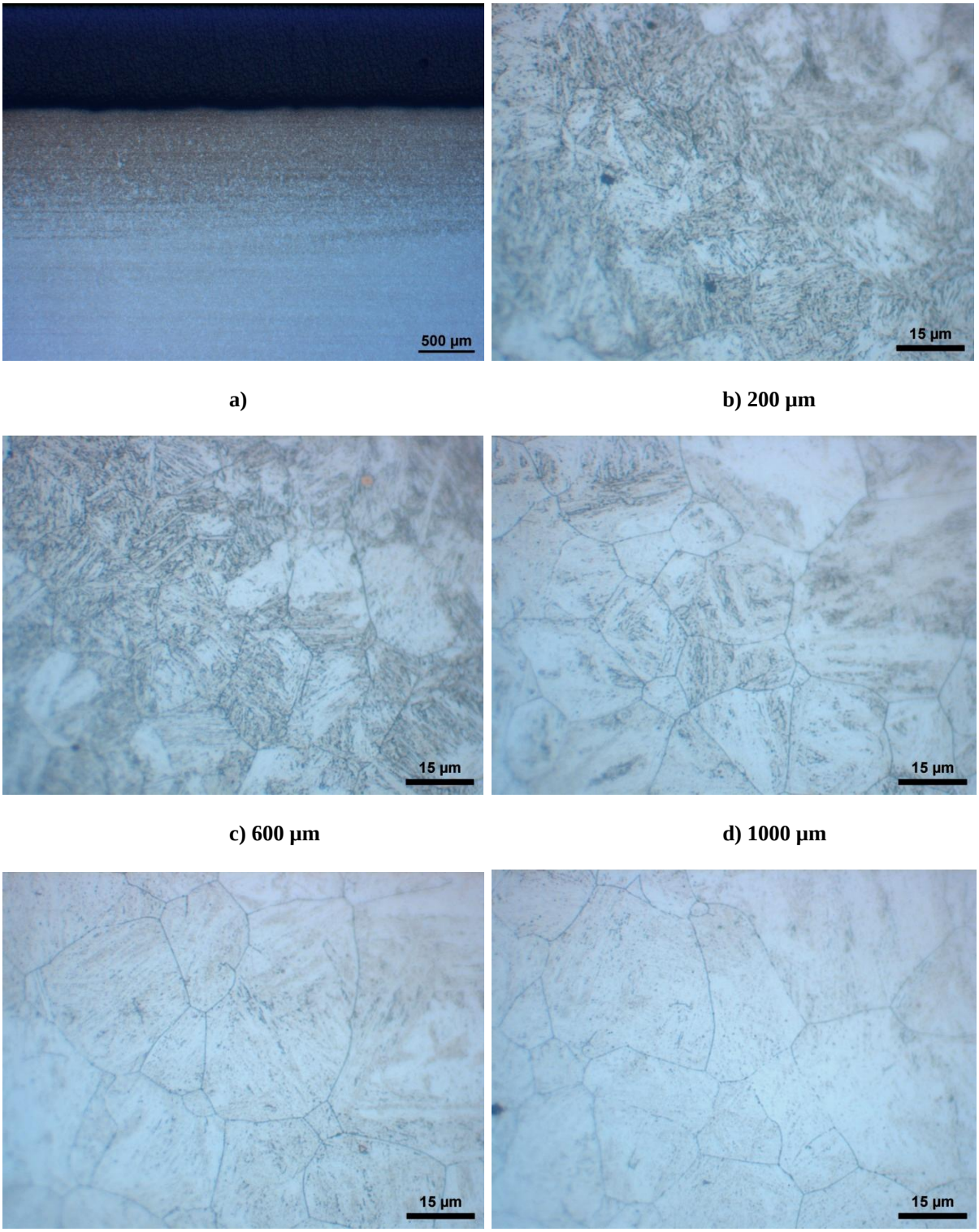

a) **b) 200 µm**

c) 600 µm **d) 1000 µm**

e) 2000 µm **f) 6000 µm**

Figure BD. Microstructure of sample 2. a): Low magnification of the sample surface. b)-f): Microstructure at different distances below the sample surface.

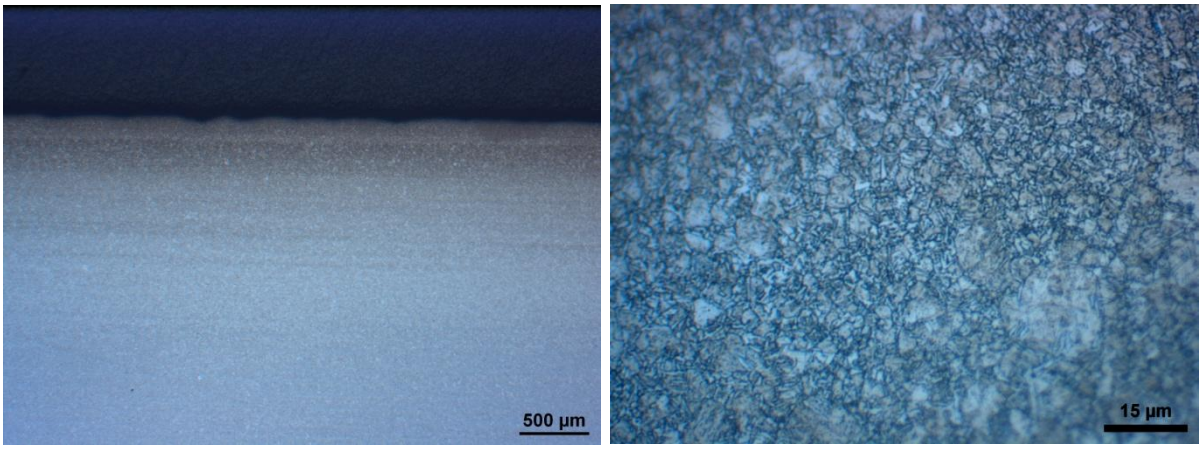

a) **b) 200 µm**

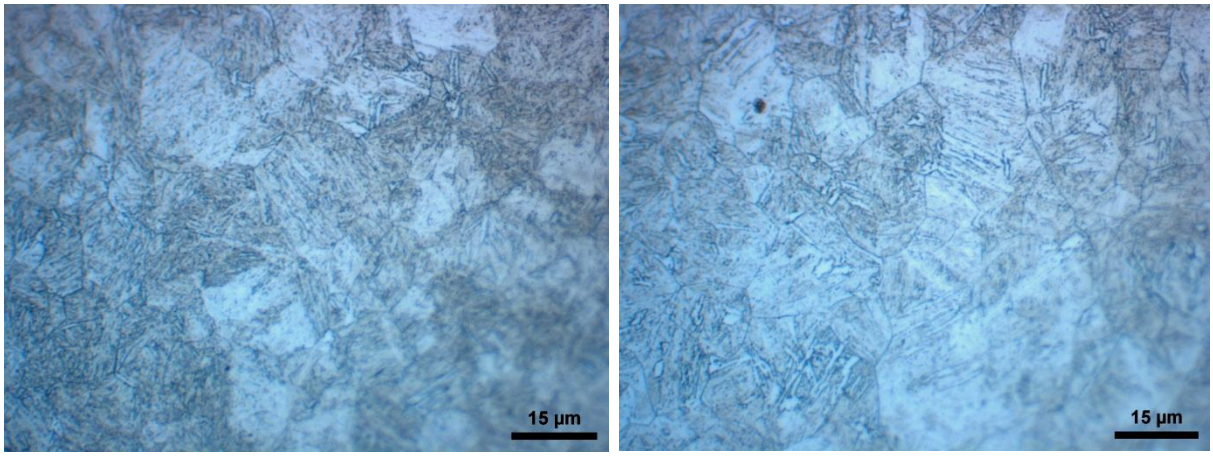

c) 600 µm **d) 1000 µm**

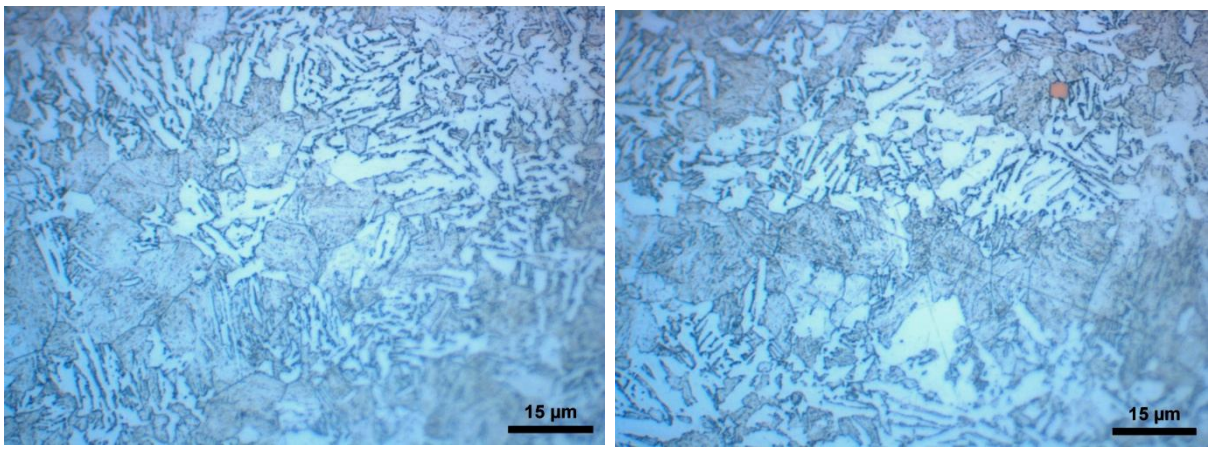

e) 2000 µm **f) 6000 µm**

Figure BE. Microstructure of sample 3. a): Low magnification of the sample surface. b)-f): Microstructure at different distances below the sample surface.

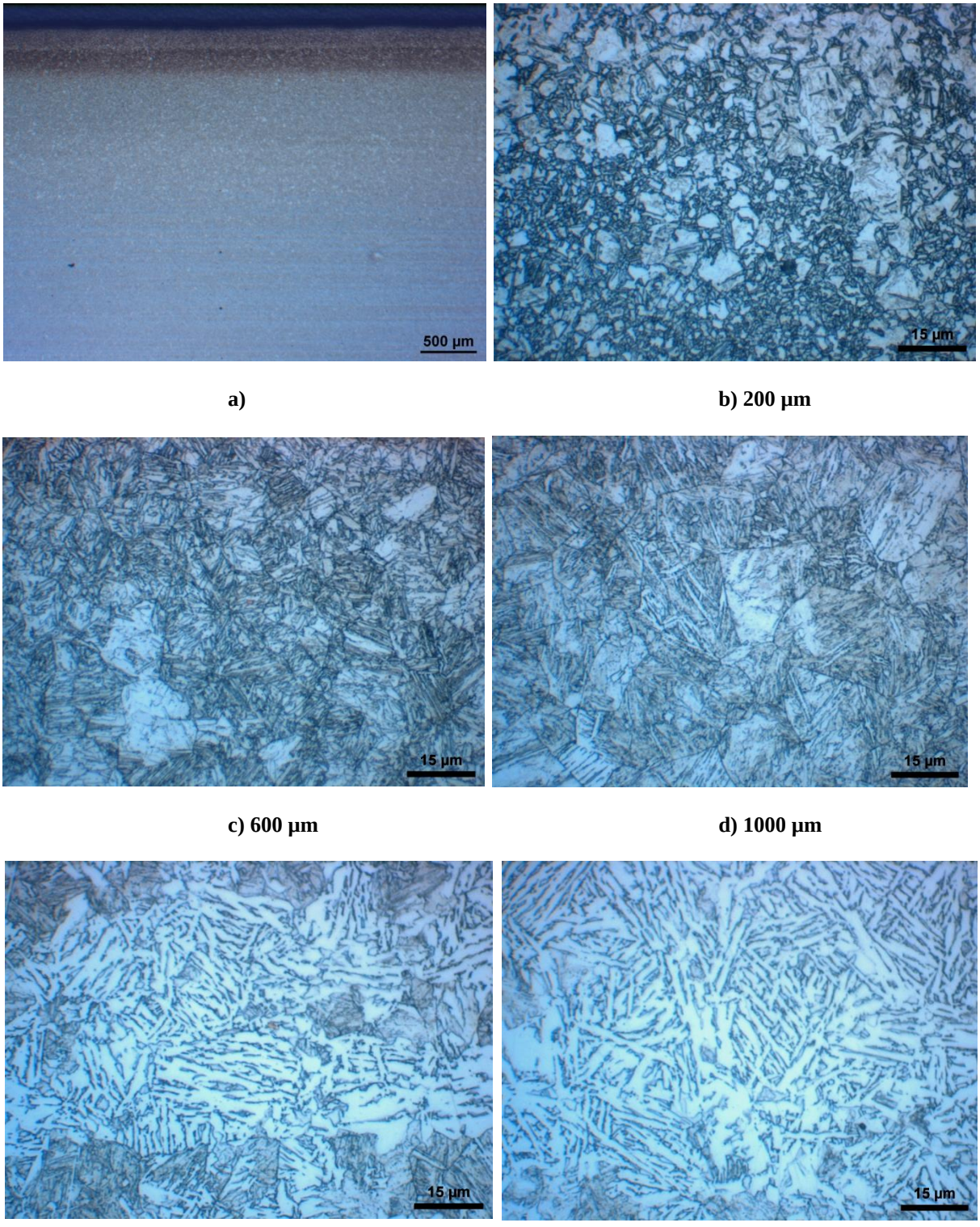

a) **b) 200 µm**

c) 600 µm **d) 1000 µm**

e) 2000 µm **f) 6000 µm**

Figure BF. Microstructure of sample 4. a): Low magnification of the sample surface. b)-f): Microstructure at different distances below the sample surface.

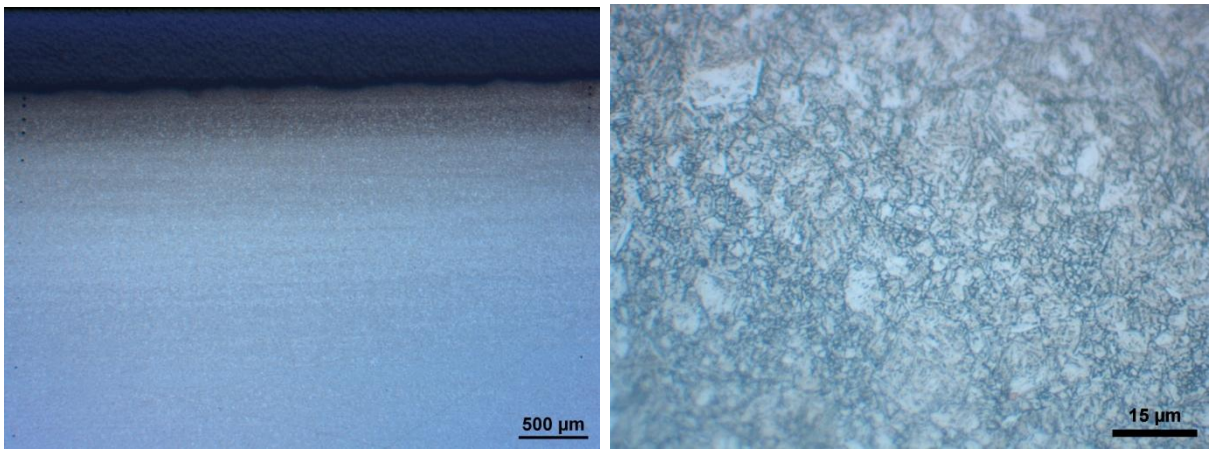

a) **b) 200 µm**

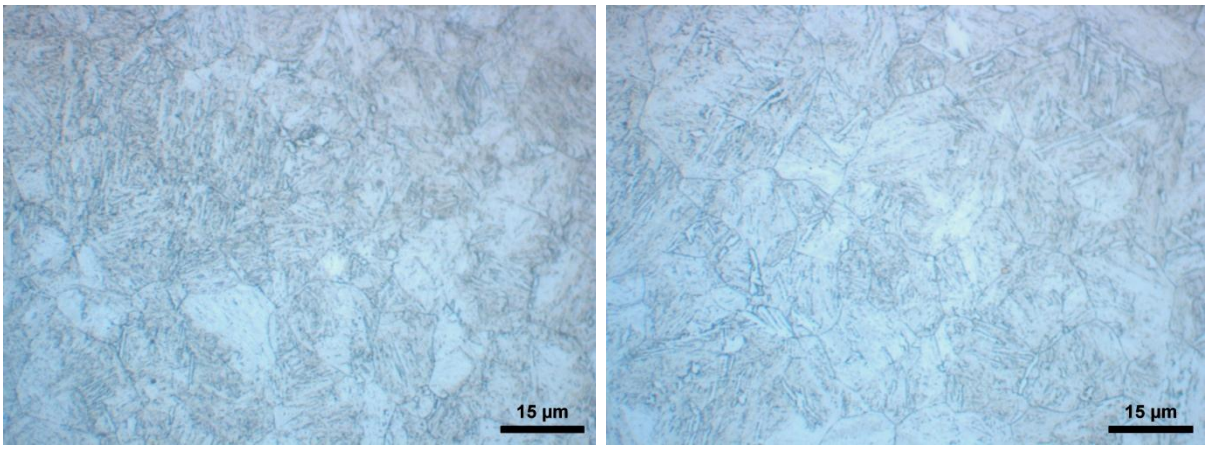

c) 600 µm **d) 1000 µm**

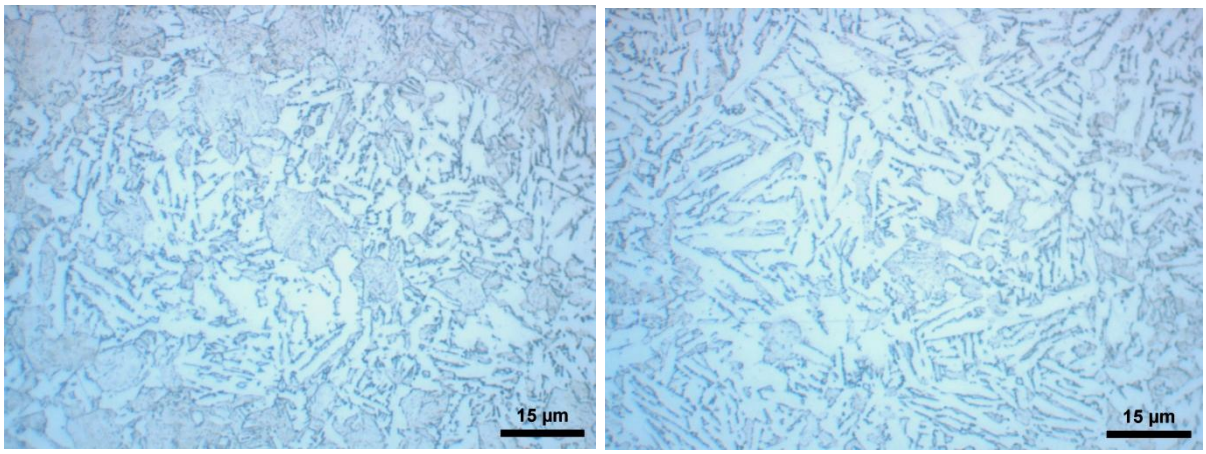

e) 2000 µm **f) 6000 µm**

Figure BG. Microstructure of sample 5. a): Low magnification of the sample surface. b)-f): Microstructure at different distances below the sample surface.

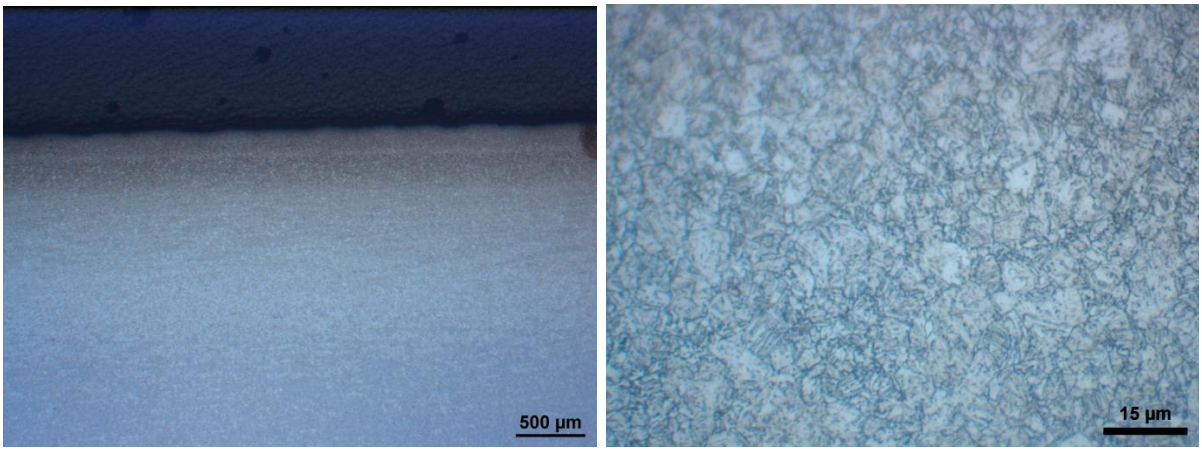

a) **b) 200 µm**

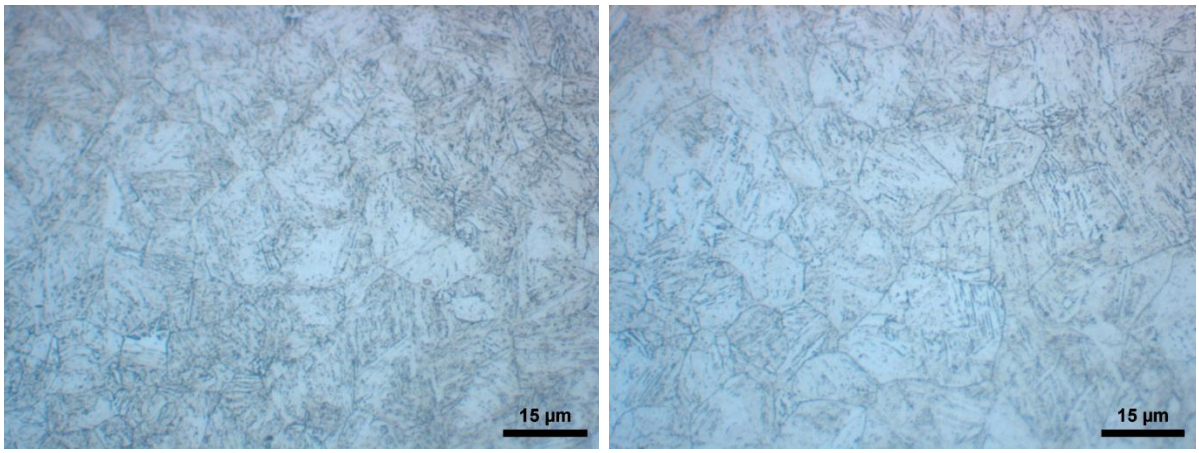

c) 600 µm **d) 1000 µm**

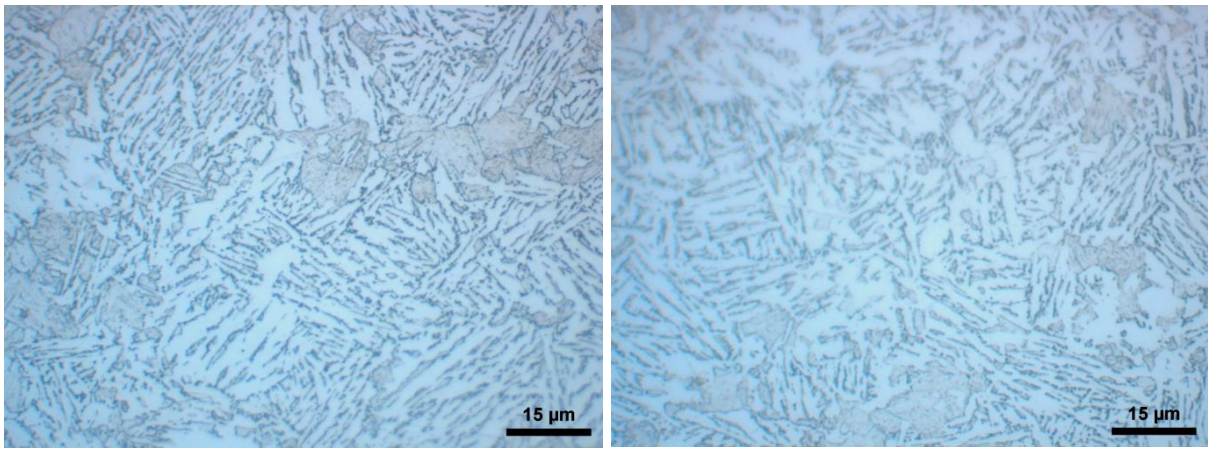

e) 2000 µm **f) 6000 µm**

Figure BH. Microstructure of sample 6. a): Low magnification of the sample surface. b)-f): Microstructure at different distances below the sample surface.

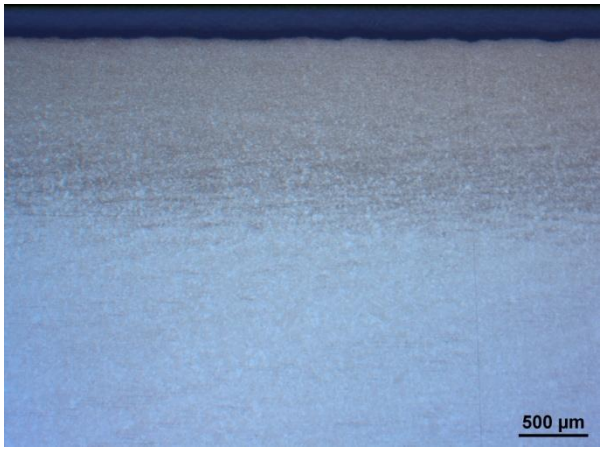

a)

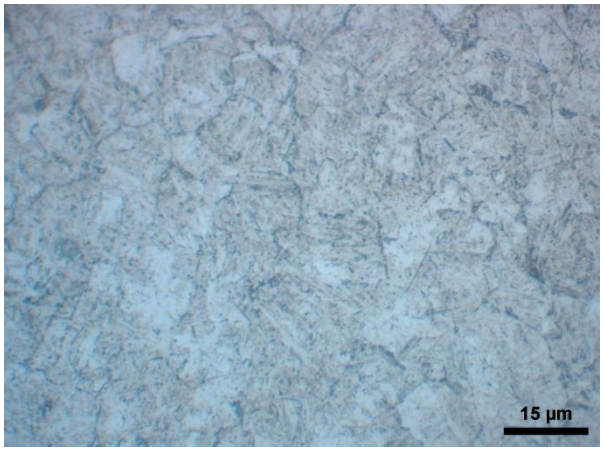

b) 200 µm

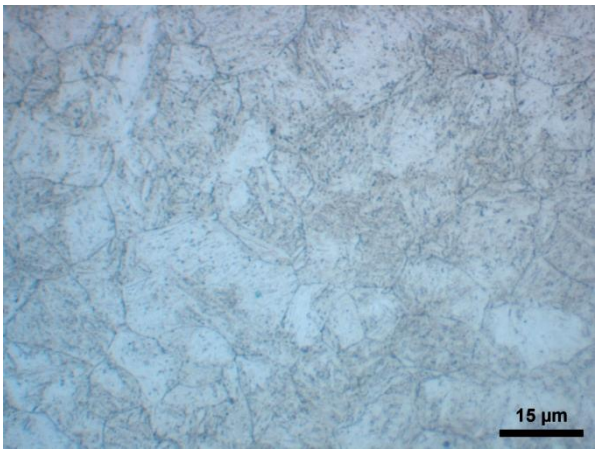

c) 600 µm

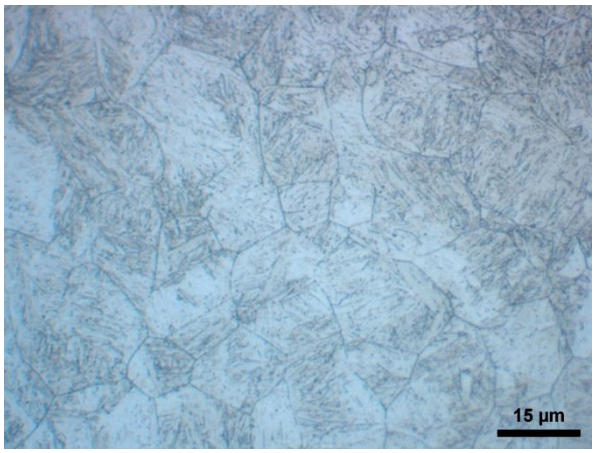

d) 1000 µm

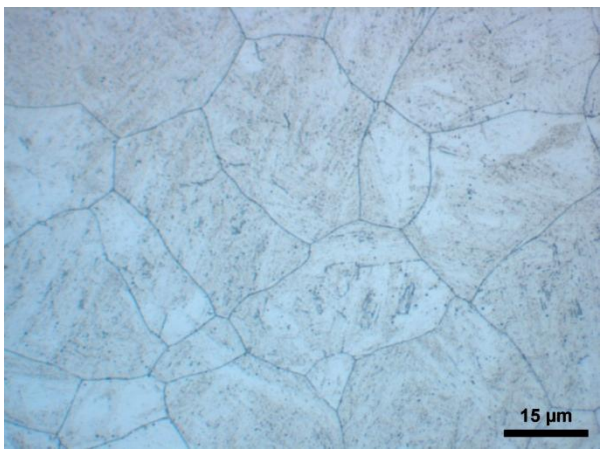

e) 2000 µm

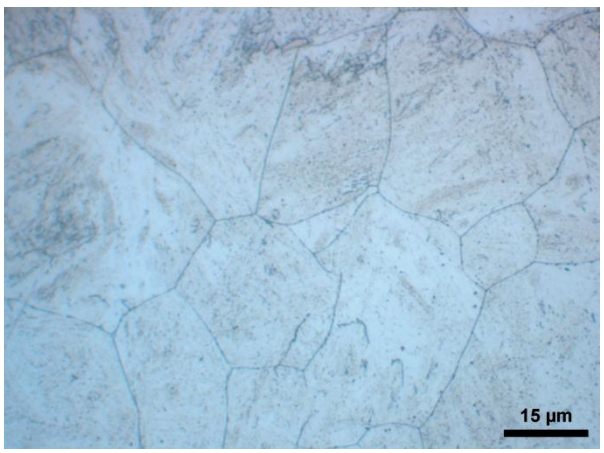

f) 6000 µm

Figure BI. Microstructure of sample 7. a): Low magnification of the sample surface. b)-f): Microstructure at different distances below the sample surface.

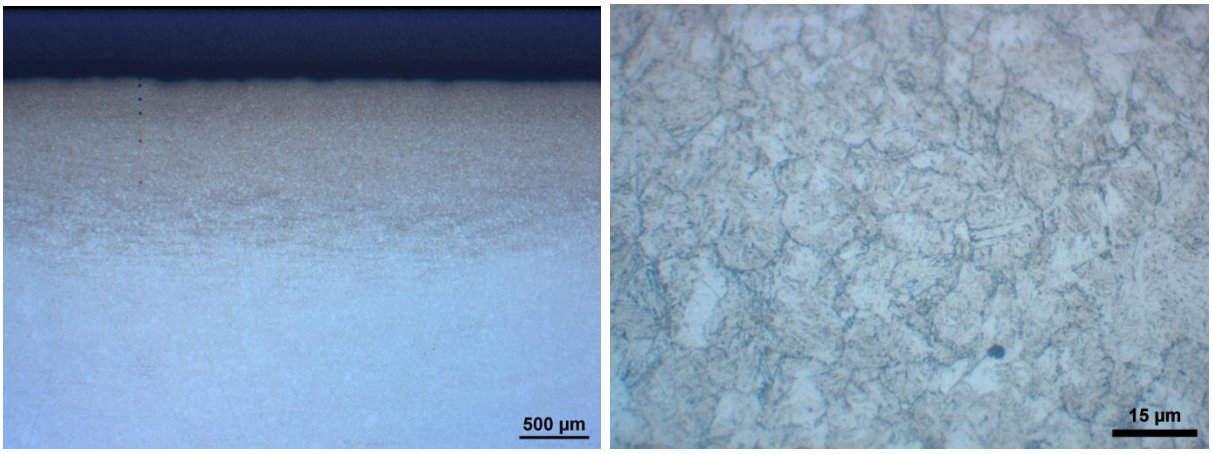

a) **b) 200 µm**

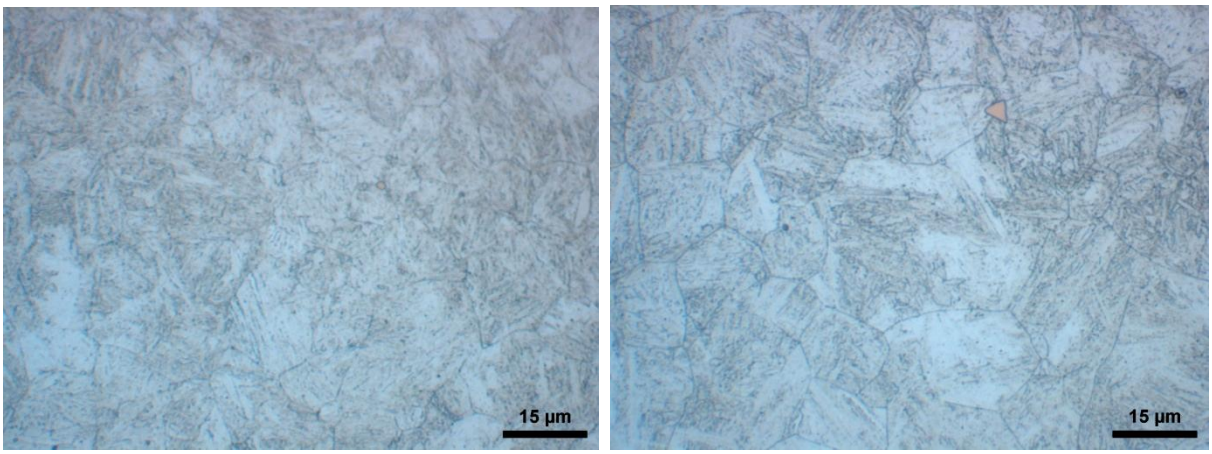

c) 600 µm **d) 1000 µm**

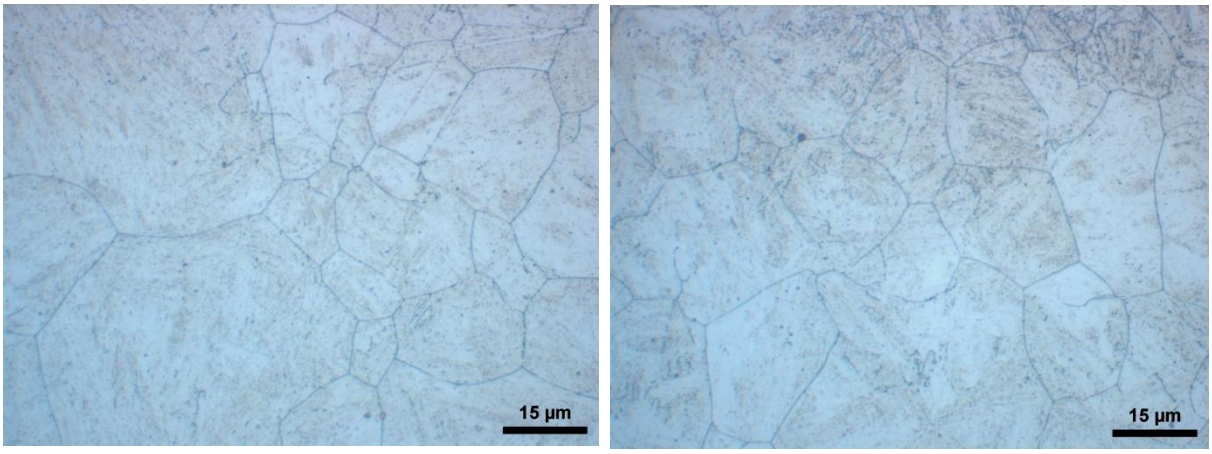

e) 2000 µm **f) 6000 µm**

Figure BJ. Microstructure of sample 8. a): Low magnification of the sample surface. b)-f): Microstructure at different distances below the sample surface.

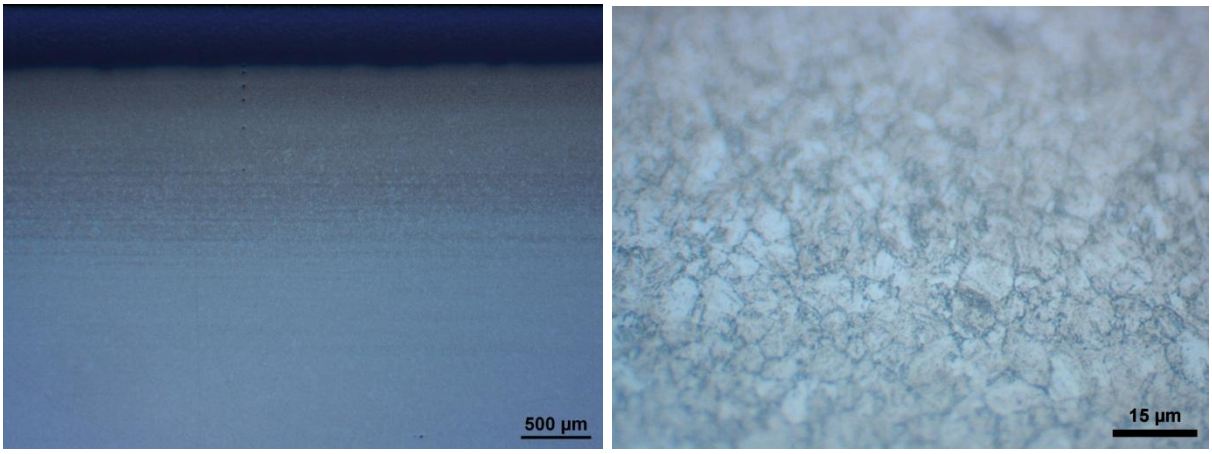

a) **b) 200 µm**

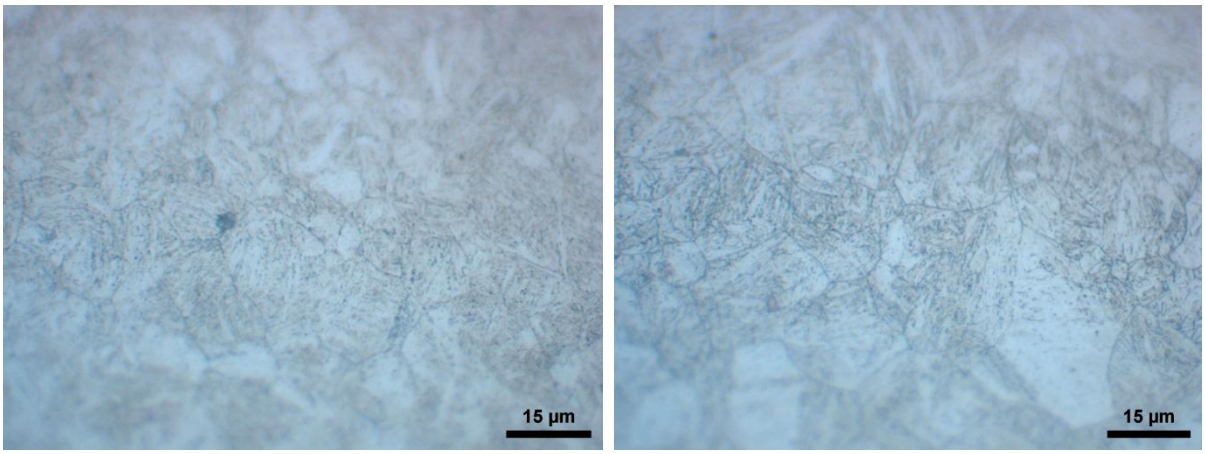

c) 600 µm **d) 1000 µm**

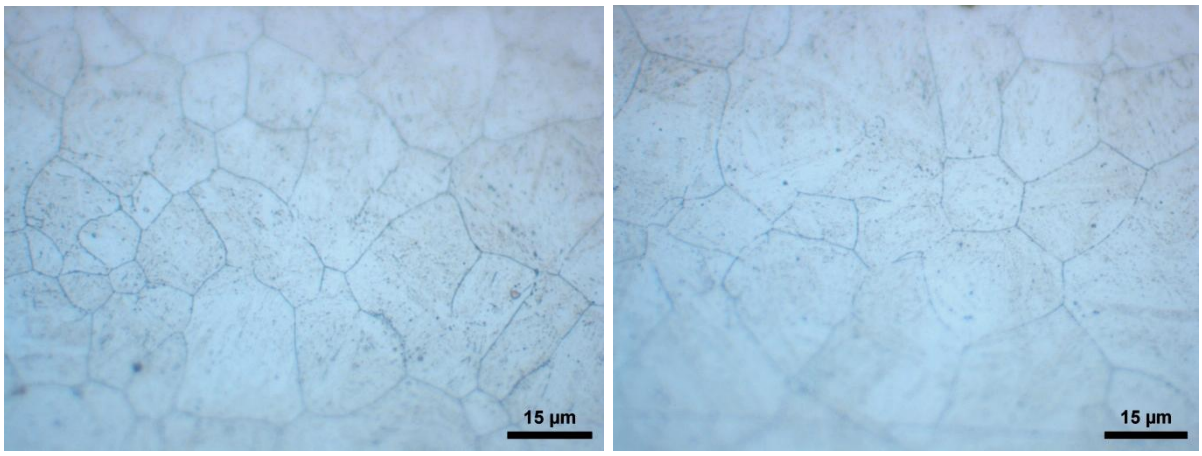

e) 2000 µm **f) 6000 µm**

Figure BK. Microstructure of sample 9. a): Low magnification of the sample surface. b)-f): Microstructure at different distances below the sample surface.

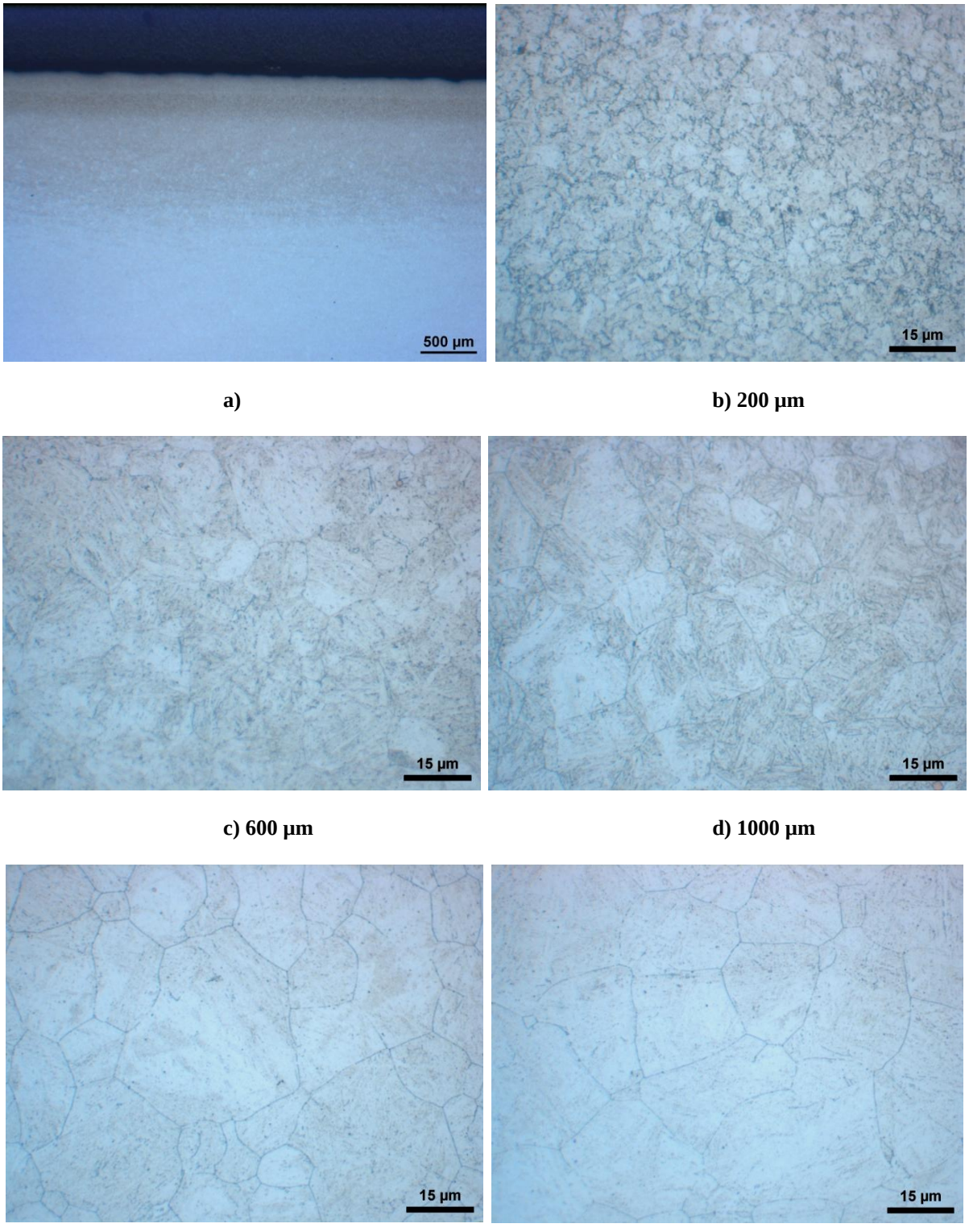

a) **b) 200 µm**

c) 600 µm **d) 1000 µm**

e) 2000 µm **f) 6000 µm**

Figure BL. Microstructure of sample 10. a): Low magnification of the sample surface. b)-f): Microstructure at different distances below the sample surface.

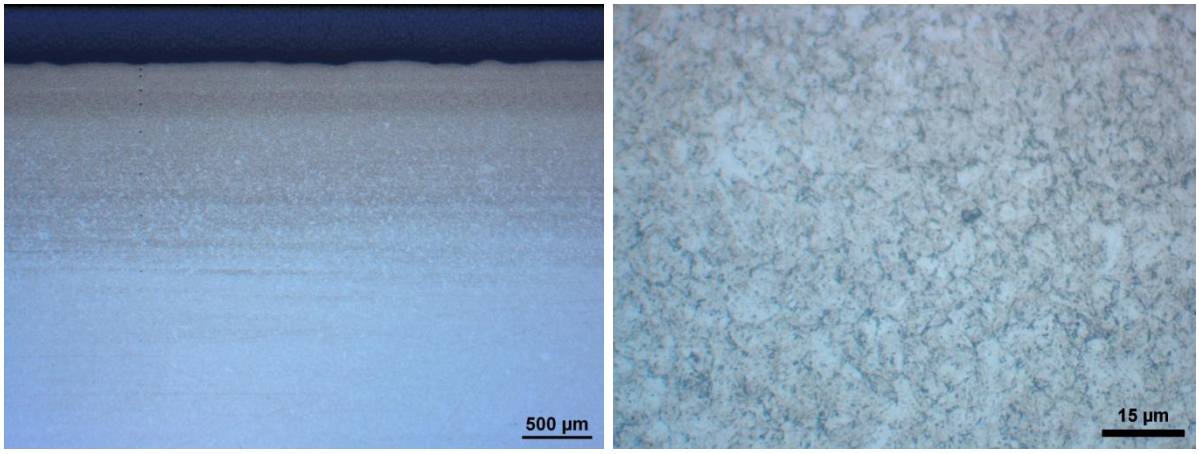

a) **b) 200 µm**

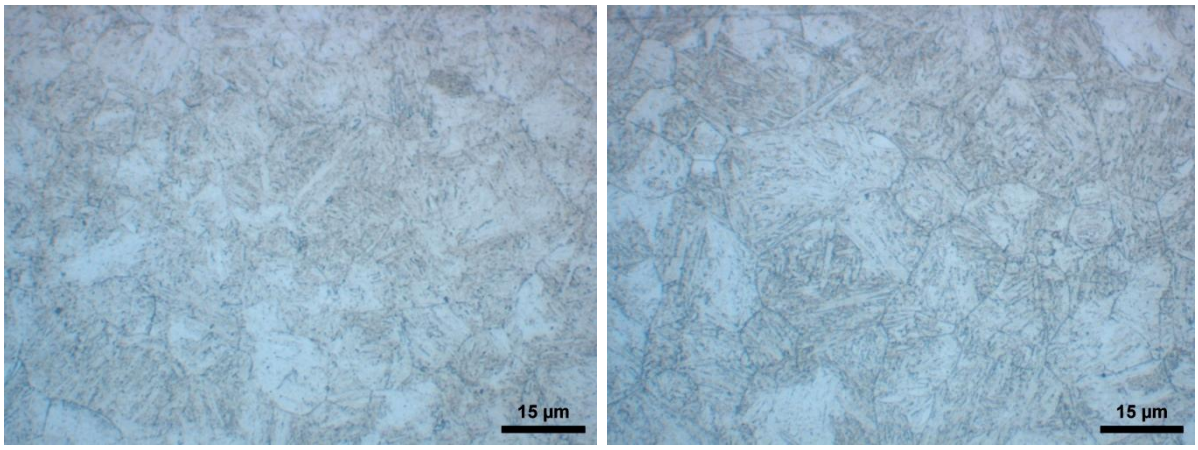

c) 600 µm **d) 1000 µm**

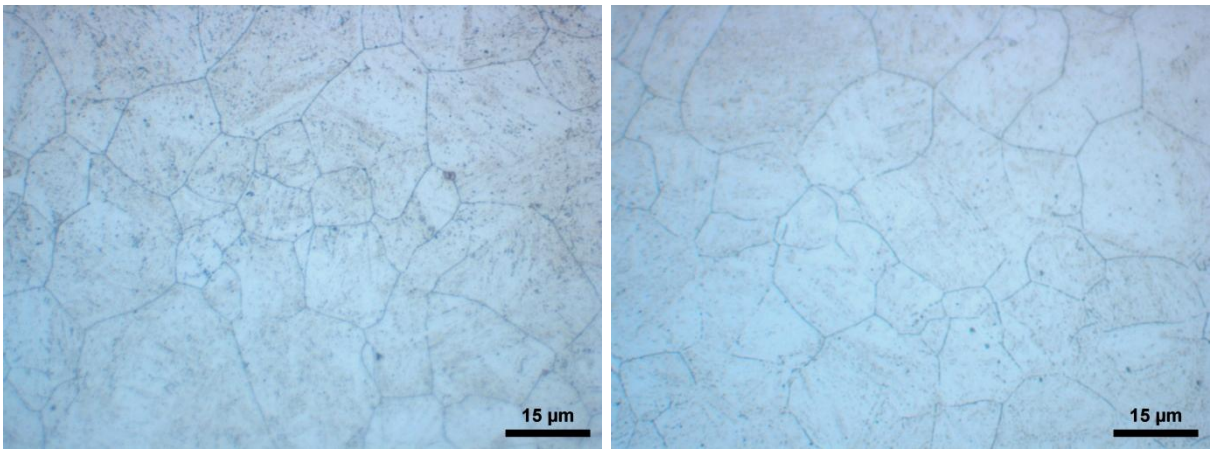

e) 2000 µm **f) 6000 µm**

Figure BM. Microstructure of sample 11. a): Low magnification of the sample surface. b)-f): Microstructure at different distances below the sample surface.

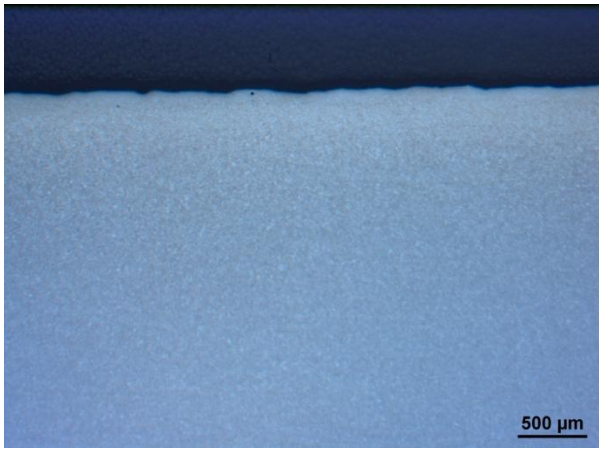

a)

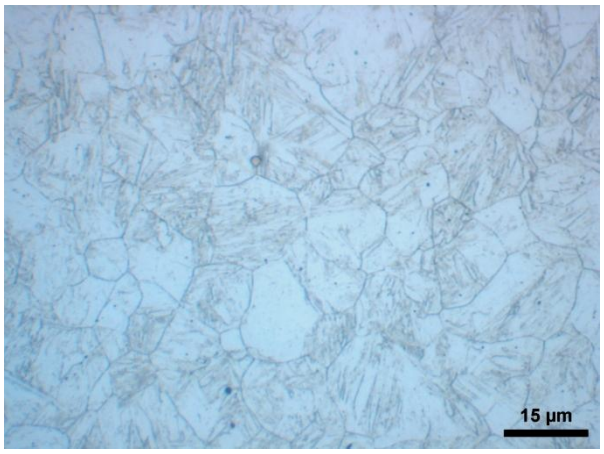

b) 200 µm

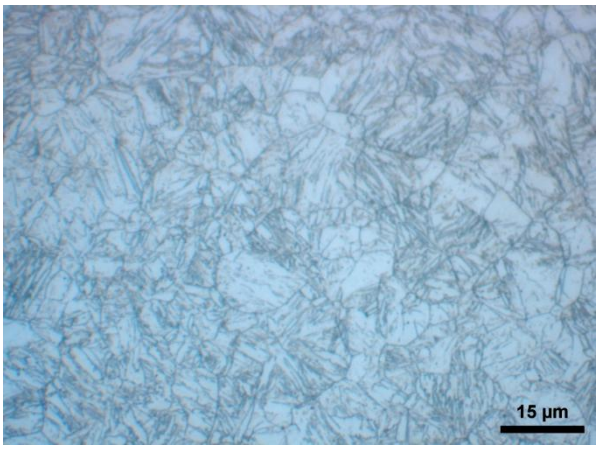

c) 600 µm

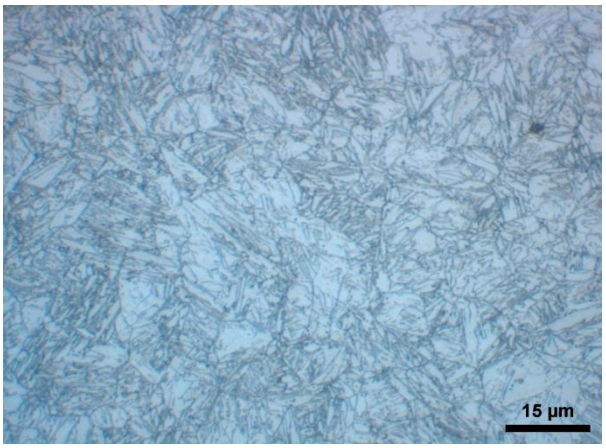

d) 1000 µm

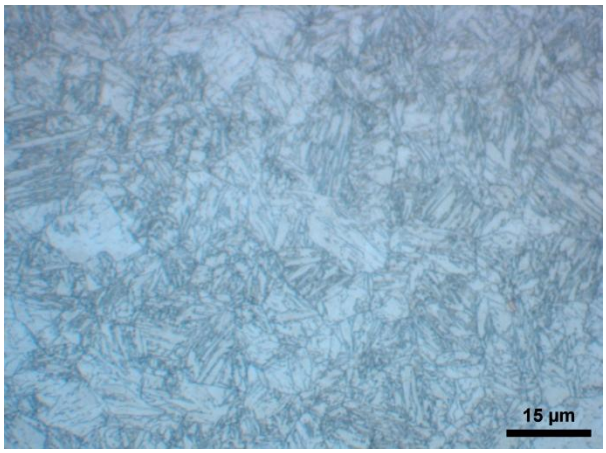

e) 2000 µm

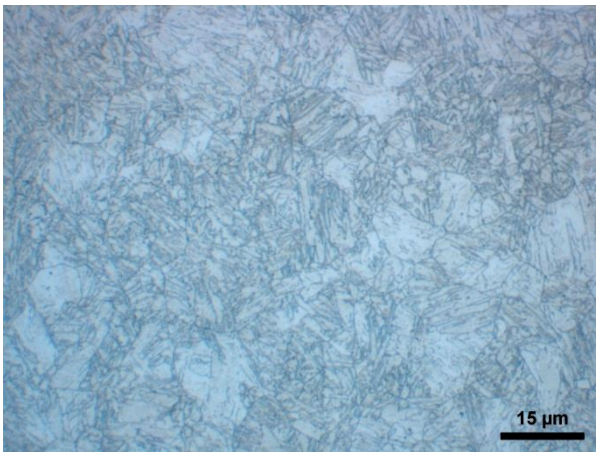

f) 6000 µm

Figure BN. Microstructure of the original Hardox 450 reference sample. a): Low magnification of the sample surface. b)-f): Microstructure at different distances below the sample surface.